Functional Polymers for Anhydrous Proton Transport

FUNCTIONAL POLYMERS FOR ANHYDROUS PROTON TRANSPORT

A Dissertation Presented

by

NAGAMANI CHIKKANNAGARI

Submitted to the Graduate School of the
University of Massachusetts Amherst in partial fulfillment
of the requirements for the degree of

DOCTOR OF PHILOSOPHY

February 2012

Chemistry

FUNCTIONAL POLYMERS FOR ANHYDROUS PROTON TRANSPORT

A Dissertation Presented

by

NAGAMANI CHIKKANNAGARI

Approved as to style and content by:

_____
Sankaran Thayumanavan, Chair

_____
Dhandapani Venkataraman, Member

_____
Mark T. Tuominen, Member

_____
Ryan C. Hayward, Member

_____
Craig T. Martin, Department Head
Chemistry

DEDICATION

To my parents and my beloved husband G. Nagarjuna

ACKNOWLEDGMENTS

A Ph.D. program is a long journey that requires a strong commitment and perseverance to succeed. This journey would not have been successful without the support and encouragement from many people. I would like to take this opportunity to express my sincere gratitude and recognize those who have helped and inspired me to come this far.

First and foremost, I wish to express my sincere respect and gratitude to my advisor Prof. S. Thayumanavan (Thai) for his guidance, encouragement, and constant support over the past five years. It has been a great privilege to work with an advisor who has a contagious enthusiasm for research and incredible management skills. His unwavering support and guidance both in research and other professional decisions has been immensely helpful and I greatly appreciate it.

I also thank my dissertation committee members, Prof. D. Venkataraman, Prof. Ryan C. Hayward, and Prof. Mark T. Tuominen for their time and constructive input on my research. I wish to thank Prof. Venkataraman for taking the time to write reference letters and also for his help during my job search; Prof. Hayward for taking the time to write reference letters and his willingness to rearrange his trip when I had a tough time scheduling my final defense; and Prof. Tuominen for providing constant support from his group in getting the conductivity measurements for most of the polymers reported in this dissertation.

I would like to acknowledge my collaborators: Dr. Akamol Klaikherd, Jing Guo, Dr. Usha Viswanathan, Craig C. Versek, Michael Thorn, and Dr. A. Chandrasekaran. It

has been a great learning experience working with you all. My special thanks to Dr. Akamol Klaikherd for being a wonderful mentor during my initial days in lab and helping me to get on my feet, and also for giving me a crash course on how to use several programs.

I would like to thank all the present and past members of *Thai Research Group* for their help and valuable advice in my research career. I also thank the administrative staff in the chemistry department for the help and support during my stay at UMass. Special thanks are due to Ms. J. M. Stowe and Karen Hakala for helping me with the logistics and making things run smoothly, and Robert Sabola for promptly fixing any broken lab equipment, particularly vacuum pumps.

Lastly, I express my deepest gratitude to my parents, brother, and sister for their unconditional love and support. My special thanks to my husband G. Nagarjuna for his love, caring attitude, and for being there for me through everything. Words cannot express my heartfelt gratitude and appreciation to you. Thank you!

ABSTRACT

FUNCTIONAL POLYMERS FOR ANHYDROUS PROTON TRANSPORT

FEBRUARY 2012

NAGAMANI CHIKKANNAGARI, B.Sc., SRI SATHYA SAI INSTITUTE OF HIGHER LEARNING

M.Sc., UNIVERSITY OF HYDERABAD

Ph.D., UNIVERSITY OF MASSACHUSETTS AMHERST

Directed by: Professor Sankaran Thayumanavan

Anhydrous proton conducting polymers are highly sought after for applications in high temperature polymer electrolyte membrane fuel cells (PEMFCs). *N*-heterocycles (eg. imidazole, triazole, and benzimidazole), owing to their amphoteric nature, have been widely studied to develop efficient anhydrous proton transporting polymers. The proton conductivity of *N*-heterocyclic polymers is influenced by several factors and the design and development of polymers with a delicate balance among various synergistic and competing factors to provide appreciable proton conductivities has been a challenging task. In this thesis, the proton transport (PT) characteristics of polymers functionalized with two diverse classes of functional groups - *N*-heterocycles and phenols have been investigated and efforts have been made to develop the molecular design criteria for the design and development of efficient proton transporting functional groups and polymers.

The proton conduction pathway in 1*H*-1,2,3-triazole polymers is probed by employing structurally analogous *N*-heterocyclic (triazole, imidazole, and pyrazole) and benz-*N*-heterocyclic (benzotriazole, benzimidazole, and benzopyrazole) polymers. *Imidazole-like* pathway was found to dominate the proton conductivity of triazole and

pyrazole-like pathway makes only a negligible contribution, if any. Polymers containing benz-*N*-heterocycles exhibited higher proton conductivity than those with the corresponding *N*-heterocycles. Pyrazole-like functional groups, *i.e*. the molecules with two nitrogen atoms adjacent to each other, were found not to be good candidates for PT applications.

A new class of proton transporting functional groups, phenols, has been introduced for anhydrous PT. One of the highlighting features of phenols over *N*-heterocycles is that the hydrogen bond donor/acceptor reorientation can happen on a single -OH site, allowing for facile reorientational dynamics in Grotthuss PT and enhanced proton conductivities in phenolic polymers. Unlike the case of *N*-heterocycles, comparable conductivities were achieved between poly (3,4,5-trihydroxy) styrene and the corresponding small molecule, pyrogallol. This observation suggests that reorientation should be considered as a crucial design parameter for PT functional groups.

The PT characteristics of phenol-based biaryl polymers are studied and compared with the analogous phenol-based linear styrenic polymers. The two-dimensional disposition of -OH moieties in biaryl polymers, although resulted in lower apparent activation energies (E_a), did not improve the net proton conductivity due to the accompanying increase in glass transition temperature (T_g). Thus, the ease of synthesis and lower T_g values of phenol-based styrene polymers make the styrenic polymer architecture preferable over the biaryl architecture. Finally, the synthesis of a series of poly(3,4-dihydroxy styrene)-b-polystyrene block copolymers has been demonstrated via anionic polymerization. These block copolymers will provide an opportunity to systematically investigate the effect of nanoscale morphology on proton transport.

TABLE OF CONTENTS

Page

LIST OF TABLES

LIST OF FIGURES

LIST OF CHARTS

LIST OF SCHEMES

CHAPTER 1

INTRODUCTION: PROTON TRANSPORTING POLYMERS

Proton transport (PT) plays an important role in many biological processes such as photosynthesis, enzyme catalysis, etc.[1] It also plays a key role in materials for renewable energy devices such as fuel cells.[2] In hydrogen fuel cells, the oxidation of hydrogen at the anode produces protons, which must be transferred to the cathode side to complete the conversion of chemical energy to electrical energy. The quest for clean and efficient sources of electrical energy and concerns about environmental pollution has intensified the research on hydrogen fuel cells. There have been increasing efforts to address the current limitations hindering the widespread commercialization of fuel cell technology. At the heart of this technology is a proton conducting polymer that can selectively and efficiently conduct protons from the anode to the cathode side. Presented here is a brief overview of fuel cells, followed by a detailed discussion about proton conducting polymers.

1.1 Fuel Cells

A fuel cell is an electrochemical device that can convert the chemical energy of a fuel (for example hydrogen) into electrical energy via redox reactions.[3, 4] A typical fuel cell consists of two electrodes, anode and cathode sandwiching a polymeric material called an electrolyte. The electrolyte serves two important purposes (i) to transfer charges across the electrodes, and (ii) to keep the fuel from mixing with the oxidant. The fuel and oxidant are supplied externally at each of the electrodes. There are various types of fuel

cells depending on the type of electrolyte and fuel. The six major types of fuel cells are polymer electrolyte membrane fuel cell (PEMFC), direct methanol fuel cell (DMFC), alkaline fuel cell (AFC), phosphoric acid fuel cell (PAFC), molten carbonate fuel cell (MCFC), and solid oxide fuel cell (SOFC). The typical characteristics of these fuel cells are summarized in Table 1.1.[5] Oxygen or air is used as the oxidant in all the fuel cells.

Table 1.1 Fuel cell types and their characteristics.

Fuel cell type	Electrode composition	Fuel	Electrolyte	Operating temperature	Efficiency
PEMFC	Carbon/Pt	H_2	Polymer membrane	RT-90 ^{o}C (Nafion) 125-200 (PBI)	50-60%
DMFC	Carbon/Pt	Methanol	Polymer membrane	60-90 ^{o}C	30-40%
AFC	Carbon/Pt	H_2	Aq. KOH, Polymer membrane	RT-90 ^{o}C	50-60%
PAFC	Carbon/Pt	H_2	Phosphoric acid	180-200 ^{o}C	40%
MCFC	Porous Ni or NiO	H_2 or natural gas	Molten Li_2CO_3	550-650 ^{o}C	45-50%
SOFC	Porous Ni or Co	Gasoline or natural gas	O^{2-} conducting ceramic oxide	800-1000 ^{o}C	55-60%

Among various types of fuel cells, PEMFCs have the well-recognized potential to supply clean energy for transportation and portable electronic systems.[6] A schematic of a PEMFC is shown in Figure 1.1. PEMFCs consist of an anode, cathode, and a proton conducting polymer electrolyte membrane (PEM) sandwiched between the electrodes. The anode and cathode typically consist of a porous carbon dispersed with platinum

catalyst. The fuel, hydrogen, is supplied externally at the anode side where it gets oxidized to produce electrons and protons. The electrons are shuttled across an external circuit and can be harnessed as electrical energy. The protons are transferred via the PEM to the cathode side. At the cathode, oxygen combines with protons and electrons to produce water and heat. Thus, water and heat are the only byproducts of the overall fuel cell reaction. The oxidation and reduction reactions at the anode and cathode respectively are catalyzed by platinum.

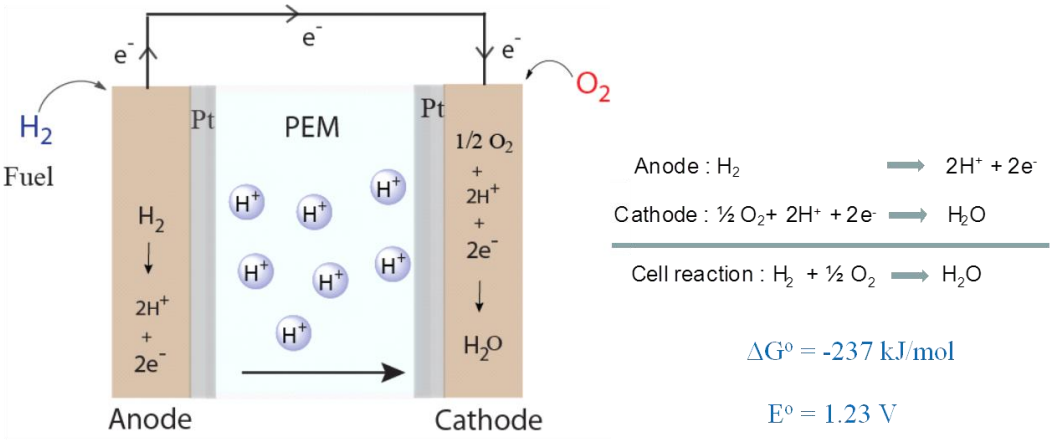

Figure 1.1 Schematic diagram of a PEMFC.

PEMFCs have gained special attention for use in automobiles and portable electronics because of their high power density, relatively low operational temperatures, non-volatile solid polymer electrolyte, and efficient energy conversion. At the heart of PEMFC technology is a PEM, a proton transporting polymer, which can selectively and efficiently transfer protons between the electrodes. The PEM is one of the most important, and often performance-limiting, components of a fuel cell. Some of the key requisites of PEMs are high proton conductivity, negligible electron conductivity, low permeability to hydrogen

and oxygen, good thermal, hydrolytic, and oxidative stability, and the ease of production with low cost. The target set by the U.S Department of Energy (DOE) for the proton conductivity of PEMs is 0.1 S cm^{-1} at 120 ^{o}C and 50% relative humidity.[7, 8] There are several key issues preventing the successful commercialization of PEMFC technology such as hydrogen production, storage and distribution, lack of robust PEMs which can withstand high operational temperatures, and lack of efficient and cost-effective catalysts. This thesis mainly deals with proton conducting polymers and hence the rest of the discussion is focused on the state-of-the art PEMs, their limitations, and the progress on developing alternate proton conducting polymers.

1.2 Proton Conducting Polymers

Two types of mechanisms are proposed for proton transfer: (i) vehicular mechanism - a solvent assisted proton transfer which involves the motion of a protonated species (for example H_3O^+ in water); and (ii) Grotthuss mechanism - proton motion via framework jumps i.e. structural diffusion which involves the hopping of protons from one site to the other mediated by an extended hydrogen bond network.[2, 9] The currently known proton conducting polymers can be broadly divided into two types (i) hydrous proton conducting polymers in which the vehicular mechanism dominates; and (ii) anhydrous proton conducting polymers in which protons are transferred via the Grotthuss mechanism.

1.2.1 Hydrous Proton Conducting Polymers

The state-of-the art PEMFCs employ perfluoro sulfonic acid (PFSA) based polymer membranes. Nafion, the first synthetic ionomer developed by Grot in 1967 at DuPont, is the most widely employed PEM polymer in the current PEMFC technology.[10, 11] Nafion

is a copolymer of tetrafluorethylene and perfluorovinyl ether terminated with sulfonic acid groups. The chemical structure of Nafion has both the hydrophobic Teflon-like backbone and the hydrophilic sulfonate side groups. Some of the other commercially available PFSA based polymers are Aciplex, Flemion, and Dow Mem.[12] The structures of Nafion and other PFSA based polymers are shown in Figure 1.2. Nafion is considered to be the benchmark for proton transporting polymers. The most striking features of Nafion are its superior proton conductivity, excellent thermal, chemical, oxidative, and hydrolytic stability, and low permeability to hydrogen and oxygen. A lifetime of over 60,000 hours has been observed with commercial Nafion membranes under fuel cell conditions.

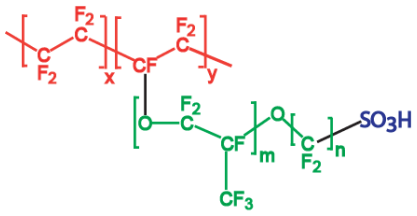

Nafion 117: m≥1, n=2, x=5-13.5, y=1000

Flemion: m=0 or 1, n=1-5

Aciplex: m=0 or 3, n=2-5, x=1.5-14

Dow Mem: m=0, n=2, x=3.6-10

Figure 1.2 Structures of Nafion and other commercially available PFSA based polymers.

Nafion relies on water-assisted proton transport i.e. the proton transport in Nafion is not the intrinsic property of the polymer itself, but is mediated by water. Despite the fluorocarbon nature of the polymer backbone, Nafion adsorbs large amounts of water. Under fully hydrated conditions, Nafion exhibits a very high proton conductivity of 0.1 S cm^{-1}. The superior proton conductivity of Nafion has been the subject of much research.

The two most popular models describing the morphology of hydrated Nafion are the cluster-network model[11] and the parallel water-channel or inverted-micelle cylinder model.[13] Both these models suggest that the hydrated Nafion self-organize to provide an inverted micelle-like structure with the sulfonate groups organized around the water clusters, creating well-organized cylindrical water nanochannels through which the 'hydrated' protons can efficiently pass through. The self assembly of Nafion providing continuous nanoscale water channels in which proton transport can take place with

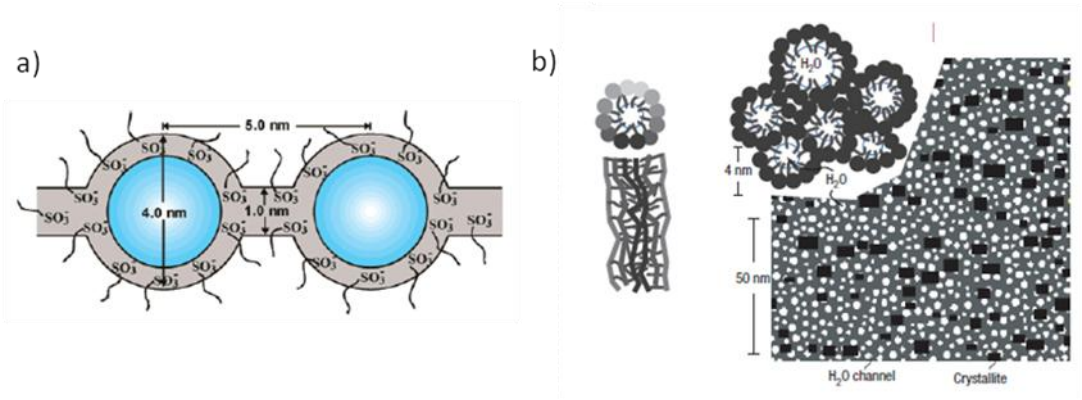

Figure 1.3 (a) Cluster-network model and (b) inverted micelle-cylinder model of hydrated Nafion (taken from references 11 and 13, respectively).

liquid-like dynamics is thought to be key for the observed superior proton transport properties of Nafion.

Despite several interesting features, Nafion suffers from two major limitations (i) high production cost; and (ii) low operational temperatures. The cost of the PEM constitutes roughly about 50% of the overall price of PEMFC, and hence is an important factor to consider. The perfluoroether comonomers employed in the synthesis of Nafion are expensive and add cost to the production of Nafion membranes. Moreover, the

handling of tetrafluorethylene in the synthesis of PFSA polymers raises safety concerns.[8] Hence, research efforts have been focused on developing alternate non-fluorinated hydrocarbon based sulfonic acid polymers. A number of partially fluorinated and fully hydrocarbon based sulfonic acid polymers have been reported.[8, 12, 14] The structures of some of these polymers are shown in Figure 1.4. Notable among these are the styrene-based polymers: BAM from Ballard Advanced Materials Corporation and styrene-ethylene-butylene-styrene (SEBS) polymer from Dais Analytic, and the poly(arylene ether) based sulfonated poly(arylene ether ether ketone) (SPEEK)[15], [16] and poly(arylene ether sulfone) (SPAES)[17, 18] polymers (Figure 1.4). Although some of the hydrocarbon

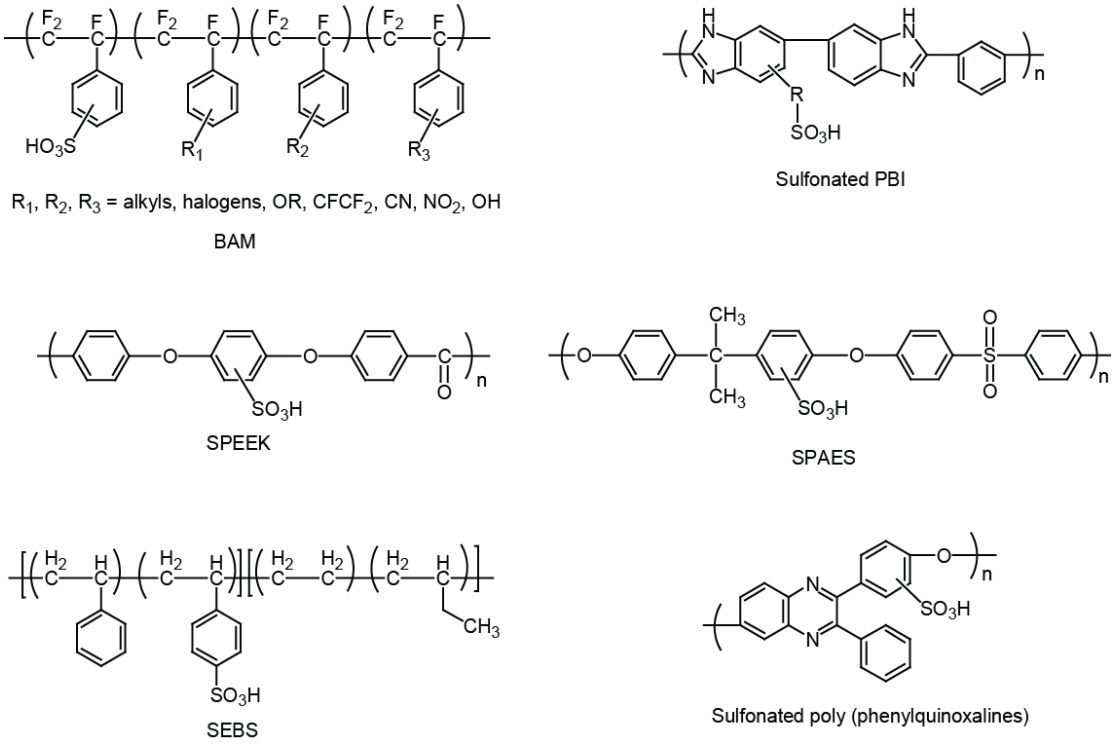

Figure 1.4 Structures of partially fluorinated and fully hydrocarbon sulfonic acid polymers.

based alternate polymers, especially SPEEK polymers, show great promise, the presence of hydrocarbon components would compromise their long term stability since the aliphatic -CH bonds are more prone to attack by radical species. Thus, there is still a need to find new polymers that could satisfactorily replace Nafion.

The other major limitation of Nafion is the low operational temperatures. As mentioned earlier, Nafion relies heavily on water for proton transport and hence the maximum operational temperatures are restricted to 80 ^{o}C since water evaporates above 100 ^{o}C. The low operational fuel cell temperatures have several disadvantages including sluggish reaction kinetics at the electrodes, reduced CO tolerance of Pt catalyst (for example the CO tolerance is reduced to 10-20 ppm at 80 ^{o}C compared to 1000 ppm at 130 ^{o}C)[14], need for ultra pure hydrogen due to the reduced CO tolerance, tedious water management (humidification must be carefully balanced to keep the polymer membrane from getting either flooded or dried),[19, 20] requirement for advanced cooling systems to maintain low operational temperatures, and poor heat recovery. To obviate these limitations, there is a need to operate fuel cells at temperatures of about 120-200 ^{o}C. Operation of fuel cells at high temperature will improve their overall efficiency as well as reduce their cost, thereby making the fuel cell technology economically viable and competitive with the existing internal combustion engine technology.

The proton conductivity of Nafion drops by about 3-4 orders of magnitude at higher temperatures, and the use of Nafion at high temperatures require tedious water management to keep the membrane fully hydrated which is practically very difficult, if not impossible.[20] Hence, there is a need for alternate proton transporting polymers that can withstand high operational temperatures and display the superior proton conductivity

and chemical robustness of Nafion. In order to reduce the dependence of proton conductivity of Nafion on water, efforts have been made to make composite membranes of Nafion by incorporating hygroscopic metal oxides such as SiO_2 and TiO_2.[21, 21]The hygroscopic metal oxides in composite membranes can hold on to water more tightly than the sulfonate groups in pristine Nafion, and hence allow for the operation of composite membranes at elevated temperatures with minimal water loss. Although there has been some success with the Nafion composite polymers, their use in actual fuel cell operating conditions has not been extensively investigated. Moreover, with the use of Nafion composite polymers in fuel cells, there will still be a need for water and heat management. Hence, the focus has been shifted to polymers which can conduct protons with minimal dependence on humidity or without the need for water - anhydrous proton transporting polymers.

1.2.2 Anhydrous Proton Conducting Polymers

As discussed in the previous section, there are several advantages to operating fuel cells at high temperatures (120-200 ^{o}C) such as the increased efficiency, increased tolerance of catalysts to high CO levels in hydrogen (1000 ppm at 130 ^{o}C and 30000 ppm at 200 ^{o}C compared to 20 ppm at 80 ^{o}C), opportunity to use reformate fuels instead of ultra pure hydrogen, reduced Pt loading on the electrodes due to enhanced redox kinetics at elevated temperatures, simplified water and heat management and hence reduced size of the fuel cell unit, significantly improved heat ejection contributing to the combined efficiency of the cell, and most importantly reduced cost.[14] While the proton conductivity of existing PFSA based polymers has already met the DOE target and is adequate for the

operation of PEMFC, their dependence on humidity and hence the need for complex water and heat management has severely hindered the advancement of PEMFC technology in terms of cell performance and cost reduction. Thus, there has been a high demand for developing anhydrous proton transporting polymers which can exhibit high proton conductivities over a wide range of temperatures (120-200 ^{o}C). Notable among the anhydrous proton transporting systems are the poly benzimidazole-phosphoric acid (PBI-PA) polymers and polymers based on *N*-heterocycles.

1.2.2.1 Polybenzimidazole-Phosphoric Acid (PBI-PA) Polymers

Phosphoric acid has a boiling point of 158 ^{o}C and it can also form extended intermolecular hydrogen bonding networks similar to that observed in water. In pure phosphoric acid, the proton transport is known to occur via Grotthuss mechanism i.e. the protons transfer through phosphate ions via structural diffusion. Unlike water, phosphoric acid has more proton donor sites than acceptors and hence exhibits high self-dissociation. In addition, the resulting phosphate ions have low diffusion coefficients. The high self-dissociation and low diffusion coefficients of phosphate ions make phosphoric acid a suitable candidate for Grotthuss proton transport.[22] Thus, blends of phosphoric acid with basic polymers such as polybenzimidazole (PBI), polyethylene oxide (PEO), and polyvinyl alcohol (PVA) have been explored. A number of polymer-phosphoric acid blends such as PEO-H_3PO_4,[23] PVA-H_3PO_4,[24] and PBI- H_3PO_4[25-27] have been studied. Among these, PBI-PA polymers are the most promising candidates with the best proton conductivities of 10^{-3}-10^{-2} S cm^{-1} from room temperature to 190 ^{o}C under anhydrous conditions. They also exhibit good mechanical properties over the temperature range of

20-220 ^{o}C as well as good thermal stability.[26] The presence of water is known to further enhance their proton conductivity and efforts are underway for the commercialization of these polymers.

Although PBI-PA polymers do satisfy the requirements for high temperature operation, they still suffer from several limitations. Some of them include (i) loss of phosphoric acid over time due to diffusion and evaporation;[27] this leads to performance loss and necessitates the use of an acid management system, (ii) cross-over of phosphoric acid to the cathode side, resulting in mixed potential,[27] (iii) condensation of phosphoric acid at high temperatures due to dehydration, and (iv) difficulty in fabricating membranes due to poor solubility. Currently, modifications to PBI polymers are being pursued to improve their processibility.[28, 29] Due to acid leaching and the condensation of PA at high temperatures, PBI-PA polymers are mainly targeted for use in fuel cells for stationery power generation where the operational temperatures can be easily regulated.

1.2.2.2 Polymers Based of *N*-heterocycles

In the case of both PFSA based polymers such as Nafion and PBI-PA polymers, the proton transport is not an inherent property of the polymer itself but of the dopant - water or H_3PO_4. Thus, these polymers provide limited opportunity to modulate the proton conductivity. There has been growing interest in developing polymers with proton conductivity as an intrinsic feature of the polymer. Although water is ubiquitous in life forms, anhydrous proton conduction pathways are also quite frequently found in Nature's PT systems.[30, 31] Histidine, an imidazole-based amino acid, has the unique ability to be present both as a proton donor (imidazolium cation, p*K*a = 6.95) and an acceptor

(imidazole) at physiological conditions (pH = 7.4) and is one of the widely exploited residues for PT in proteins.[32, 33] Inspired by Nature, *N*-heterocycles such as imidazole, triazole, and benzimidazole have been extensively employed to develop polymers for anhydrous proton transport.[34-42]

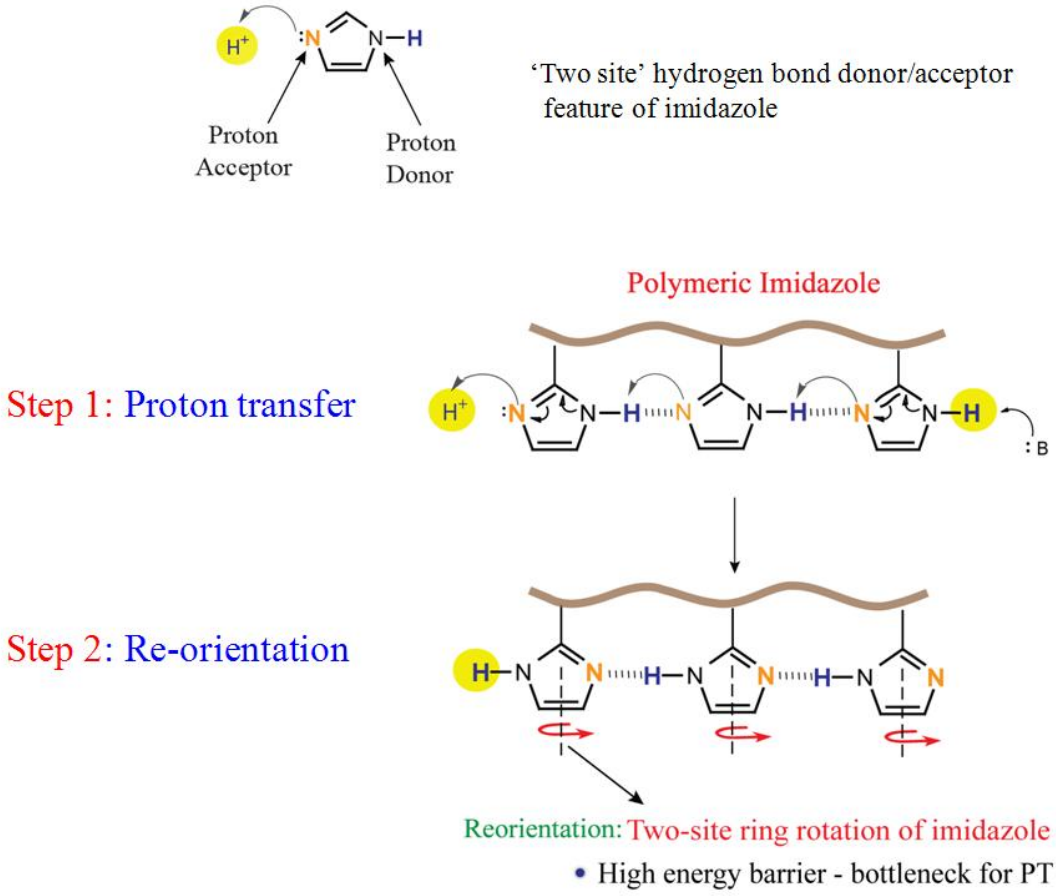

Figure 1.5 Illustration of the Grotthuss proton transfer processes in polymeric imidazole.

N-heterocycles, for example imidazole, are amphoteric in nature i.e. they can act both as proton donors and acceptors. Due to the amphoteric nature, imidazoles can interact with each other via intermolecular hydrogen bonding forming extended hydrogen bond

networks similar to that observed in water and phosphoric acid. In addition, imidazole also exhibits high proton conductivities of 10^{-2} S cm^{-1} in the molten state.[43, 36, 22] All these features make heterocycles ideal candidates for Grotthuss proton transport. Kreuer was the first to propose the use of heterocycles for anhydrous proton transport.[36] The Grotthuss proton transfer in imidazole is illustrated in Figure 1.5. Imidazole and imidazolium salts were used as proton dopants to replace water in Nafion. Although conductivities on the order of 10^{-3}-10^{-2} S cm^{-1} were achieved up to 200 ^{o}C, the small molecule heterocycles were found to leach out of the polymers at high temperatures resulting in a gradual decrease in proton conductivity.[44]

In contrast to water, *N*-heterocycles can be covalently attached to a polymer backbone. Thus, to avoid leaching, immobilization of heterocycles onto polymers has been proposed.[40] In the case of *N*-heterocyclic polymers, since the diffusion of heterocycles is restricted, the proton conduction happens predominantly via Grotthuss mechanism (Figure 1.5).[9, 2] Grotthuss mechanism of proton transfer involves two steps: (i) inter-functional group proton transfer across the scaffold and (ii) reorientation of the scaffold for subsequent PT. The reorientation step involves the reorganization or flipping of the PT moieties and is recognized to be the rate limiting step for proton transfer in *N*-heterocyclic polymers.[45-47]

A number of polymers based on *N*-heterocycles have been studied for anhydrous proton transport.[34-42, 48-50] The structures of some of these polymers are shown in Figure 1.6. The bulk proton conductivity of polymers can be described by Equation 1.1, where n

$$\sigma = n\mu q \qquad (1.1)$$

is the number of charge carriers (charge carrier density), μ is the mobility of the protons, and q is the charge of the proton. The proton conductivity of polymers is known to be influenced by several factors such as the nature of heterocycle, glass transition temperature (T_g) of the polymer, polymer architecture, and the proton charge carrier density. This thesis mainly focuses on two aspects (i) to gain a fundamental understanding of the proton transport mechanism in heterocycle polymers, in particular polymers based on 1*H*-1,2,3-triazole and (ii) to rationally design new proton transporting functional groups to address the limitations imposed by the 'two-site' hydrogen bond donor/acceptor feature of heterocycles on proton transport. In line with the focus of this thesis, the rest of the discussion will be focused on highlighting the effect of the above mentioned factors on proton conductivity of heterocyclic polymers, rather than providing a comprehensive overview of the entire *N*-heterocyclic proton conducting polymers reported till date.

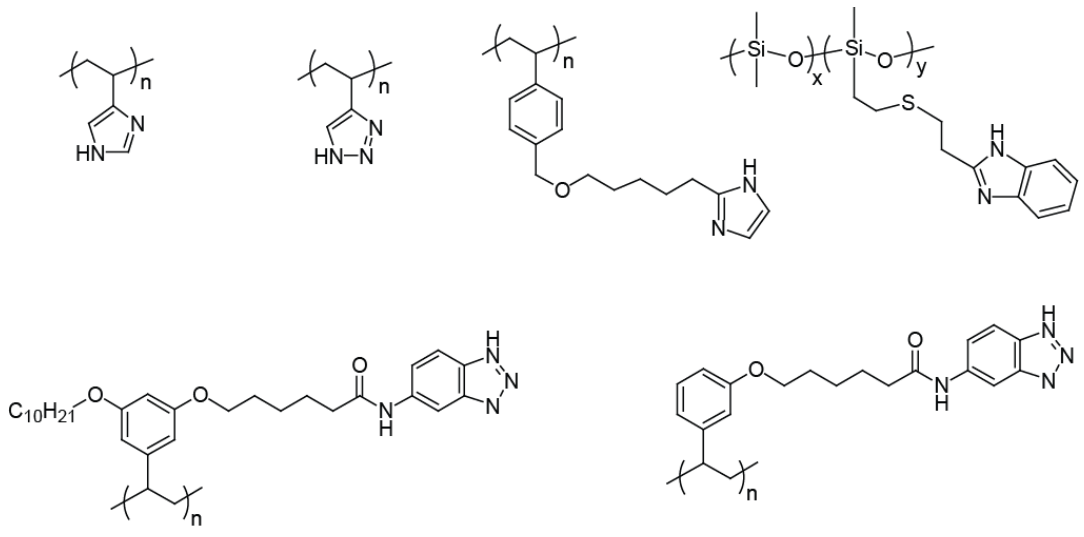

Figure 1.6 Structures of *N*-heterocyclic proton transporting polymers.

1.2.2.2.1 Effect of the Nature of Heterocycle

As mentioned earlier, *N*-heterocyclic polymers conduct protons via Grotthuss mechanism, and the reorientation step has been established to be the rate-determining step for PT. In *N*-heterocycles (eg. imidazole), one nitrogen atom accepts a proton while the other nitrogen donates a proton. This 'two-site' feature would necessitate the rotation of the entire heterocycle during reorientation (Figure 1.6). When heterocycles are immobilized onto a polymer, the reorientation step requires the concerted rotation of all the imidazole units involved for the subsequent proton transfer to happen in the same direction. This concerted 'two-site' ring rotation of imidazole units would in turn impose significant neighboring molecule rearrangements and hence is energetically demanding.[2, 51] Thus, while immobilizing heterocycles onto polymers, care must be exercised to warrant facile reorientational dynamics.

The existence of multiple tautomers is expected to assist the reorientation step in the Grotthuss mechanism of proton transfer, while the interconversion among the tautomers would facilitate the proton transfer dynamics. It has been reported that the proton conductivity of poly(4-vinyl-1*H*-1,2,3-triazole) is 10^5 times higher than that of poly(4-vinyl-imidazole) over the entire temperature range of 50-150 ^{o}C.[52] Unlike imidazole, 1*H*-1,2,3-triazole has an additional 2*H*-1,2,3 triazole tautomer and it has been speculated that the presence of the 2*H*-1,2,3 triazole tautomer in triazole would promote intramolecular proton transfer, thereby facilitating reorientational dynamics and long-range proton transport. However, there have also been reports where similar or even slightly higher proton conductivities were observed for imidazole polymers compared to triazole when they are tethered to siloxane backbones via flexible spacers.[34] Thus the enhancement in

conductivity from imidazole to triazole does not appear to be universal. These contrary observations clearly highlight the need to allow for the local mobility of heterocycles in polymers to form dynamical hydrogen bonds. These results also suggest that it is difficult to deconvolute the effect of individual factors on proton conductivity. An effort has been made by us to study the effect of the heterocycle on proton conductivity by keeping all the possible variations with respect to polymer architecture, molecular weight, T_g, and charge carrier density to a minimum and it is discussed in Chapter 2.[53]

1.2.2.2.2 Effect of T_g and Charge Carrier Density

The glass transition temperature (T_g) of polymers influences the flexibility of the polymer side chains, which in turn will influence the local mobility and reorientational dynamics of heterocycles. To investigate the effect of T_g on proton conductivity, several polymers based on benzimidazole and triazole have been studied. Polysiloxanes grafted with varying mol% of benzimidazole units have been studied by Persson and Jannasch.[39] The charge carrier density and T_g were found to act in opposition to each other. Low benzimidazole content resulted in lower T_g values and enhanced proton conductivities at lower temperatures due to higher segmental mobility. However, the conductivities at high temperatures were low due to the reduced benzimidazole concentration. Similarly, while the polymers with high benzimidazole content displayed increased high temperature conductivity, the low temperature conductivity was compromised due to the subsequent increase in T_g accompanied with the increased benzimidazole content.

Polyacrylates with a systematic increase in the number of 1*H*-1,2,3-triazole units were studied to investigate the effect of charge carrier density on proton conductivity.[54]

The increase in the number of triazole units per repeat unit (charge carrier density) did not result in enhanced proton conductivity as there was an accompanying increase in T_g, which severely restricts the mobility and reorientational dynamics of heterocycles. Thus, T_g and charge carrier density are the two competing factors influencing the proton conductivity. While the effect of T_g is more pronounced at low temperatures, the charge carrier density takes over at higher temperatures.

1.2.2.2.3 Effect of Polymer Architecture

While variations in the polymer backbone (eg. polystyrene, polyacrylate, polysiloxane, etc.) and flexibility of the spacer tethering *N*-heterocycles to the polymer backbone do affect proton conductivity, supramolecular organization of PT functionalities is yet another key factor that can significantly influence the macroscopic proton transport in polymers. In the case of Nafion,[13, 55, 56] sulfonated block copolymers,[8, 57-64] and lithium ion transporting ionic liquid block copolymers,[65-67] the role of the self-assembly of polymers providing well-defined nanoscale ion conducting pathways on macroscopic proton conductivity has been well studied. In a recent study, similar observations were made for anhydrous proton transport in styrene-based facially amphiphilic comb polymers.[49] Imidazole and benzotriazole polymers that can self-assemble to provide organized supramolecular assemblies were observed to provide 2-3 orders of magnitude enhancement in proton conductivity compared to the analogous polymers which lack the ability to self-assemble. Thus, proton conductivity of polymers is a bulk property that is influenced by several factors and the design and development of

polymers with a delicate balance among various synergistic and competing factors to provide appreciable proton conductivities is a challenging task.

1.3 Summary

PT is a chemical process that plays a crucial role in biology as well as in materials used for generating electricity in an environmentally friendly way, for example hydrogen fuel cells. A brief overview of how fuel cells function and various types of fuel cells are presented. PEMFCs are discussed in detail, with a special focus on proton transporting polymers. The interesting features as well as the limitations of the state-of-the art PFSA based polymers, particularly Nafion, are discussed in the context of proton transport. The most promising PBI-PA based anhydrous proton transporting polymers for applications in high temperature fuel cells have also been discussed. Their limitations are also pointed out to hint that there is still room for further improvement. In the final section, a detailed discussion about anhydrous proton transporting *N*-heterocyclic polymers with an insight into the effect of various factors on proton transport is presented. *N*-heterocyclic polymers are still in the development stage and their use in actual fuel cells is yet to be demonstrated.

1.4 Outline of the Dissertation

In this thesis, the proton transporting characteristics of polymers functionalized with two diverse classes of functional groups - *N*-heterocycles and phenols have been investigated. In Chapter 2, structurally analogous polymers based on *N*-heterocycles (triazole, imidazole, and pyrazole) and benz- *N*-heterocycles (benzotriazole, benzimidazole, and benzopyrazole) are employed to probe the most probable proton

conduction pathway in 1*H*-1,2,3-triazole polymers. Since polymers were assembled modularly to minimize the variations in terms of polymer architecture, T_g, and charge carrier density, the same polymer platform has also been useful to probe the effect of the nature of the heterocycle on proton conductivity. Chapter 3 introduces a new class of functional groups, phenols, for anhydrous proton transport. One of the highlighting features of phenols over *N*-heterocycles is that the hydrogen bond donor/acceptor reorientation can happen on a single -OH site, allowing for facile reorientational dynamics in Grotthuss proton transport. The proton transport characteristics of a series of styrene-based phenolic polymers with varying number of -OH moieties are studied. The effect of the 'single-site' hydrogen bond donor/acceptor feature of phenols on reorientational dynamics and proton transport is probed both theoretically and experimentally. In Chapter 4, the proton transfer characteristics of phenolic biaryl polymers in which the -OH moieties are presented in orthogonal planes are studied and compared with the analogous one-dimensional linear phenolic styrene polymers. Finally, in Chapter 5, the synthetic route allowing facile access to poly (styrene-b-3,4-dihydroxy styrene) block copolymers is outlined. These block copolymers would allow for systematically investigating the effect of nanoscale morphology on proton transport in anhydrous systems.

1.5 References

1. Williams, R. J. P., Proton circuits in biological energy interconversions. *Annual Review of Biophysics and Biophysical Chemistry* **1988**, *17*, 71-97.

2. Kreuer, K. D., Proton conductivity: Materials and applications. *Chem. Mat.* **1996**, *8*, 610-641.

3. Winter, M.; Brodd, R. J., What are batteries, fuel cells, and supercapacitors? *Chem. Rev.* **2004**, *104*, 4245-4269.

4. Carrette, L.; Friedrich, K. A.; Stimming, U., Fuel cells - fundamentals and applications. *Fuel Cells* **2001**, *1*, 5-39.

5. Whittingham, M. S.; Savinell, R. F.; Zawodzinski, T., Introduction: Batteries and fuel cells. *Chem. Rev.* **2004**, *104*, 4243-4244.

6. Costamagna, P.; Srinivasan, S., Quantum jumps in the PEMFC science and technology from the 1960s to the year 2000 Part I. Fundamental scientific aspects. *J. Power Sources* **2001**, *102*, 242-252.

7. Wycisk, R.; Chisholm, J.; Lee, J.; Lin, J.; Pintauro, P. N., Direct methanol fuel cell membranes from Nafion-polybenzimidazole blends. *J. Power Sources* **2006**, *163*, 9-17.

8. Hickner, M. A.; Ghassemi, H.; Kim, Y. S.; Einsla, B. R.; McGrath, J. E., Alternative polymer systems for proton exchange membranes (PEMs). *Chem. Rev.* **2004**, *104*, 4587-4611.

9. Agmon, N., The Grotthuss mechanism. *Chem. Phys. Lett.* **1995**, *244*, 456-462.

10. Steele, B. C. H.; Heinzel, A., Materials for fuel-cell technologies. *Nature* **2001**, *414*, 345-352.

11. Mauritz, K. A.; Moore, R. B., State of understanding of Nafion. *Chem. Rev.* **2004**, *104*, 4535-4585.

12. Rikukawa, M.; Sanui, K., Proton-conducting polymer electrolyte membranes based on hydrocarbon polymers. *Prog. Polym. Sci.* **2000**, *25*, 1463-1502.

13. Schmidt-Rohr, K.; Chen, Q., Parallel cylindrical water nanochannels in Nafion fuel-cell membranes. *Nat. Mater.* **2008**, *7*, 75-83.

14. Li, Q. F.; He, R. H.; Jensen, J. O.; Bjerrum, N. J., Approaches and recent development of polymer electrolyte membranes for fuel cells operating above 100 degrees C. *Chem. Mat.* **2003**, *15*, 4896-4915.

15. Bae, J. M.; Honma, I.; Murata, M.; Yamamoto, T.; Rikukawa, M.; Ogata, N., Properties of selected sulfonated polymers as proton-conducting electrolytes for polymer electrolyte fuel cells. *Solid State Ionics* **2002**, *147*, 189-194.

16. Li, X. F.; Na, H.; Lu, H., Novel sulfonated poly(ether ether ketone ketone) derived from bisphenol S. *J. Appl. Polym. Sci.* **2004**, *94*, 1569-1574.

17. Summer, M. J.; Harrison, W. L.; Weyers, R. M.; Kim, Y. S.; McGrath, J. E.; Riffle, J. S.; Brink, A.; Brink, M. H., Novel proton conducting sulfonated poly(arylene ether) copolymers containing aromatic nitriles. *J. Membr. Sci.* **2004**, *239*, 199-211.

18. Shin, C. K.; Maier, G.; Scherer, G. G., Acid functionalized poly(arylene ether)s for proton-conducting membranes. *J. Membr. Sci.* **2004**, *245*, 163-173.

19. Chen, C.; Fuller, T. F., The effect of humidity on the degradation of Nafion (R) membrane. *Polym. Degrad. Stabil.* **2009**, *94*, 1436-1447.

20. Pozio, A.; Cemmi, A.; Mura, F.; Masci, A.; Serra, E.; Silva, R. F., Long-term durability study of perfluoropolymer membranes in low humidification conditions. *J. Solid State Electrochem.* **2011**, *15*, 1209-1216.

21. Baradie, B.; Dodelet, J. P.; Guay, D., Hybrid Nafion (R)-inorganic membrane with potential applications for polymer electrolyte fuel cells. *J. Electroanal. Chem.* **2000**, *489*, 101-105.

22. Kreuer, K. D.; Paddison, S. J.; Spohr, E.; Schuster, M., Transport in proton conductors for fuel-cell applications: Simulations, elementary reactions, and phenomenology. *Chem. Rev.* **2004**, *104*, 4637-4678.

23. Donoso, P.; Gorecki, W.; Berthier, C.; Defendini, F.; Poinsignon, C.; Armand, M. B., NMR, conductivity and neutron scattering investigation of ionic dynamics in the anhydrous polymer protonic conductor PEO(H3PO4)X *Solid State Ionics* **1988**, *28*, 969-974.

24. Pettyweeks, S.; Zupancic, J. J.; Swedo, J. R., Proton conducting interpenetrating polymer networks. *Solid State Ionics* **1988**, *31*, 117-125.

25. Mader, J. A.; Benicewicz, B. C., Synthesis and Properties of Segmented Block Copolymers of Functionalised Polybenzimidazoles for High-Temperature PEM Fuel Cells. *Fuel Cells* **2011**, *11*, 222-237.

26. Yu, S.; Xiao, L.; Benicewicz, B. C., Durability studies of PBI-based high temperature PEMFCs. *Fuel Cells* **2008**, *8*, 165-174.

27. Jayakody, J. R. P.; Chung, S. H.; Durantino, L.; Zhang, H.; Xiao, L.; Benicewicz, B. C.; Greenbaum, S. G., NMR studies of mass transport in high-acid-content fuel cell membranes based on phosphoric acid and polybenzimidazole. *J. Electrochem. Soc.* **2007**, *154*, B242-B246.

28. Berrada, M.; Anbaoui, Z.; Lajrhed, N.; Knouzi, N.; Vaultier, M.; Sekiguchi, H.; Carriere, F., Synthesis, characterization, and studies of heat-resistant poly(ether benzimidazole)s. *Chem. Mat.* **1997**, *9*, 1989-1993.

29. Berrada, M.; Carriere, F.; Abboud, Y.; Abourriche, A.; Benamara, A.; Lajrhed, N.; Kabbaj, M., Preparation and characterization of new soluble benzimidazole-imide copolymers. *J. Mater. Chem.* **2002**, *12*, 3551-3559.

30. Schnell, J. R.; Chou, J. J., Structure and mechanism of the M2 proton channel of influenza A virus. *Nature* **2008**, *451*, 591-U512.

31. Khurana, E.; Dal Peraro, M.; DeVane, R.; Vemparala, S.; DeGrado, W. F.; Klein, M. L., Molecular dynamics calculations suggest a conduction mechanism for the M2 proton channel from influenza A virus. *Proc. Natl. Acad. Sci. U. S. A.* **2009**, *106*, 1069-1074.

32. Silverman, D. N.; Lindskog, S., The catalytic mechanism of carboinc-anhydrase - Implications of rate-limiting protolysis of water. *Accounts Chem. Res.* **1988**, *21*, 30-36.

33. Lesburg, C. A.; Christianson, D. W., X-ray crystallographic studies of engineered hydrogen-bond networks in a protein-zinc binding site. *J. Am. Chem. Soc.* **1995**, *117*, 6838-6844.

34. Granados-Focil, S.; Woudenberg, R. C.; Yavuzcetin, O.; Tuominen, M. T.; Coughlin, E. B., Water-free proton-conducting polysiloxanes: A study on the effect of heterocycle structure. *Macromolecules* **2007**, *40*, 8708-8713.

35. Herz, H. G.; Kreuer, K. D.; Maier, J.; Scharfenberger, G.; Schuster, M. F. H.; Meyer, W. H., New fully polymeric proton solvents with high proton mobility. *Electrochim. Acta* **2003**, *48*, 2165-2171.

36. Kreuer, K. D.; Fuchs, A.; Ise, M.; Spaeth, M.; Maier, J., Imidazole and pyrazole-based proton conducting polymers and liquids. *Electrochim. Acta* **1998**, *43*, 1281-1288.

37. Narayanan, S. R.; Yen, S. P.; Liu, L.; Greenbaum, S. G., Anhydrous proton-conducting polymeric electrolytes for fuel cells. *J. Phys. Chem. B* **2006**, *110*, 3942-3948.

38. Persson, J. C.; Jannasch, P., Block copolymers containing intrinsically proton-conducting blocks tethered with benzimidazole units. *Chem. Mat.* **2006**, *18*, 3096-3102.

39. Persson, J. C.; Jannasch, P., Intrinsically proton-conducting benzimidazole units tethered to polysiloxanes. *Macromolecules* **2005**, *38*, 3283-3289.

40. Schuster, M. E.; Meyer, W. H., Anhydrous proton-conducting polymers. *Ann. Rev. Mater. Res.* **2003**, *33*, 233-261.

41. Schuster, M. F. H.; Meyer, W. H.; Schuster, M.; Kreuer, K. D., Toward a new type of anhydrous organic proton conductor based on immobilized imidazole. *Chem. Mat.* **2004**, *16*, 329-337.

42. Woudenberg, R. C.; Yavuzeetin, O.; Tuominen, M. T.; Coughlin, E. B., Intrinsically proton conducting polymers and copolymers containing benzimidazole moieties: Glass transition effects. *Solid State Ionics* **2007**, *178*, 1135-1141.

43. Kawada, A.; McGhie, A. R.; Labes, M. M., Protonic conductivity in imidazole single crystal. *J. Chem. Phys.* **1970**, *52*, 3121-3125.

44. Sun, J. Z.; Jordan, L. R.; Forsyth, M.; MacFarlane, D. R., Acid-organic base swollen polymer membranes. *Electrochim. Acta* **2001**, *46*, 1703-1708.

45. Bredas, J. L.; Poskin, M. P.; Delhalle, J.; Andre, J. M.; Chojnacki, H., Electronic-structure of hydrogen-bonded imidazole chains - Influence of the proton position *J. Phys. Chem.* **1984**, *88*, 5882-5887.

46. Daycock, J. T.; Jones, G. P.; Evans, J. R. N.; Thomas, J. M., Rotation of imidazole in solid state and its significance in deciding nature of charge migration in biological materials. *Nature* **1968**, *218*, 672-673.

47. Munch, W.; Kreuer, K. D.; Silvestri, W.; Maier, J.; Seifert, G., The diffusion mechanism of an excess proton in imidazole molecule chains: first results of an ab initio molecular dynamics study. *Solid State Ionics* **2001**, *145*, 437-443.

48. Celik, S. U.; Bozkurt, A., Proton conduction promoted by 1H-1,2,3-benzotriazole in non-humidified polymer membranes. *Electrochim. Acta* **2011**, *56*, 5961-5965.

49. Chen, Y. B.; Thorn, M.; Christensen, S.; Versek, C.; Poe, A.; Hayward, R. C.; Tuominen, M. T.; Thayumanavan, S., Enhancement of anhydrous proton transport by supramolecular nanochannels in comb polymers. *Nat. Chem.* **2010**, *2*, 503-508.

50. Wang, J. T. W. W. J. T. W.; Hsu, S. L. C., Enhanced high-temperature polymer electrolyte membrane for fuel cells based on polybenzimidazole and ionic liquids. *Electrochim. Acta* **2011**, *56*, 2842-2846.

51. Goward, G. R.; Schuster, M. F. H.; Sebastiani, D.; Schnell, I.; Spiess, H. W., High-resolution solid-state NMR studies of imidazole-based proton conductors: Structure motifs and chemical exchange from H-1 NMR. *J. Phys. Chem. B* **2002**, *106*, 9322-9334.

52. Zhou, Z.; Li, S. W.; Zhang, Y. L.; Liu, M. L.; Li, W., Promotion of proton conduction in polymer electrolyte membranes by 1H-1,2,3-triazole. *J. Am. Chem. Soc.* **2005**, *127*, 10824-10825.

53. Nagamani, C.; Versek, C.; Thorn, M.; Tuominen, M. T.; Thayumanavan, S., Proton Conduction in 1H-1,2,3-triazole Polymers: Imidazole-Like or Pyrazole-Like? *J. Polym. Sci. Pol. Chem.* **2010**, *48*, 1851-1858.

54. Martwiset, S.; Yavuzcetin, O.; Thorn, M.; Versek, C.; Tuominen, M.; Coughlin, E. B., Proton Conducting Polymers Containing 1H-1,2,3-Triazole Moieties. *J. Polym. Sci. Pol. Chem.* **2009**, *47*, 188-196.

55. Diat, O.; Gebel, G., Proton channels. *Nat. Mater.* **2008**, *7*, 13-14.

56. Elliott, J. A.; Hanna, S.; Elliott, A. M. S.; Cooley, G. E., Interpretation of the small-angle X-ray scattering from swollen and oriented perfluorinated ionomer membranes. *Macromolecules* **2000**, *33*, 4161-4171.

57. Bae, B.; Yoda, T.; Miyatake, K.; Uchida, H.; Watanabe, M., Proton-Conductive Aromatic Ionomers Containing Highly Sulfonated Blocks for High-Temperature-Operable Fuel Cells. *Angew. Chem.-Int. Edit.* **2010**, *49*, 317-320.

58. Elabd, Y. A.; Hickner, M. A., Block Copolymers for Fuel Cells. *Macromolecules* **2011**, *44*, 1-11.

59. Kishimoto, K.; Suzawa, T.; Yokota, T.; Mukai, T.; Ohno, H.; Kato, T., Nano-segregated polymeric film exhibiting high ionic conductivities. *J. Am. Chem. Soc.* **2005**, *127*, 15618-15623.

60. Lee, H. C.; Lim, H.; Su, W. F.; Chao, C. Y., Novel Sulfonated Block Copolymer Containing Pendant Alkylsulfonic Acids: Syntheses, Unique Morphologies, and Applications in Proton Exchange Membrane. *J. Polym. Sci. Pol. Chem.* **2011**, *49*, 2325-2338.

61. Rubatat, L.; Shi, Z. Q.; Diat, O.; Holdcroft, S.; Frisken, B. J., Structural study of proton-conducting fluorous block copolymer membranes. *Macromolecules* **2006**, *39*, 720-730.

62. Sodeye, A. I. I.; Huang, T.; Gido, S. P.; Mays, J. W., Polymer electrolyte membranes from fluorinated polyisoprene-block-sulfonated polystyrene: Membrane structure and transport properties. *Polymer* **2011**, *52*, 1963-1970.

63. Takamuku, S.; Jannasch, P., Fully Aromatic Block Copolymers for Fuel Cell Membranes with Densely Sulfonated Nanophase Domains. *Macromol. Rapid Commun.* **2011**, *32*, 474-480.

64. Won, J.; Park, H. H.; Kim, Y. J.; Choi, S. W.; Ha, H. Y.; Oh, I. H.; Kim, H. S.; Kang, Y. S.; Ihn, K. J., Fixation of nanosized proton transport channels in membranes. *Macromolecules* **2003**, *36*, 3228-3234.

65. Cho, B. K.; Jain, A.; Gruner, S. M.; Wiesner, U., Mesophase structure-mechanical and ionic transport correlations in extended amphiphilic dendrons. *Science* **2004**, *305*, 1598-1601.

66. Wanakule, N. S.; Panday, A.; Mullin, S. A.; Gann, E.; Hexemer, A.; Balsara, N. P., Ionic Conductivity of Block Copolymer Electrolytes in the Vicinity of Order-Disorder and Order-Order Transitions. *Macromolecules* **2009**, *42*, 5642-5651.

67. Weber, R. L.; Ye, Y. S.; Schmitt, A. L.; Banik, S. M.; Elabd, Y. A.; Mahanthappa, M. K., Effect of Nanoscale Morphology on the Conductivity of Polymerized Ionic Liquid Block Copolymers. *Macromolecules* **2011**, *44*, 5727-5735.

CHAPTER 2

PROTON CONDUCTION IN 1*H*-1,2,3-TRIAZOLE POLYMERS: IMIDAZOLE-LIKE OR PYRAZOLE-LIKE?

2.1 Introduction

N-heterocyclic polymers based on imidazole, benzimidazole and triazole have been studied extensively for applications in anhydrous proton transport (PT) materials.[1-10] Several polymers exhibiting moderate to appreciable conductivities have been developed. However, the current understanding of the functional group requirements and the mechanistic aspects of PT is limited. Gaining insights into functional group requirements for PT would provide the necessary design guidelines to rationally tailor new PT materials with enhanced proton conduction. In this Chapter, we outline our efforts to understand the most probable proton conduction pathway in 1*H*-1,2,3-triazole systems.

N-heterocyclic polymers conduct protons via Grotthuss mechanism, which involves two steps: (*i*) intermolecular proton transfer across the scaffold and (*ii*) reorientation of the scaffold for subsequent PT. The reorientation step involves reorganization or flipping of the PT moieties and is recognized to be the rate limiting step for proton transfer in *N*-heterocyclic polymers.[11-13] Triazole-based systems have been reported to provide an advantage in proton transfer.[14] This is attributed to the presence of multiple tautomers for triazole, which would reduce the number of conformational changes required during the reorientation step. Triazole can be viewed as a scaffold that can simultaneously provide PT pathways both in the imidazole and the pyrazole modes (Figure 2.1). Proton transfer barriers for short range proton conduction in 1,2,3-triazole systems have been computed

theoretically and it is reported that proton transfer is equally feasible in both imidazole-like and pyrazole-like dimers of triazole.[15] Thus, theoretically triazole can utilize both imidazole-like and pyrazole-like pathways to conduct protons. Furthermore, the activation energies for the tautomerization in 1,2,3-triazole, imidazole and pyrazole are known to be similar, and are about 50 kcal/mol.[16-18]

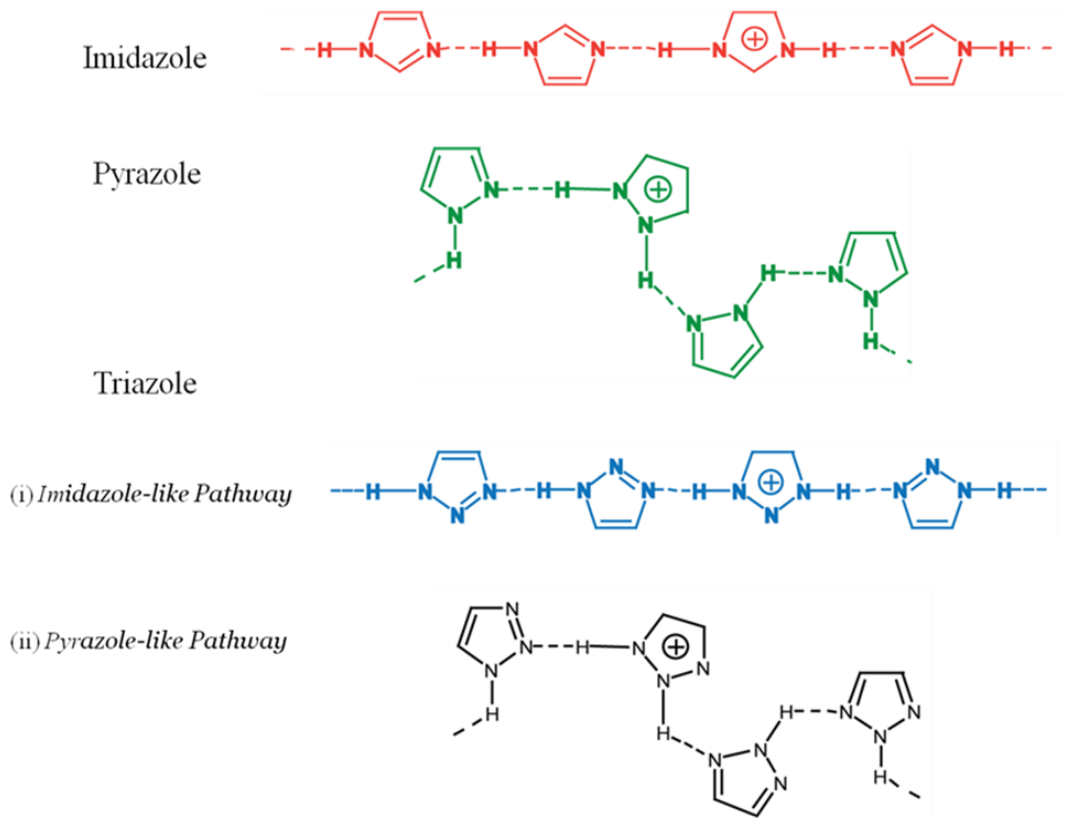

Figure 2.1 Illustration of the proton conduction pathways in 1,2,3-triazole.

Prompted by the above observations and considering that triazole resembles the imidazole-pyrazole couple, it is fundamentally interesting to ask: does the triazole have both imidazole-like and pyrazole-like pathways equally accessible experimentally for proton conduction? Probing this question might provide insights into the mechanistic

details of PT and help understand why certain functional groups provide facile proton transport while others do not. We do recognize that most of the theoretical studies investigating proton transfer processes in heterocycles are based on small molecules and hence consider very limited number of interactions among the PT functionalities.[11-13,15, 19-20] However, in a polymeric system each of the PT moieties will be surrounded by multiple neighboring molecules and hence involve complex interactions. Thus, the low barriers observed for short range proton transfer in small molecules may or may not translate into fast proton transfer dynamics in a polymeric system. Nonetheless, polymeric systems are closer to the practical systems for PT applications. Hence, it is imperative to systematically investigate the structural details of PT in polymeric systems.

2.2 Results and Discussion

2.2.1 Molecular Design

To discern the predominant proton conducting pathway in triazole, we chose to study the proton transfer characteristics of 1*H*-benzotriazole based polymer in comparison with that of 1*H*-benzimidazole and 1*H*-benzopyrazole systems. Besides providing a systematic comparison, these systems are also interesting, because: (*i*) though benzimidazole based polymers have been explored,[7,10, 21-23] benzotriazole and benzopyrazole polymers are unexplored for PT applications, and (*ii*) we would be able to investigate if the benzene ring in benz-*N*-heterocycles provides any advantages over the corresponding *N*-heterocyclic molecules towards proton conductivity. It is possible that the benzene ring might contribute towards stabilizing the existing tautomers by delocalization of the positive charge of the protonated azolium cations on to the ring or open room for new

tautomers, thereby facilitating the proton transfer dynamics. Finally, though a number of polymers based on heterocycles have been studied by several groups, the diversity in the polymeric architecture itself has been an impediment in the systematic comparison of the effect of the nature of heterocycle on proton conductivity.[1-10, 21-23] Thus, we adopted a modular approach to synthesize the polymers, which would not only allow for rapid assembly of the polymers, but also would eliminate possible variations with respect to the polymeric architecture, molecular weights, and polydispersity (PDI). In this report, we reveal our findings regarding the proton conducting behavior of 1*H*-benzotriazole based polymer in comparison to that of 1*H*-benzimidazole and 1*H*-benzopyrazole systems and thereby shed light on which pathway (imidazole-like or pyrazole-like) is more accessible to triazole systems experimentally to shuttle protons in a polymeric scaffold.[24] The structures of the proton conducting polymers used in this study are shown in Chart 2.1.

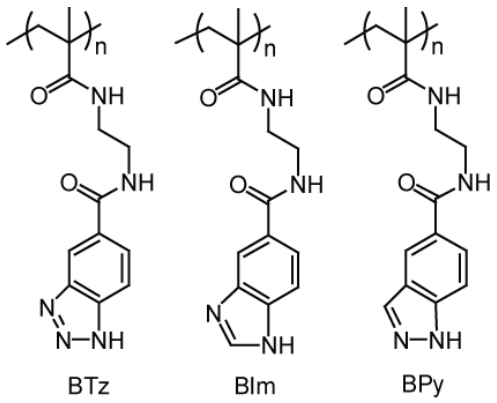

Chart 2.1 Structures of proton conducting polymers based on benz-*N*-heterocycles.

2.2.2 Synthesis and Characterization

As mentioned earlier, we adopted a modular approach to assemble proton conducting polymers in order to eliminate the inherent heterogenieties of polymers. Polymers based on active ester functionalities have been widely employed to generate new polymers by post-polymerization modification.[25-27] We made use of *N*-hydroxysuccinimide methacrylate (NHSMA) polymer (**5)** as the parent polymer. *N*-hydroxysuccinimidyl ester is an activated ester and has been widely exploited as a handle to install various functionalities with high fidelity. NHSMA **4** was polymerized using ATRP,[28-30] a well known controlled radical polymerization technique. Ethyl-2-bromo isobutyrate (EBiB) was used as an initiator. Polymer **5** was obtained with a narrow polydispersity of 1.26 and molecular weight of 11 kg/mol.

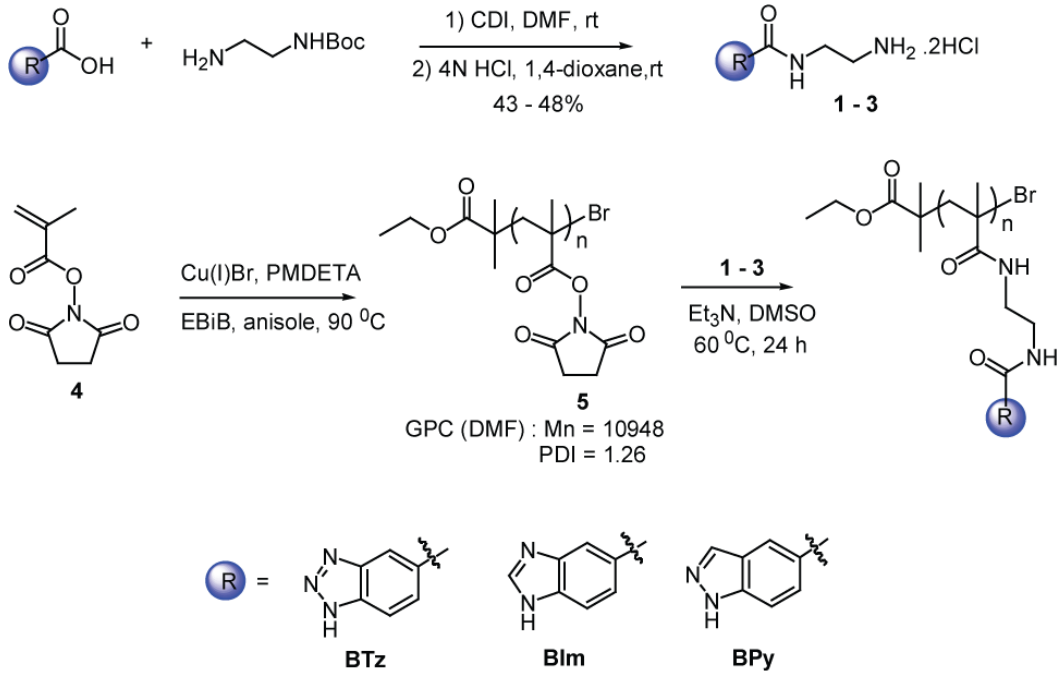

Scheme 2.1 General procedure for the modular synthesis of proton conducting polymers.

The activated ester of the polymer was subsequently substituted with various amine-terminated PT functionalities (**1-3**) to generate the proton conducting polymers (**BTz, BIm** and **BPy**) (Scheme 2.1). Amine terminated PT groups were synthesized starting from the corresponding carboxylic acids with carbonyl diimidazole (CDI) as the coupling reagent. An excess of amine-terminated PT group (4 equiv. with respect to the NHS ester) was utilized to ensure complete substitution of NHS ester. The covalent incorporation of the PT groups was confirmed by ^{1}H NMR (Figure 2.2), which indicated the complete disappearance of the peak at δ = 2.79-2.88 ppm corresponding to the

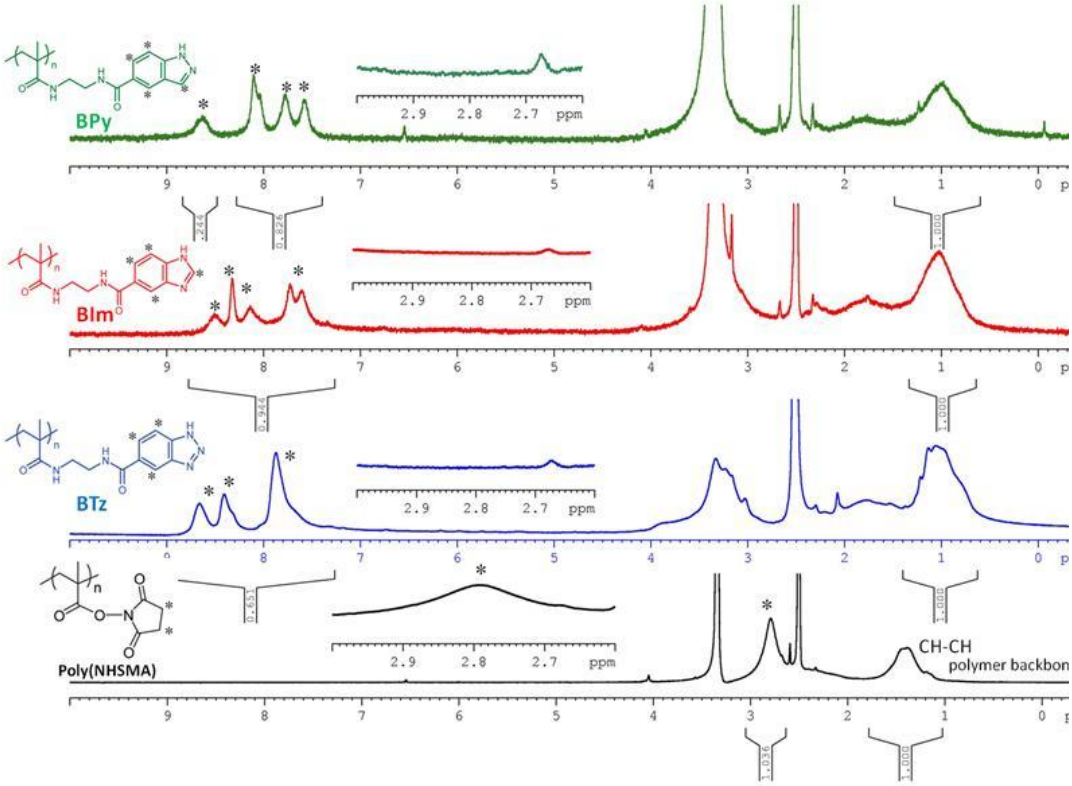

Figure 2.2 ^{1}HNMR spectra of proton conducting polymers, indicating the quantitative substitution of NHS ester of poly(NHSMA).

methylene protons of *N*-hydroxy succinimidyl ester and the concomitant appearance of peaks in the aromatic region. ^{1}H NMR of the polymers indicated the substitution to be greater than 95%. The polymers were also characterized by FTIR spectroscopy (Figure 2.9). All the polymers exhibited a broad band at around 3500-2900 cm^{-1}, with a maximum at ~3400 cm^{-1} characteristic of hydrogen bonded N-H stretch. The peaks around 1530-1670 cm-1 could be attributed to the amide bands, as well as the stretching vibrations of the aromatic C=C and the heterocyclic C=N bonds.

Since the proton conductivity measurements were carried out under variable temperature conditions, it is necessary that we investigate the thermal stability of these polymers by thermogravimetric analysis (TGA). Similarly, since proton conductivities could be affected by the glass transition temperature (T_g) of the polymer, we also carried out the differential scanning calorimetry (DSC) analyses of these polymers. Thermal analyses results of the polymers are shown in Table 2.1 and Figure 2.8. The decomposition temperatures are reported at 5% weight loss. While **BTz** polymer is stable

Table 2.1 Decomposition onset temperatures and molecular weights of proton conducting polymers.

Polymer	Decomposition Onset (^{o}C) (5% weight loss)	Molecular Weight (Mn, g/mol)*
BTz	234	16,000
BIm	184	16,000
BPy	190	16,000

* Estimated based on the quantitative substitution of NHS ester (Figure 2.2)

up to 234 ^{o}C, **BIm** and **BPy** polymers were found to be stable only up to 180-190 ^{o}C. The polymers exhibited neither a clearly discernible glass transition nor a melting transition up to 160 ^{o}C (Figure 2.7). The reasons for this observation are not clear to us at this time.

2.2.3 Proton Conductivity

Proton conductivity of the polymers is known to be influenced by several factors such as the nature of the heterocycle, glass transition temperature of the polymer, variations in polymeric architecture and proton charge carrier density.[3,31,14] Since the polymers were assembled modularly and the incorporation of PT groups on to the polymer was greater than 95% in all polymers, variations in the polymeric architecture and the charge carrier density would be minimal. Furthermore, since all the polymers possess identical polymeric architecture, the variations in the glass transition temperatures are also expected to be minimal. Thus, the chemical structure of the PT group will be the key determining factor of the proton conductivity of polymers **BTz, BIm** and **BPy**.

Proton conductivities of **BTz, BIm** and **BPy** are shown in Figure 2.3a. The conductivities of all the polymers steadily increased with temperature, which would be due to the increased segmental motion of the PT groups at higher temperatures, facilitating rapid formation and breaking of hydrogen bonding, resulting in fast proton transfer dynamics. It can be seen from Figure 3a that **BTz** exhibits better performance among all with the conductivity of 1.2 x 10^{-4} S/cm at 170 ^{o}C under anhydrous conditions. The benzimidazole based polymer, **BIm**, behaves similar to **BTz** in all temperature ranges, and its conductivity is slightly lesser. Contrary to **BTz** and **BIm**, benzopyrazole polymer (**BPy**) is a very poor conductor of protons. Its conductivities are lower than 10^{-8}

S/cm at all temperatures, about 4 orders of magnitude lower than that of **BTz** and **BIm**. Doping with acids, such as H_3PO_4, CF_3SO_3H and CF_3COOH (TFA), has been known to enhance the proton conductivities of the polymers, which is due to the increase in the number of mobile protons in the polymer matrix. Hence, polymers were doped with 30% TFA and the proton conductivities were measured (Figure 2.3b). Doping with TFA slightly improved the conductivity of **BIm** and **BPy** polymers at lower temperatures, while it had negligible effect on **BTz**. Furthermore, the conductivity of TFA doped **BPy** did not exhibit any dependence on temperature.

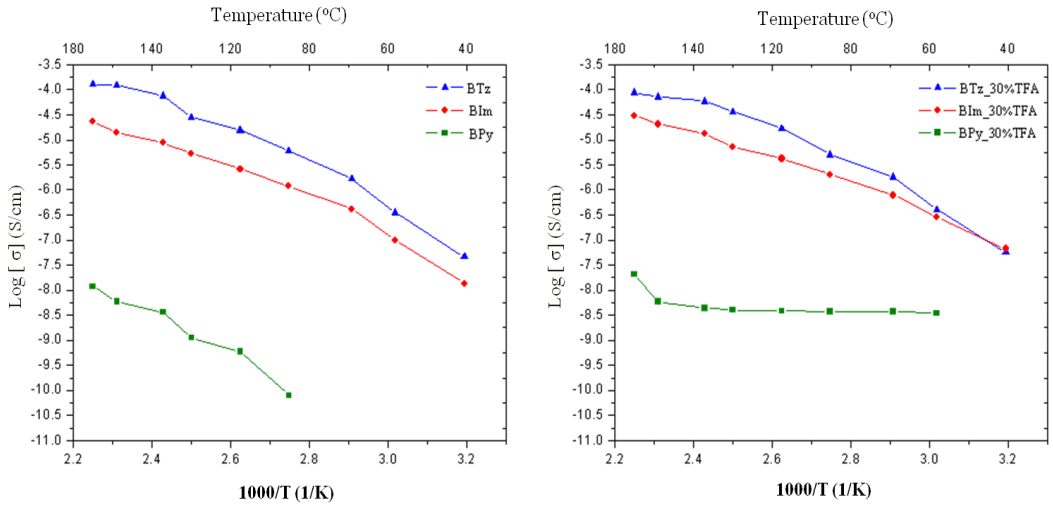

Figure 2.3 Proton conductivity of benz-*N*-heterocyclic polymers: neat samples (left) and doped with 30% TFA (right).

The existence of multiple tautomers is known to assist the reorientation step in the Grotthuss mechanism of proton transfer, while the interconversion among the tautomers would facilitate the proton transfer dynamics. To understand the similar behavior of **BTz** and **BIm** and the poor performance of **BPy** towards proton conductivity, we examined

the possible tautomers of benzotriazole, benzimidazole and benzopyrazole (Figure 2.4). Benzopyrazole has 1*H*- and 2*H*- tautomers. It is reasonable to suggest that the 2*H*-tautomer is less stable, because the benzene ring in benzopyrazole system is in the quinonoid form.[32-33] Therefore, the poor performance of **BPy** might be due to the restricted interconversion between 1*H*- and 2*H*- tautomers of benzopyrazole, which can severely impede the dynamics (formation and breaking) of hydrogen bonding and hence the proton transfer.

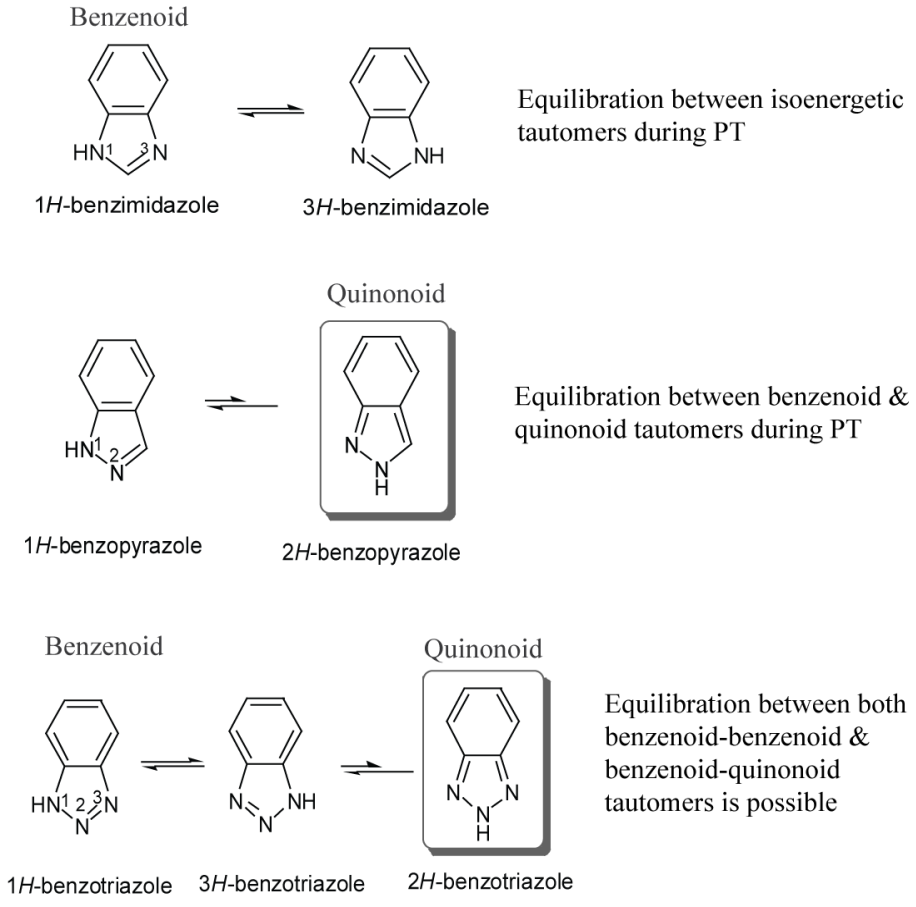

Figure 2.4 Illustration of the tautomers of benz-*N*-heterocycles.

Benzotriazole and benzimidazole, contrary to benzopyrazole, can tautomerize between the isoenergetic 1*H*- and 3*H*- forms without going through the quinonoid form of the benzene ring. Thus, the facile interconversion among the tautomers would provide a better opportunity for the neighboring PT moieties to interact with each other and hence rapidly shuttle the protons across the polymer, resulting in higher conductivities. Therefore, although benzotriazole theoretically has access to both 1,2- and 1,3- pathways, it is less likely to utilize the pyrazole-like pathway due to the quinonoid-type tautomer. Thus, the similar proton conducting behavior of **BTz** and **BIm** polymers might be due to the unavailability of pyrazole-like pathway in **BTz**, rather than the predominance of imidazole-like pathway for proton conduction.

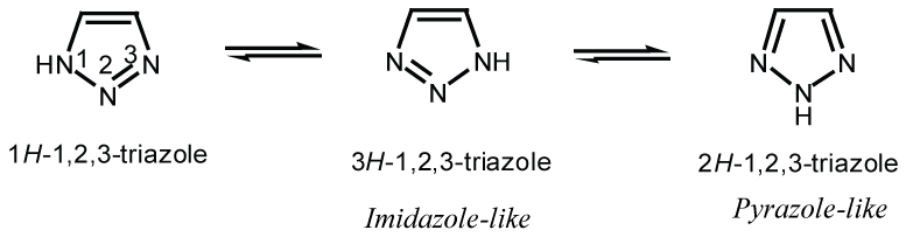

Figure 2.5 Illustration of the tautomers of 1*H*-1,2,3-triazole.

To overcome the above restriction and to unambiguously establish if both the pathways (imidazole-like and pyrazole-like) are equally accessible experimentally in triazoles, we further investigated the proton conductivities of triazole, imidazole and pyrazole containing polymers. Unlike benzotriazole, triazole has access to both imidazole-like (1*H*- and 3*H*-) and pyrazole-like (1*H*- and 2*H*-) tautomers without any possible contribution from quinonoid *vs*. benzenoid stability differences (Figure 2.5). Furthermore, triazole, imidazole and pyrazole have similar activation energies for

tautomerization. Hence, comparative study of the proton conducting behavior of triazole, imidazole and pyrazole systems would help us unequivocally establish the proton conduction pathway differences in triazole.

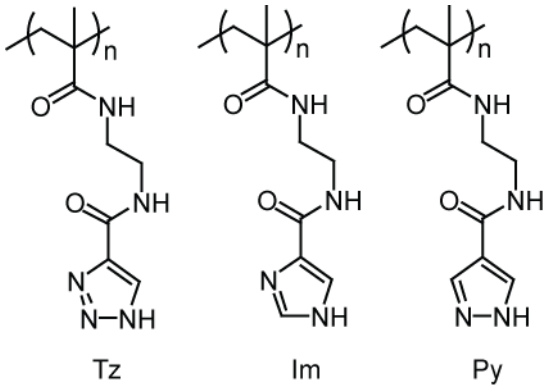

Chart 2.2 Structures of proton conducting polymers based on *N*-heterocycles.

Polymers based on triazole, imidazole and pyrazole were also assembled modularly following similar procedure described above for benz-*N*-heterocyclic polymers. PT groups with an amine terminus were synthesized via CDI coupling procedure and were then covalently tethered to poly (NHSMA) **5** to obtain **Tz, Im** and **Py** polymers (Chart 2.2). ^{1}H NMR indicated the incorporation of PT groups to be quantitative. TGA and DSC analysis were carried out and the results are summarized in Table 2.2. Polymers are found to be thermally stable up to 180-190 ^{o}C (Table 2.2, Figure 2.8). Similar to benz-*N*-heterocyclic polymers, these polymers also did not exhibit any measurable glass transition up to 180 ^{o}C (Figure 2.7). [16] As in the case of benz-*N*-heterocyclic polymers, the nature of the heterocycle will primarily govern the proton conductivity.

TGA and DSC analysis were carried out and the results are summarized in Table 2.2. Polymers are found to be thermally stable up to 180-190 ^{o}C (Table 2.2, Figure 2.8). Similar to benz-*N*-heterocyclic polymers, these polymers also did not exhibit any measurable glass transition up to 180 ^{o}C (Figure 2.7). [16] As in the case of benz-*N*-heterocyclic polymers, the nature of the heterocycle will primarily govern the proton conductivity.

Table 2.2 Decomposition onset temperatures and molecular weights of proton conducting polymers.

Polymer	Decomposition Onset (^{o}C) (5% weight loss)	Molecular Weight (Mn)*
Tz	181	13K
Im	183	13K
Py	193	13K

* Estimated based on the quantitative substitution of NHS ester

The proton conductivity of **Tz, Im** and **Py** polymers (neat and 30% TFA doped samples) are shown in Figure 2.6. Polymers based on triazole, **Tz** and imidazole, **Im** exhibited comparable conductivities at all temperature ranges, which varies from 10^{-9} S/cm at 40 ^{o}C to about 3.4 x 10^{-5} S/cm at 170 ^{o}C. It had been reported earlier that the proton conductivity of 1*H*-1,2,3-triazole based polymer is a few orders of magnitude higher than that of imidazole.[14] But, it has also been shown that the proton conductivity of imidazole containing polysiloxanes is about an order of magnitude higher than those of triazole.[3] Contrary to the above observations, we did not find any striking difference in conductivity between the imidazole and triazole based polymers, provided all the other

factors were held constant. Thus, the enhancement in conductivity of triazole to imidazole does not appear to be universal.

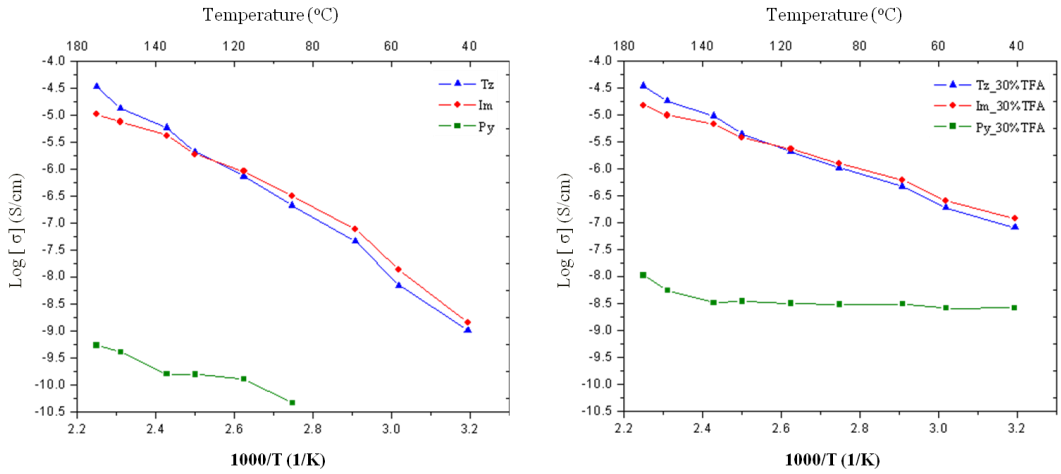

Figure 2.6 Proton conductivity of *N*-heterocyclic polymers: neat samples (left) and doped with 30% TFA (right).

Pyrazole based polymer, **Py**, is once again found to consistently perform poorly. **Py** did not exhibit any appreciable conductivity even at higher temperatures. Its conductivities were always lesser than 10^{-9} S/cm, a few orders of magnitude lower than those of **Tz** and **Im**. Doping with TFA enhanced the conductivity by about two orders of magnitude at lower temperatures, but had less pronounced effect at higher temperatures. Similar to **BPy**, the conductivity of **Py** also did not exhibit any dependence on temperature. The relative behavior of **Tz**, **Im** and **Py** towards proton conductivity is in good agreement with that of **BTz, BIm** and **BPy** polymers. Thus, based on the above observations, it would be reasonable to suggest that the imidazole-like pathway is the predominant contributor towards the proton conductivity of triazole, while contribution from the pyrazole-like pathway is negligible.

The poor proton conducting ability of pyrazole systems might be due to the inability of the polymer bound pyrazole moieties to pack well to provide an extended hydrogen bonded network. It can be visualized from Figure 2.1 that neighboring imidazoles in **Im** polymer can easily pack well to form an extended linear hydrogen bonded network. On the otherhand, in case of pyrazole, since the nitrogen's are in 1, 2 positions the neighboring pyrazoles in **Py** polymer need to pack in more or less a zig-zag fashion to form continuous hydrogen bonded network. Since the pyrazole moieties are covalently bound to the polymer backbone, the proper packing of the pyrazole groups to form an extended hydrogen bonded network would be sterically demanding and is less likely, resulting in low proton conductivity.

2.3 Summary

In aiming to gain insights into the mechanistic details of proton transport in triazole systems, we synthesized and characterized a range of polymers containing *N*-heterocycles (triazole, imidazole, pyrazole) as well as benz-*N*-heterocycles (benzotriazole, benzimidazole and benzopyrazole) by adopting a modular synthetic approach. We have shown that: (*i*) triazole (benzotriazole) and imidazole (benzimidazole) containing polymers behave similarly in proton conductivity and exhibit enhanced proton transfer dynamics compared to those with pyrazole (benzopyrazole). Similar behavior of triazole & imidazole (benzotriazole and benzimidazole) polymers has led us to believe that imidazole-like pathway dominates the proton conductivity of triazole and pyrazole-like pathway makes only a negligible contribution, if any. (*ii*) Pyrazole-like functional groups, *i.e*. the molecules with two nitrogen atoms adjacent to each other are not good candidates

to consider for proton transport applications, as pyrazole and benzopyrazole based polymers exhibited poor proton conductivity. (*iii*) Polymers containing benz-*N*-heterocycles performed better than those with the corresponding *N*-heterocycles, which might be due to the effective stabilization of the azolium cations via delocalization of the charge on to the benzene ring, thereby facilitating the dynamics of proton transfer. By comprehensively studying the PT behavior of structurally-related heterocycles under a common polymer platform, we believe that this study provides fundamental insights into structural characteristics of functional groups for anhydrous proton transport, which could have implications in proton exchange membranes.

2.4 Experimental Details

2.4.1 General Materials and Methods

All the reagents were purchased from commercial sources and were used as received. *N*-hydroxysuccinimide methacrylate (NHSMA) monomer[1] and benzopyrazole-5-carboxylic acid[2] were prepared following reported literature procedures. ^{1}H NMR (400 MHz) spectra were recorded on a Bruker 400 MHz NMR spectrometer using the residual proton and carbon resonance of the solvent, respectively as internal standards. Chemical shifts (δ) are reported in parts per million (ppm). The following abbreviations are used for the peak multiplicities: s, singlet; d, doublet; t, triplet; m, multiplet; dd, doublet of doublet; bs, broad singlet; bm, broad multiplet. ^{13}C NMR spectra were proton decoupled and recorded on a Bruker 100 MHz NMR spectrometer using the carbon signal of the dueterated solvent as the internal standard. Flash chromatography was performed using combiflash with normal phase Redi*sep R*f silica columns. Silica plates with F-254

indicator were used for analytical thin layer chromatography. The molecular weight of poly (NHSMA) **5** was determined by gel permeation chromatography (GPC) using PMMA standard employing RI detector. DMF with 0.1M LiCl at 50 °C was used as the eluent (flow rate: 1.0 mL/min). FTIR spectra were recorded on a MIDAC M1200 spectrometer.

Thermal stability of polymers was determined by thermogravimetric analysis (TGA) using TA Instruments TGA 2950 thermogravimetric analyzer (Figure 2.8). Samples were heated at a rate of 10 ^{o}C/min from room temperature to 600 ^{o}C under a flow of nitrogen. Glass transition temperature (T_g) of the polymers were obtained by differential scanning calorimeter (DSC) using TA instruments Dupont DSC 2910 (Figure 2.7). Measurements were conducted with a heating rate of 10 ^{o}C /min from -50 ^{o}C to 180 ^{o}C under a flow of nitrogen (50 mL/min). Each sample was measured through two heating cycles and the data from the second heating cycle is considered.

Proton conductivity of the polymers was measured under anhydrous conditions using impedance spectroscopy. Electrochemical impedance of the polymers was measured from 0.1 Hz-300 kHz with a sinusoidal excitation voltage of 0.1 V_{rms} using Solartron 1287 potentiostat and 1252A frequency response analyzer. Conductivity measurements were carried out under vacuum from 40 ^{o}C to 200 ^{o}C. Kapton tape with a hole of thickness 127 μm and diameter of 0.414 cm was placed onto a gold coated electrode and the polymer films were drop cast from solution onto the hole. Polymer film thickness and the contact area between the membrane and the electrode were determined by the dimensions of the hole and hence were held constant. Films were dried at 50 ^{o}C for 15 h prior to measurements and were then placed between two gold coated electrodes and

characterized by impedance spectroscopy. Conductivities lower than 10^{-9} S/cm are generally considered to be below the sensitivity of the instrument and hence the absolute numbers below this value are not considered accurate. Since the conductivities of BPy and Py polymers are lower than 10^{-9} S/cm at most temperature ranges, the conductivity data for these polymers should be treated as a representation of the poor proton conducting ability of BPy and Py polymers.

In order to measure the proton conductivity of polymers as a function of temperature, a vacuum oven was controlled to set points from 40 ^{o}C up to 200 ^{o}C and back down to 40 ^{o}C. Because of positional gradients in the system and heating time-lag effects, the temperature in the sample environment was consistently lower than that reported by the oven's built in thermocouple. Thus, in order to mitigate the temperature discrepancy, a calibration experiment was performed by embedding a standardized thermistor into the sample holder, and a correction was derived to apply to all of the data sets reported here. The largest correction at the 200 ^{o}C set point amounted to a sample temperature of about 170 ^{o}C.

2.4.2 Polymerization of NHSMA using ATRP

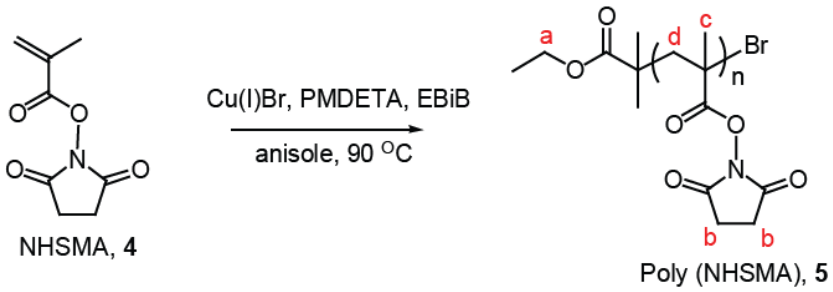

NHSMA, **4** Poly (NHSMA), **5**

The polymerization was carried out with a ratio of [NHSMA]c: [Cu(I)Br]: [PMDETA]: [EBiB] = 100:1:2:1. 23.3 mg (0.16 mmol) of Cu(I)Br was taken in a 25 mL round bottom flask equipped with a septum and gas inlet/outlet. The flask was degassed with argon for 5 min. Then 69.4 µL (0.32 mmol) of *N, N ,N' ,N'',N'''* pentamethyl-diethylenetriamine (PMDETA) was added, followed by a solution of *N*-hydroxysuccinimide methacrylate monomer (3.0g, 16.3 mmol) in 5.0 mL degassed anisole. The reaction mixture was stirred at room temperature for 5 min and 24 µL (0.16 mmol) of the initiator was added. Three cycles of freeze-pump thaw was carried out and the flask was transferred to a preheated oil bath at 90 °C. The polymerization was carried out at the same temperature for 2 h and then quenched and concentrated under reduced pressure. The crude mixture was dissolved in a minimum amount of DMF and precipitated twice from acetone, washed with DCM and MeOH. The white powder obtained was dried under vacuum for 12 h. GPC (DMF): Mn = 11 kg/mol; PDI = 1.26. ^{1}H NMR (400 MHz, DMSO-d6): δ: 4.0 (bs, 2H, a), 2.79-2.88 (bs, 4H, b), 2.08 (bs, 3H, c), 1.29-1.42 (bs, 2H, d).

2.4.3 General Procedure 1

Synthesis of 1*H*-benzotriazole-5-carboxylic acid (2-amino-ethyl)-amide-dihydrochloride (1)

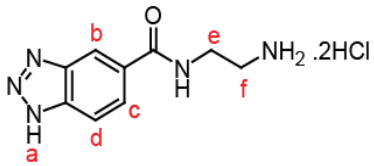

Benzotriazole-5-carboxylic acid (1.0 g, 6.13 mmol) was taken in 10 mL DMF and CDI (1.19 g, 7.35 mmol) was added to it. The reaction mixture was stirred at room

temperature for 30 min, followed by the addition of mono-Boc protected ethylene diamine (1.45 mL, 9.19 mmol). The reaction mixture was allowed to stir at room temperature and the completion of the reaction was followed by thin layer chromatography (MeOH/DCM, 5:95). The reaction mixture was then concentrated under reduced pressure and extracted with ethyl acetate and water. The organic layers were dried over Na_2SO_4 and concentrated using rotary evaporator. The crude mixture was then purified by column chromatography over silica with MeOH/DCM (5:95) as an eluent. The Boc protected compound was carried to the next step without further characterization. It was taken in 5 mL 1, 4-dioxane at room temperature and 5 mL 4N HCl was added to it. The reaction mixture was stirred at room temperature for 3 h and concentrated under reduced pressure. The crude mixture was dissolved in a minimum amount of methanol and triturated with excess diethyl ether. The solid obtained was filtered, washed with excess ether and dried under vacuum to obtain compound **1** as light brown solid. The combined yields are reported. Yield = 43%, light brown solid. ^{1}H NMR (400 MHz, DMSO-d6): δ (ppm): 8.93 (t, *J* = 5.60 Hz, 1H, a), 8.55 (s, 1H, b), 7.9-8.1 (m, 2H, c, d), 3.57 (m, 2H, e), 3.03 (m, 2H, f). ^{13}C NMR (100 MHz, DMSO-d6): δ (ppm): 166.9, 139.9, 131.4, 125.7, 119.6, 116.2, 114.2, 39.0, and 37.7.

Synthesis of 1*H*-benzimidazole-5-carboxylic acid (2-amino-ethyl)-amide-dihydrochloride (2)

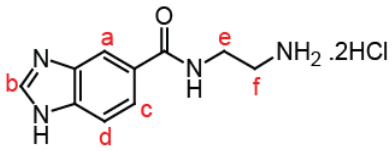

The compound was synthesized following general procedure **1**. Yield = 46%, dark brown solid. ^{1}H NMR (400 MHz, MeOD-d4): δ (ppm): 9.53 (s, 1H, a), 8.45 (s, 1H, b), 8.17 (d, *J* = 8.64 Hz, 1H, c), 7.94 (d, *J* = 8.64 Hz, 1H, d), 3.74 (m, 2H, e), 3.23 (m, 2H, f). ^{13}C NMR (100 MHz, MeOD-d4); δ (ppm): 168.3, 141.9, 132.8, 132.68, 130.7, 125.9, 114.4, 114.3, 39.7, 37.7.

Synthesis of 1*H*-benzopyrazole-5-carboxylic acid (2-amino-ethyl)-amide-dihydrochloride (3)

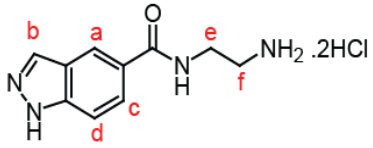

The compound was synthesized following general procedure **1**. Yield = 48%, light yellow solid. ^{1}H NMR (400 MHz, DMSO-d6): δ (ppm): 8.83 (s, 1H, a), 8.12 (s, 1H, b), 7.83 (d, *J* = 8.61 Hz, 1H, c), 7.64 (d, *J* = 8.61 Hz, 1H, d), 3.55 (m, 2H, e), 3.02 (m, 2H, f). ^{13}C NMR (100 MHz, DMSO-d6); δ (ppm): 167.6, 139.9, 133.9, 132.2, 125.2, 120.7, 119.9, 110.4, 39.0, 37.7.

Synthesis of 1*H*-triazole-4- carboxylic acid (2-amino-ethyl)-amide-dihydrochloride

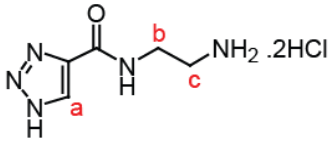

The compound was synthesized following general procedure **1**. Yield = 23%, off white solid. ^{1}H NMR (DMSO-d6): δ (ppm): 8.58 (s, 1H, a), 3.23 (m, 2H, b), 2.92 (m, 2H, c). ^{13}C NMR (100 MHz, DMSO-d6); δ (ppm): 167.9, 134.7, 134.4, 36.8, 34.6.

Synthesis of 1*H*-pyrazole-4- carboxylic acid (2-amino-ethyl)-amide-dihydrochloride

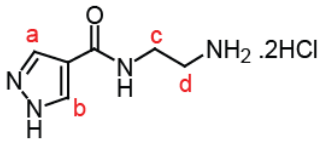

The compound was synthesized following general procedure **1**. Yield = 50%, light yellow solid. ^{1}H NMR (400 MHz, DMSO-d6): δ (ppm): 7.63 (s, 1H, a), 6.98 (s, 1H, b), 3.08 (m, 2H, c), 2.58 (m, 2H, d). ^{13}C NMR (100 MHz, DMSO-d6); δ (ppm): 164.6, 134.7, 119.7, 114.9, 37.0, 34.6.

Synthesis of 1*H*-imidazole-4- carboxylic acid (2-amino-ethyl)-amide-dihydrochloride

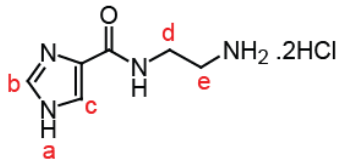

Imidazole-4- carboxylic acid (500 mg, 4.46 mmol) was refluxed with $SOCl_2$ (10 mL) for 36 h to obtain the corresponding acid chloride.[3] The reaction mixture was concentrated and the crude was triturated with excess diethyl ether. The white powder obtained was filtered, dried and then reacted with mono-Boc protected ethylene diamine (1.05 mL, 6.69 mmol) in $CHCl_3$ (5 mL). The reaction mixture was stirred at room temperature for 6 h, concentrated and extracted with ethylacetate and water. The combined organic layers were dried over Na_2SO_4 and concentrated using rotary evaporator. The crude mixture was then purified by column chromatography over silica with MeOH/DCM (5:95) as an eluent. The Boc protected compound was carried to the

next step without further characterization. It was taken in 5 mL 1, 4-dioxane at room temperature and 5 mL 4N HCl was added to it. The reaction mixture was allowed to stir at room temperature for 3 h and concentrated under reduced pressure. The crude mixture was dissolved in a minimum amount of methanol and triturated with excess diethyl ether. The solid obtained was filtered, washed with excess ether and dried under vacuum to obtain the pure compound as off white solid in 33% overall yield. ^{1}H NMR (400 MHz, DMSO-d6): δ (ppm): 9.38 (bs, 1H, a), 9.03 (s, 1H, b), 8.36 (s, 1H, c), 3.53 (m, 2H, d), 3.00 (m, 2H, e). ^{13}C NMR (100 MHz, DMSO-d6); δ (ppm): 158.3, 136.3, 128.7, 121.1, 38.9, 37.2.

2.4.4 General Procedure 2

Substitution of NHS Ester of Poly (NHSMA) 5 with Amine Terminated PT Groups

200 mg of poly (NHSMA) 5 was taken in 20 mL vial and dissolved in 3 mL anhydrous DMSO. Amine terminated PT groups (4 mmol w.r.t NHS ester moiety) and triethyl amine (10 mmol w.r.t to the amine functionality) were added and the reaction mixture was flushed with argon and stirred at 60 ^{o}C for 24 h. The polymers were then precipitated from excess diethyl ether, washed with copious amounts of methanol and dried under vacuum at 40 ^{o}C for 24 h. The polymers were obtained in about 60-70% yield. ^{1}H NMR indicated the substitution of NHS ester to be greater than 95%.

Synthesis of Benzotriazole Polymer BTz

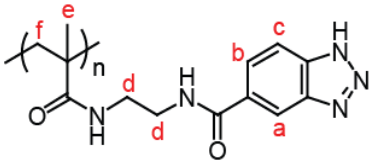

The polymer was synthesized following general procedure **2.** ^{1}H NMR (400 MHz, DMSO-d6): δ (ppm): 8.66 (bs, 1H, a), 8.41 (bs, 1H, b), 7.88 (bs, 1H, c), 3.17-3.33 (bm, 1H, d), 1.73-1.76 (bs, 3H, e), 0.94 - 1.03 (bs, 2H, f).

Synthesis of Benzimidazole Polymer BIm

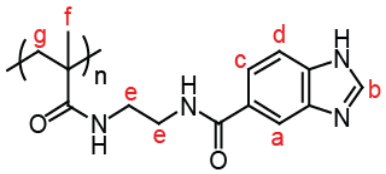

^{1}H NMR (400 MHz, DMSO-d6): δ (ppm): 8.51 (bs, 1H, a), 8.32 (bs, 1H, b), 8.13 (bs, 1H, c), 7.60 - 7.72 (bd, 1H, d), 3.17-3.33 (bm, 4H, e), 1.73-1.76 (bs, 3H, f), 0.94 - 1.03 (bs, 2H, g).

Synthesis of Benzopyrazole Polymer BPy

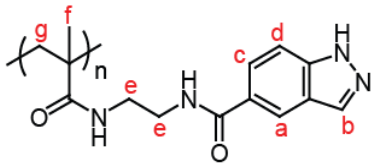

The polymer was synthesized following general procedure **2.** ^{1}H NMR (400 MHz, DMSO-d6): δ (ppm): 8.53 (bs, 1H, a), 8.08 (bm, 1H, b), 7.56 (bs, 1H, c), 7.54 (bs, 1H, d), 3.17-3.33 (bm, 4H, e), 1.73-1.76 (bs, 3H, f), 1.02 (bs, 2H, g).

Synthesis of Triazole Polymer Tz

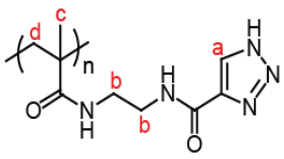

The polymer was synthesized following general procedure **2.** ^{1}H NMR (400 MHz, DMSO-d6): δ (ppm): 8.53-8.56 (bs, 1H, a), 3.17-3.33 (bm, 4H, b), 1.73-1.76 (bs, 3H, c), 0.94-1.03 (bs, 2H, d).

Synthesis of Imidazole Polymer Im

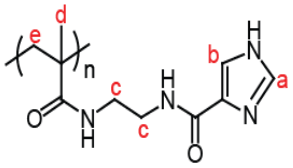

The polymer was synthesized following general procedure **2.** ^{1}H NMR (400 MHz, DMSO-d6): δ (ppm): 8.76 (bs, 1H, a), 7.98 (bs, 1H, b), 3.17-3.33 (bm, 4H, c), 1.73-1.76 (bs,3H, d), 0.94-1.03 (bs, 2H, e).

Synthesis of Pyrazole Polymer Py

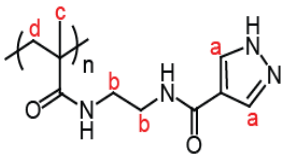

The polymer was synthesized following general procedure **2.** ^{1}H NMR (400 MHz, DMSO-d6): δ (ppm): 7.3-6.8 (bs, 2H, a), 3.17-3.33 (bm, 4H, b), 1.73-1.76 (bs, 3H, c), 0.94-1.03 (bs, 2H, d).

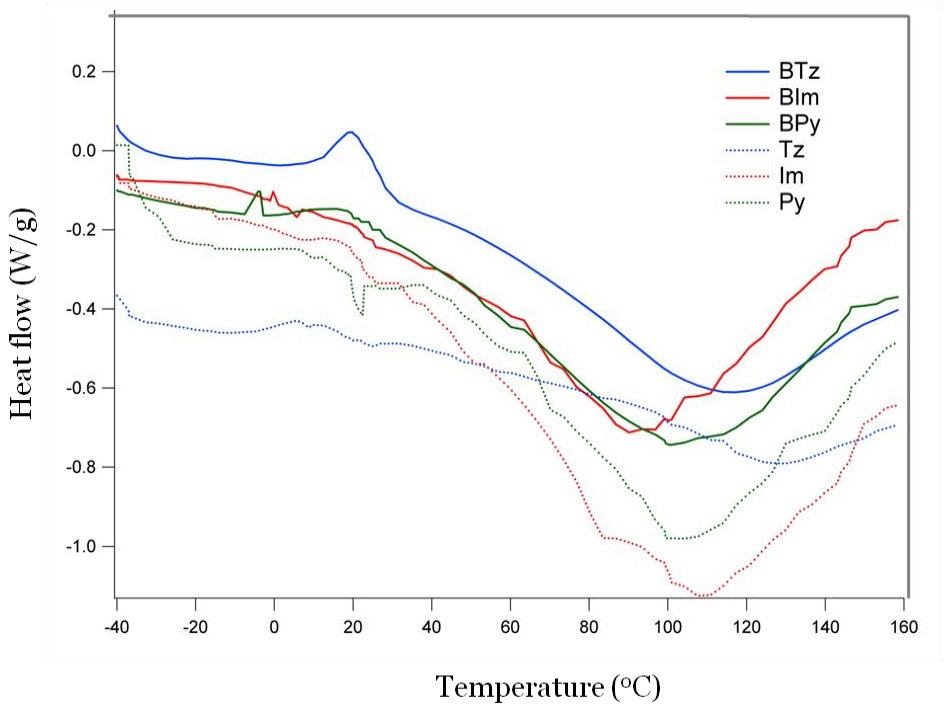

Figure 2.7 DSC traces of proton conducting polymers.

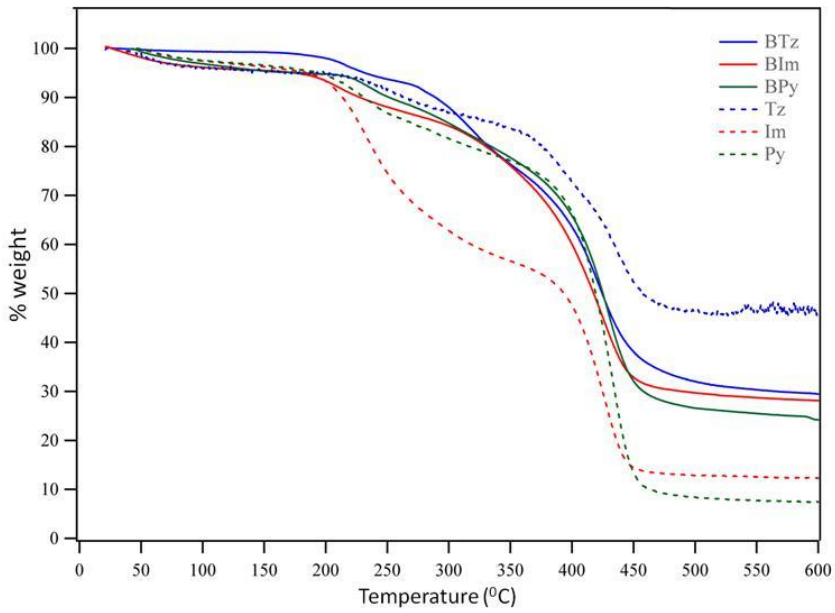

Figure 2.8 TGA traces of proton conducting polymers.

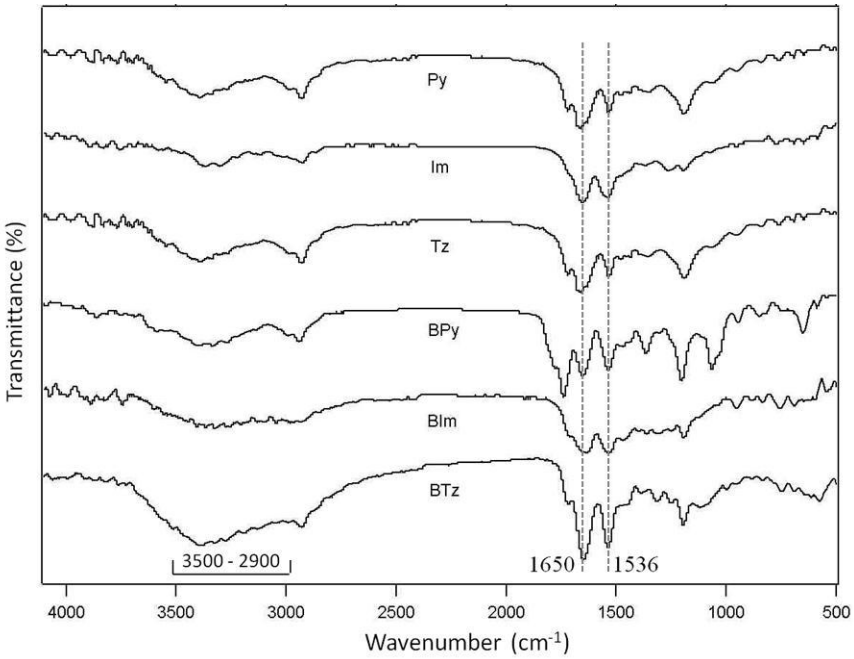

Figure 2.9 FTIR spectra of proton conducting polymers.

2.5 References

1. Celik, S. U.; Bozkurt, A., Proton conduction promoted by 1H-1,2,3-benzotriazole in non-humidified polymer membranes. *Electrochim. Acta* **2011**, *56*, 5961-5965.

2. Chen, Y. B.; Thorn, M.; Christensen, S.; Versek, C.; Poe, A.; Hayward, R. C.; Tuominen, M. T.; Thayumanavan, S., Enhancement of anhydrous proton transport by supramolecular nanochannels in comb polymers. *Nat. Chem.* **2010**, *2*, 503-508.

3. Granados-Focil, S.; Woudenberg, R. C.; Yavuzcetin, O.; Tuominen, M. T.; Coughlin, E. B., Water-free proton-conducting polysiloxanes: A study on the effect of heterocycle structure. *Macromolecules* **2007**, *40*, 8708-8713.

4. Herz, H. G.; Kreuer, K. D.; Maier, J.; Scharfenberger, G.; Schuster, M. F. H.; Meyer, W. H., New fully polymeric proton solvents with high proton mobility. *Electrochim. Acta* **2003**, *48*, 2165-2171.

5. Kreuer, K. D.; Fuchs, A.; Ise, M.; Spaeth, M.; Maier, J., Imidazole and pyrazole-based proton conducting polymers and liquids. *Electrochim. Acta* **1998**, *43*, 1281-1288.

6. Narayanan, S. R.; Yen, S. P.; Liu, L.; Greenbaum, S. G., Anhydrous proton-conducting polymeric electrolytes for fuel cells. *J. Phys. Chem. B* **2006**, *110*, 3942-3948.

7. Persson, J. C.; Jannasch, P., Intrinsically proton-conducting benzimidazole units tethered to polysiloxanes. *Macromolecules* **2005**, *38*, 3283-3289.

8. Schuster, M. E.; Meyer, W. H., Anhydrous proton-conducting polymers. *Ann. Rev. Mater. Res.* **2003**, *33*, 233-261.

9. Schuster, M. F. H.; Meyer, W. H.; Schuster, M.; Kreuer, K. D., Toward a new type of anhydrous organic proton conductor based on immobilized imidazole. *Chem. Mat.* **2004**, *16*, 329-337.

10. Wang, J. T. W. W. J. T. W.; Hsu, S. L. C., Enhanced high-temperature polymer electrolyte membrane for fuel cells based on polybenzimidazole and ionic liquids. *Electrochim. Acta* **2011**, *56*, 2842-2846.

11. Bredas, J. L.; Poskin, M. P.; Delhalle, J.; Andre, J. M.; Chojnacki, H., Electronic-structure of hydrogen-bonded imidazole chains - Influence of the proton position *J. Phys. Chem.* **1984**, *88*, 5882-5887.

12. Daycock, J. T.; Jones, G. P.; Evans, J. R. N.; Thomas, J. M., Rotation of imidazole in solid state and its significance in deciding nature of charge migration in biological materials. *Nature* **1968**, *218*, 672-673.

13. Munch, W.; Kreuer, K. D.; Silvestri, W.; Maier, J.; Seifert, G., The diffusion mechanism of an excess proton in imidazole molecule chains: first results of an ab initio molecular dynamics study. *Solid State Ionics* **2001**, *145*, 437-443.

14. Zhou, Z.; Li, S. W.; Zhang, Y. L.; Liu, M. L.; Li, W., Promotion of proton conduction in polymer electrolyte membranes by 1H-1,2,3-triazole. *J. Am. Chem. Soc.* **2005**, *127*, 10824-10825.

15. Zhou, Z.; Liu, R.; Wang, J. H.; Li, S. W.; Liu, M. L.; Bredas, J. L., Intra- and intermolecular proton transfer in 1H(2H)-1,2,3-triazole based systems. *J. Phys. Chem. A* **2006**, *110*, 2322-2324.

16. Alkorta, I.; Rozas, I.; Elguero, J., A computational approach to intermolecular proton transfer in the solid state: assistance by proton acceptor molecules. *J. Chem. Soc.-Perkin Trans. 2* **1998**, 2671-2675.

17. Elguero, J.; Fruchier, A.; Pellegrin, V., Annular tautomerism in the solid state - A high resolution NMR study. *J. Chem. Soc.-Chem. Commun.* **1981**, 1207-1208.

18. Jimenez, V.; Alderete, J. B., Complete basis set calculations on the tautomerism and protonation of triazoles and tetrazole. *Theochem-J. Mol. Struct.* **2006**, *775*, 1-7.

19. Catalan, J.; Sanchezcabezudo, M.; Depaz, J. L. G.; Elguero, J.; Taft, R. W.; Anvia, F., The tautomerism of 1,2,3-triazole, 3(5)-methylpyrazole and their cations. *J. Comput. Chem.* **1989**, *10*, 426-433.

20. Scheiner, S.; Yi, M. Y., Proton transfer properties of imidazole. *J. Phys. Chem.* **1996**, *100*, 9235-9241.

21. Mader, J. A.; Benicewicz, B. C., Synthesis and Properties of Segmented Block Copolymers of Functionalised Polybenzimidazoles for High-Temperature PEM Fuel Cells. *Fuel Cells* **2011**, *11*, 222-237.

22. Persson, J. C.; Jannasch, P., Block copolymers containing intrinsically proton-conducting blocks tethered with benzimidazole units. *Chem. Mat.* **2006**, *18*, 3096-3102.

23. Woudenberg, R. C.; Yavuzeetin, O.; Tuominen, M. T.; Coughlin, E. B., Intrinsically proton conducting polymers and copolymers containing benzimidazole moieties: Glass transition effects. *Solid State Ionics* **2007**, *178*, 1135-1141.

24. Nagamani, C.; Versek, C.; Thorn, M.; Tuominen, M. T.; Thayumanavan, S., Proton Conduction in 1H-1,2,3-triazole Polymers: Imidazole-Like or Pyrazole-Like? *J. Polym. Sci. Pol. Chem.* **2010**, *48*, 1851-1858.

25. Godwin, A.; Hartenstein, M.; Muller, A. H. E.; Brocchini, S., Narrow molecular weight distribution precursors for polymer-drug conjugates. *Angew. Chem. Int. Ed.* **2001**, *40*, 594-597.

26. Shunmugam, R.; Tew, G. N., Efficient route to well-characterized homo, block, and statistical polymers containing terpyridine in the side chain. *J. Polym. Sci. Pol. Chem.* **2005**, *43*, 5831-5843.

27. Wong, S. Y.; Putnam, D., Overcoming limiting side reactions associated with an NHS-activated precursor of polymethacrylamide-based polymers. *Bioconjugate Chem.* **2007**, *18*, 970-982.

28. Braunecker, W. A.; Matyjaszewski, K., Controlled/living radical polymerization: Features, developments, and perspectives. *Prog. Polym. Sci.* **2007**, *32*, 93-146.

29. Kamigaito, M.; Ando, T.; Sawamoto, M., Metal-catalyzed living radical polymerization. *Chem. Rev.* **2001**, *101*, 3689-3745.

30. Matyjaszewski, K.; Xia, J. H., Atom transfer radical polymerization. *Chem. Rev.* **2001**, *101*, 2921-2990.

31. Martwiset, S.; Yavuzcetin, O.; Thorn, M.; Versek, C.; Tuominen, M.; Coughlin, E. B., Proton Conducting Polymers Containing 1H-1,2,3-Triazole Moieties. *J. Polym. Sci. Pol. Chem.* **2009**, *47*, 188-196.

32. Teixeira, F. C.; Ramos, H.; Antunes, I. F.; Curto, M. J. M.; Duarte, M. T.; Bento, I., Synthesis and structural characterization of 1-and 2-substituted indazoles: Ester and carboxylic acid derivatives. *Molecules* **2006**, *11*, 867-889.

33. Tomas, F.; Abboud, J. L. M.; Laynez, J.; Notario, R.; Santos, L.; Nilsson, S. O.; Catalan, J.; Claramunt, R. M.; Elguero, J., Tautomerism and aromaticity in 1,2,3-triazole - The caseof benzotriazole. *J. Am. Chem. Soc.* **1989**, *111*, 7348-7353.

CHAPTER 3

IMPORTANCE OF DYNAMIC HYDROGEN BONDS AND REORIENTATION BARRIERS IN PROTON TRANSPORT

3.1 Introduction

N-heterocycles such as imidazole[1-3] and triazole[4] exhibit high proton conductivities in their molten state. Nonetheless, the corresponding polymers' conductivities fall far short (2-3 orders of magnitude lower).[3, 5-9] The differences in conductivity between the polymers and the corresponding small molecule heterocycles are understood to arise in part due to the restricted rotation of the heterocycles when they are immobilized on to a polymer scaffold. While small molecule heterocycles can conduct protons by both the vehicular mechanism as well as the Grotthuss mechanism, proton transport in polymers is facilitated exclusively via the Grotthuss mechanism. Grotthuss proton transfer (PT) involves two steps: (i) inter-functional group proton transfer and (ii) reorientation of the scaffold for subsequent PT. The reorientation step involves reorganization or flipping of the PT moieties and is recognized to be the rate limiting step for proton transfer in *N*-heterocyclic polymers.[10-12]

In *N*-heterocycles, one nitrogen atom accepts a proton while the other nitrogen donates a proton. This 'two-site' feature would necessitate the rotation of the entire heterocycle during reorientation. When heterocycles are immobilized onto a polymer, the reorientation step requires a concerted rotation of all the imidazole units involved for this to be a proton wire after the first pass of protons (*i.e.* subsequent proton transfer). The concerted 'two-site' ring rotation of imidazole units would in turn impose significant

neighboring molecule rearrangements and hence is energetically demanding, resulting in high reorientation barriers. The rotation of heterocycles in polymers (reorientational dynamics) would be restricted to a far greater extent compared to that of small molecules. This restricted mobility of heterocycles in a tethered polymeric scaffold would adversely affect the overall PT, resulting in lower proton conductivities in polymers; thereby increasing the gap in conductivity between polymers and the corresponding small molecules.

We hypothesized that utilizing a 'single-site' moiety, which acts as both a hydrogen bond donor and acceptor, would likely provide lower reorientational barriers and thus improve the proton conductivity; thereby lowering the gap in conductivity between polymers and the corresponding small molecules. In contrast to the 'two-site' system, reorientation in a 'single-site' system is 'local' on a functional group level and hence would impose minimal neighboring molecule rearrangements. A new class of functional groups, phenols, has been identified to possess the 'single-site' hydrogen bond donor/acceptor feature. The molecular design and synthesis, conductivity measurements, and molecular theory of phenolic polymers will be discussed in this Chapter.

3.2 Results and Discussion

3.2.1 Molecular Design

Our molecular design hypothesis is to seek a functional group where hydrogen bond donor/acceptor reorientation can occur in a single site and also affords a dynamic and labile hydrogen bond network. This design is reminiscent of the hydrogen bond network found in water, which is interestingly one of the best Grotthuss proton transporters.[13] We

hypothesized that phenols are suitable for this purpose; because they have the functional component found in water (-OH), while providing handles for polymerization. Moreover, a single hydroxyl moiety (-OH) acts as both a proton donor and acceptor. Therefore, we hypothesized that reorientation in phenols might proceed via C-O bond rotation involving just the -OH moiety and not the entire phenyl ring, and hence would exhibit lower barrier rotations (Figure 3.1b). To test this hypothesis, we studied the phenolic polymers shown in Chart 3.1. We carried out quantum calculations using simple model oligomers to test if (*i*) reorientation in phenols proceeds via C-O bond rotation involving just the –OH moiety, and (*ii*) the reorientation barrier observed for the PS-4-OH dimer is lower than that reported for *N*-heterocyclic systems.[14]

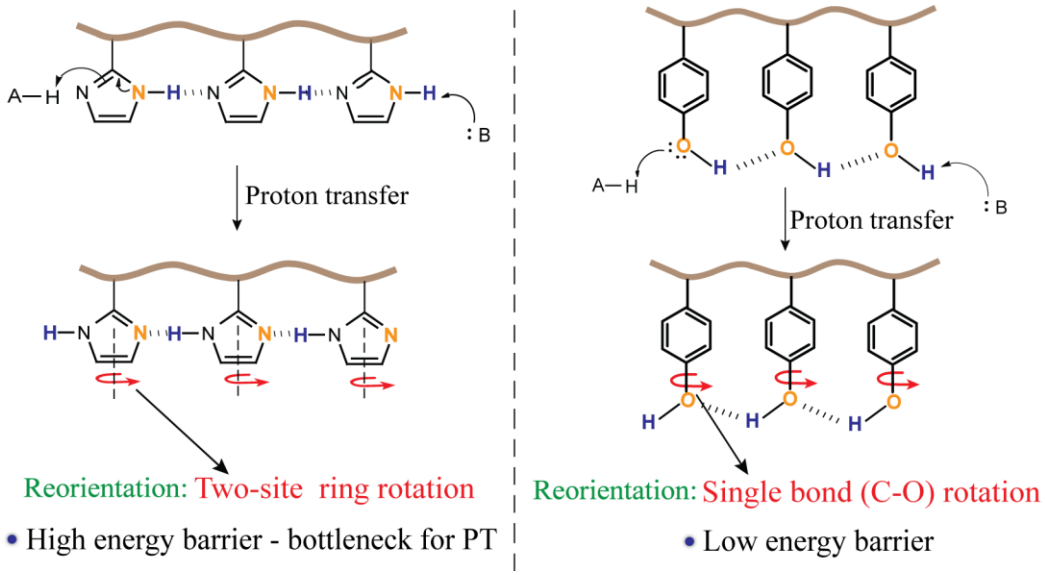

Figure 3.1 Schematic representation of Grotthuss proton transfer processes in polymeric imidazole (left) and phenol (right).

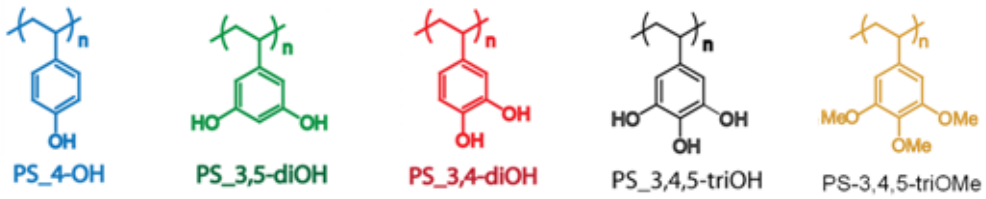

Chart 3.1 Structures of phenolic polymers.

3.2.2 Quantum Calculations

To test if regeneration in phenols involves the rotation of just C-O bonds, structures of PS-4-OH dimer and the reoriented dimer were modeled using density functional theory (DFT) LSDA/6-311G(d,p), with transition states found using the quadratic synchronous transit method (Figure 3.2). The local spin-density approximation (LSDA) has been found to capture the energetics of π-π stacking remarkably well,[15] while most other correlation potentials miss this form of van der Waals attraction. The imaginary frequency so obtained (332*i*) corresponds to the C-O rotation of the proton around the

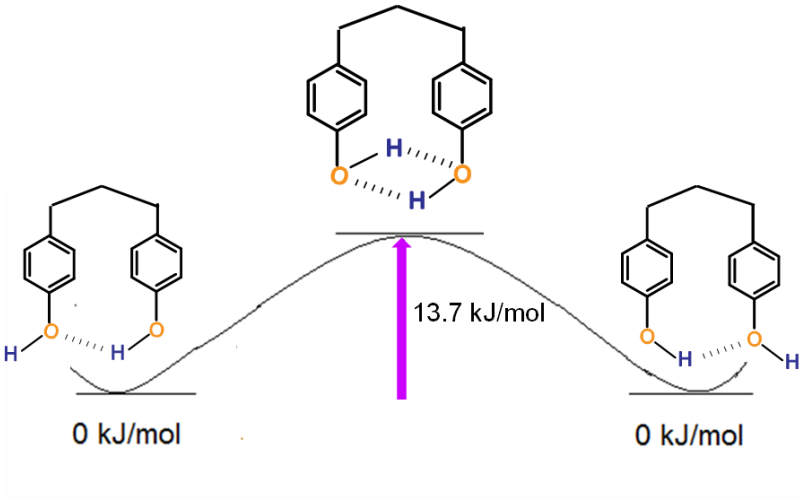

Figure 3.2 Structures of PS-4-OH dimer and the transition state modeled using LSDA/6-311G(d,p).

oxygen atom.[16] The barrier for reorientation was found to be 13.7 kJ/mol, which is comparable to that observed for water in nano-confined systems (12 kJ/mol).[17-18] These computational results lend credence to our hypothesis, by showing that C-O rotation in these phenolic species is responsible for Grotthuss regeneration with barriers similar to those in water.

3.2.3 Synthesis and Characterization

All the polymers were synthesized starting from the corresponding hydroxy benzaldehydes (Scheme 3.1). The hydroxyl groups were first protected with t-butoxycarbonyl (Boc) and the aldehyde was subsequently converted to a polymerizable double bond using Wittig reaction. The monomers were polymerized via free radical polymerization with AIBN as the initiator. The Boc groups were then deprotected using trifluoroacetic acid (TFA) to obtain the corresponding phenolic polymers. The GPC traces of the Boc protected polymers are shown in Figure 3.9 and the polymer details are summarized in Table 3.1. The molecular weights of the hydroxy polymers were

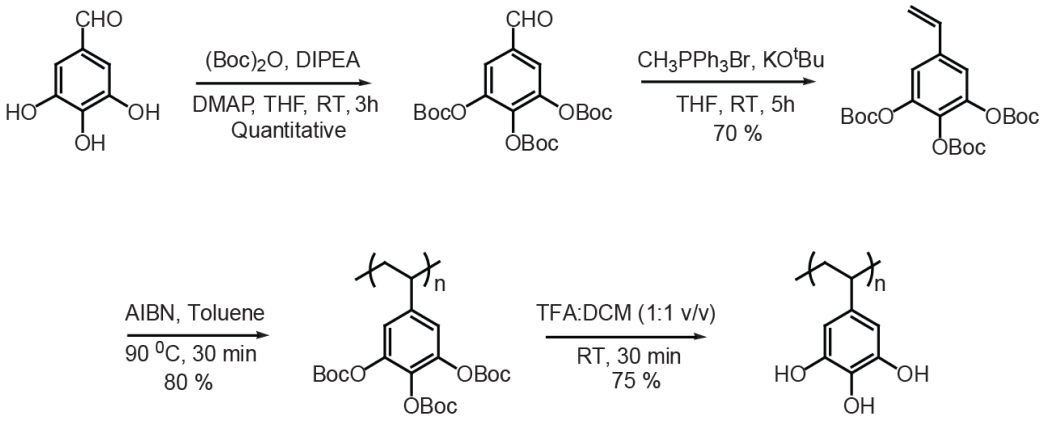

Scheme 3.1 Synthetic scheme for PS-3,4,5-triOH polymers.

determined based on the complete deprotection of the Boc protecting groups, which was confirmed by both ^{1}H NMR (Figure 3.10) and FTIR (Figure 3.11). The molecular weights obtained from GPC (DMF, 0.1 M LiCl, 50 ^{o}C) were greater than 100 kg/mol for all the polymers. We suspect that the polymers might be aggregating due to the strong hydrogen bonding interactions between the hydroxyl groups.

3.2.4 Thermal Analysis

The thermal stability of polymers was determined by thermogravimetric analysis (TGA) under nitrogen atmosphere and the results are summarized in Table 3.2 and Figure 3.14b. All the polymers were found to be stable up to atleast 250 ^{o}C. Since phenol based polymers are susceptible to oxidation, the polymers were also analyzed for thermo-oxidative stability i.e. the thermal stability of polymers was examined under air atmosphere. The thermo-oxidative results are also tabulated in Table 3.2 and shown in Figure 3.14a. All the polymers were found to be stable up to atleast 230 ^{o}C both under nitrogen and air atmospheres.

The glass transition temperatures (T_g values) of polymers were determined by differential scanning Calorimetry (DSC) and are shown in Table 3.2 and Figure 3.13. The glass transition temperature steadily increases with increasing number of -OH groups from PS-4-OH to PS-3,4,5-triOH. This is expected because the hydrogen bonding interactions among polymer side chains would increase with increasing number of -OH groups. Although PS-3,4-diOH and PS-3,5-diOH have same number of –OH groups, PS-3,4-diOH exhibits lower T_g compared to PS-3,5-diOH. This is because the -OH groups in PS-3,4-diOH are in *ortho* position and hence can also participate in intramolecular

hydrogen bonding besides intermolecular hydrogen bonding, thereby lowering the extent of intermolecular interactions in a polymer chain.

Table 3.1 Polymer details, thermal stability ($T_{d,5\%}$, under nitrogen), thermo-oxidative stability ($T_{d,5\%}$, under air), and glass transition temperature (T_g) of phenolic polymers.

Polymer	Mn[a] (g/mol)	PDI	Polymer	Mn[b] (g/mol)	$T_{d,5\%}$ [c] (^oC)	$T_{d,5\%}$ [d] (^oC)	T_g (^oC)
PS-3,4,5-triBoc	60,000	1.5	PS-3,4,5-triOH	20,000	267	265	233
PS-3,4-diBoc	63,000	1.6	PS-3,4-diOH	26,000	267	308	199
PS-3,5-diBoc	64,000	1.4	PS-3,5-diOH	25,000	239	258	227
PS-4-Boc	NA	NA	PS-4-OH	25,000	285	347	187

[a] estimated by GPC (THF) using PS standards.

[b] estimated based on the complete deprotection of Boc groups, which was confirmed by both ^{1}H NMR (Figure 3.10) and FT-IR (Figure 3.11).

[c] Temperature at 5% weight loss when heated under air at 1 ^{o}C/min

[d] Temperature at 5% weight loss when heated under nitrogen at 10 ^{o}C/min

3.2.5 Proton Conductivity

We first wanted to test if -OH groups can conduct protons under anhydrous conditions. To test this, the proton conductivities of commercially available poly(4-vinyl phenol) (PS-4-OH) and the control polymers polystyrene (PS) and PS-3,4,5-triOMe, neither of which contain -OH groups, were measured. PS-4-OH was found to indeed conduct protons under water-free conditions ($\sigma = 10^{-7.5}$ S cm^{-1} at 160 ^{o}C) (Figure 3.3). On the other hand, the proton conductivities of PS and PS-3,4,5-triOMe, neat as well as with

30% TFA doping, were below the sensitivity of the instrument (<10^{-9} S/cm) over the entire temperature range. This observation is consistent with our hypothesis that -OH groups can indeed assist proton conduction under anhydrous conditions.

Although PS-4-OH can conduct protons, the observed proton conductivity is not substantial. This might be due to its inability to provide a continuous hydrogen bond pathway with just one -OH group per monomer unit, *i.e.* the fraction of conducting functionalities within the polymer may be too low. To improve the conductivity, PS-3,5-diOH, PS-3,4-diOH, and PS-3,4,5-triOH polymers (see Chart 3.1) were synthesized and evaluated for thermal stability (under nitrogen), thermo-oxidative stability (under air) and proton conductivity. These polymers provide a systematic variation in the number as well as the position (ortho *vs.* meta) of –OH groups and hence establish structure-property

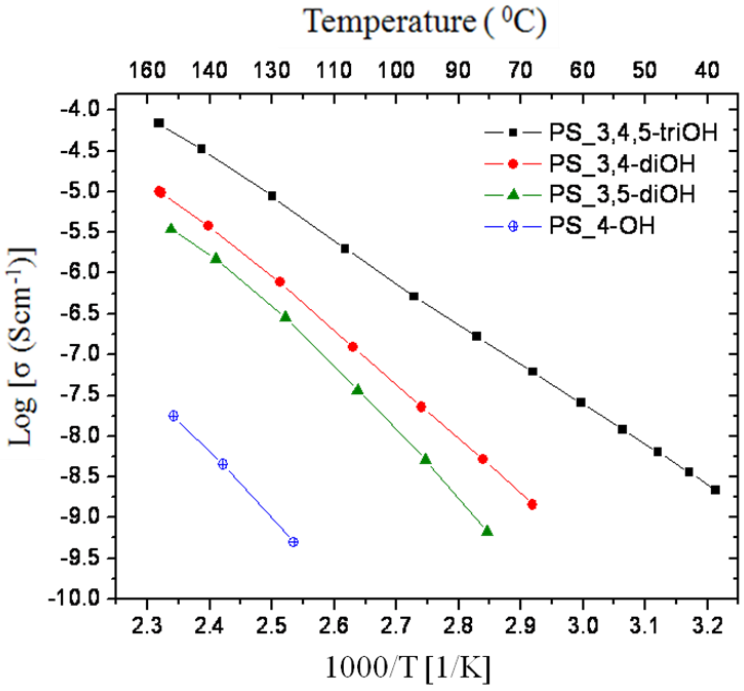

Figure 3.3 Proton conductivity of phenolic polymers under vacuum.

relationships. All these polymers are stable up to at least 230 ^{o}C both under nitrogen and air atmospheres (Table 3.2).

3.2.5.1 Temperature Dependence of Conductivity in Phenolic Polymers

The nature of the temperature dependence of the proton conductivity in polymer electrolytes is an indicative of the type of conduction mechanism. In general, two different behaviors are observed: (i) polymers exhibiting a Vogel-Tamman-Fulcher (VTF) behavior. These systems show a curvature in the plots of log σ versus inverse temperature (1/T), indicating that the conductivity mechanism is predominantly governed by the segmental motion of the polymeric side chains,[19,9,20] (ii) polymers exhibiting an Arrhenius-type behavior, in which log σ follows a simple Arrhenius relationship with (1/T) according to Equation 3.1. The proton transport in these systems is essentially governed by a hopping mechanism i.e. rapid exchange of protons via hydrogen bonds. where σ_o is a pre-exponential factor, E_a is the apparent activation energy and T is the temperature in Kelvin.

$$\sigma = \sigma_o \exp(-E_a/RT) \quad (3.1)$$

The proton conductivity of the phenolic polymers is shown in Figure 3.3. The phenolic polymers exhibit an Arrhenius-type behavior over the entire temperature range studied here. The conductivity plots were fitted by Arrhenius equation and the activation energies (E_a) were computed from the slope of the linear fit of ln σ vs. 1/T (Table 3.2). All polymers show enhanced proton conductivities compared to PS-4-OH (Figure 3.3 and Table 3.2). The activation energy decreases and the proton conductivity increases with increasing number of –OH groups. PS-3,4,5-triOH is the best performing polymer. The

ortho (PS-3,4-diOH) *vs.* meta (PS-3,5-diOH) placement of -OH groups does not cause significant difference in proton conductivity.

Table 3.2 Proton conductivity (σ, under vacuum), apparent activation energy (E_a), and glass transition temperature (T_g) of phenolic polymers.

Polymer	Log [σ (S cm^{-1})] at 140 ^oC	E_a/kJ mol^{-1}	T_g (^oC)
PS-3,4,5-triOH	-4.5	94	233
PS-3,4-diOH	-5.5	110	199
PS-3,5-diOH	-5.8	114	227
PS-4-OH	-8.4	154	187

3.2.5.2 Reorientational Dynamics in Phenolic Polymers

The Arrhenius-type behavior of proton transport in phenolic polymers suggests that the proton transport in these systems is primarily governed by the initial proton transfer step and the contribution of segmental motions is low over the temperature range investigated here. The following discussion highlighting the differences in proton conducting behavior between *N*-heterocyclic and phenolic polymers further supports this assumption (*i*) It has been well established that the PT in *N*-heterocycle-based polymers (for e.g. imidazole) is limited by the reorientation step.[10-12] A consequence of this is that lower T_g values are known to assist the reorientational dynamics in *N*-heterocyclic polymers due to the enhanced flexibility of the system.[8-9,21] Since proton transport in *N*-heterocycles is limited by reorientation, E_a for PT can be directly correlated to the reorientation barrier, which in turn is favored by lower T_g values (enhanced segmental

motion of polymer side chains). Thus, if reorientation is the rate-determining step for PT, then one should observe a direct correlation between E_a and T_g. If our hypothesis that phenols exhibit a low barrier for reorientation were correct, we do not expect to see a correlation between T_g and E_a in phenolic polymers. Indeed, we find that PS-3,4,5-triOH, with the highest T_g has the lowest E_a of all the polymers, while PS-4-OH with the lowest T_g has the highest E_a (Table 3.2); and (*ii*) The proton conductivity in phenolic polymers increases with the increasing number of hydroxyl groups and is not offset by the accompanying increase in T_g, which further supports the hypothesis that proton conductivity is independent of the segmental motion of polymer side chains. This observation is in sharp contrast to that observed with *N*-heterocycle-based polymers where the density of PT moieties did not result in enhanced conductivity.[6] This is attributed to the increase in T_g, which in turn hampers the segmental motion of polymer side chains. Thus, considering the Arrhenius-type proton conduction, inverse correlation between T_g and E_a, and the increase in conductivity with increasing density of PT moieties, it is reasonable to suggest that the PT in phenols is not limited by reorientation over the temperature range investigated here.

3.2.5.3 Proton Conductivity of PS-3,4,5-triOH versus Pyrogallol

We had hypothesized that utilizing a functional moiety which lowers the reorientational barrier would enhance the overall PT and hence would help lower the gap in conductivity between polymers and the corresponding small molecules. Having demonstrated that polymers based on phenols exhibit lower barrier rotations, we wanted to test if the gap in conductivity between polymers and the corresponding small

molecules can be bridged. To test this, the proton conductivity of pyrogallol, small molecule analog of the best performing PS-3,4,5-triOH polymer, was evaluated and compared with PS-3,4,5-triOH (Figure 3.4). As expected, the proton conductivity of PS-3,4,5-triOH polymer indeed compares very well with the molten state conductivities of the corresponding small molecule, pyrogallol. In contrast, the proton conductivities observed in imidazole based homopolymers are at least two orders of magnitude lower than the molten state conductivity of imidazole, which is attributed to be arising from the restricted reorientational dynamics with immobilization.[3]

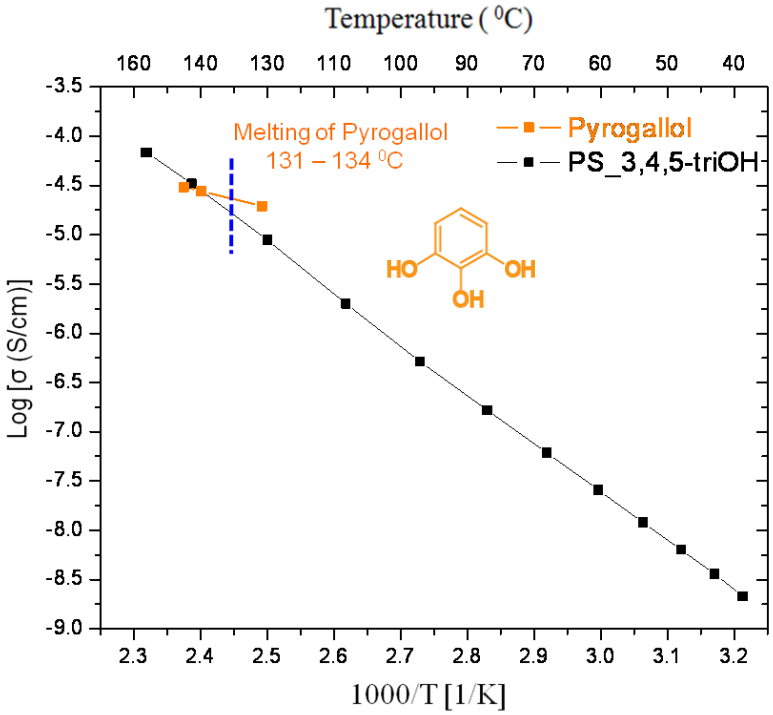

Figure 3.4 Proton conductivity of PS-3,4,5-triOH in comparison with the corresponding small molecule, pyrogallol.

3.2.5.4 Hydrogen Bond Network in Protonated Pentamers of Phenolic Polymers

Although the proton conductivity of phenolic polymers increases with increasing number of –OH moieties, the increase is not linear. That is, while the difference in conductivities between PS-3,4,5-triOH and PS-3,4-diOH is only an order of magnitude, the difference between PS-3,4-diOH and PS-4-OH is more than 3 orders of magnitude (Table 3.2). This difference cannot simply be explained based on the number of –OH groups. To gain insights into the observed trend in proton conductivity, hydrogen-bond networks in protonated pentamers of these polymers were investigated using DFT (LSDA/6-311G(d,p)) (Figure 3.5). PS-4-OH was not found to form a continuous hydrogen bond network; instead it splits into dimers with the extra proton localized between the first dimer. For further proton translocation, the dimer between the first two

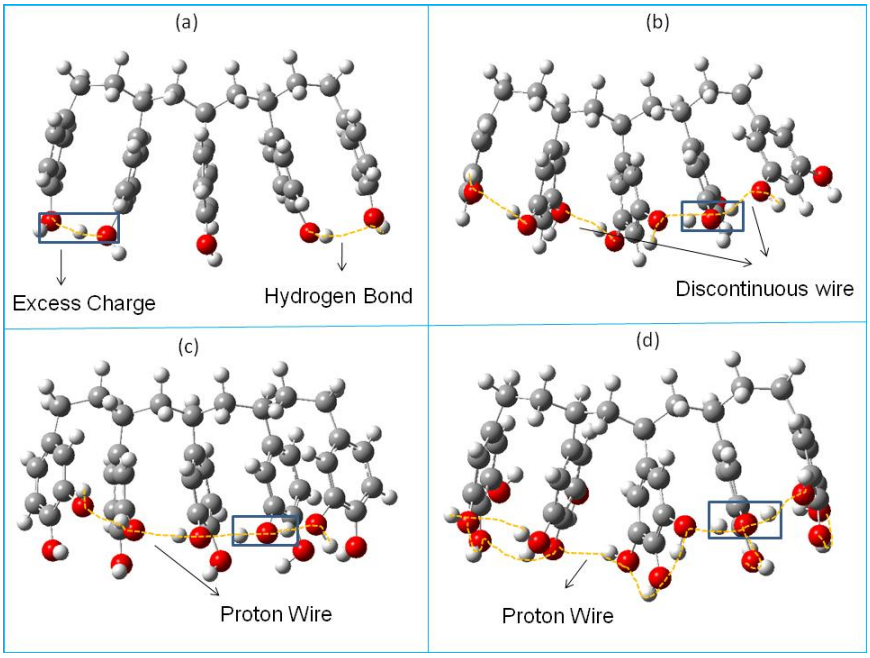

Figure 3.5 Proton wires of pentamers: (a) PS-4-OH; (b) PS-3,5-diOH; (c) PS-3,4-diOH; and (d) PS-3,4,5-triOH.

units has to break and a dimer between the second and the third units must form. As such, proton translocation in PS-4-OH requires a series of hydrogen-bond breaking and forming events, which are likely limited by higher barriers. PS-3,5-diOH also does not form an extended hydrogen bond network. However, it does form localized continuous networks of a trimer and dimer. Thus, proton translocation proceeds with minimal hydrogen bond breaking and forming events compared to PS-4-OH.

On the other hand, PS-3,4-diOH and PS-3,4,5-triOH form extended networks with both inter- and intra-molecular hydrogen bonds over the entire proton wire, which presumably facilitates proton translocation with lower barriers. Thus, the functional groups capable of forming both inter- and intra-molecular hydrogen bonds have greater propensities of providing continuous pathways for efficient proton shuttling across the scaffold. These same groups exhibit the highest proton conductivities in Figure 3.3. The modeling studies are carried out for simple oligomers and for intramolecular proton hopping. Although this provides fundamental insights into the need for multiple hydroxyl groups and thus the trends, it should be noted that they do not capture the complexities of proton transfer in bulk material where interchain hydrogen bonds also play a key role.

3.2.5.5 Effect of Humidity on Proton Conductivity

Finally, we also envisaged the possibility that conductivities would be enhanced with humidity, as water would add to the available pathways for proton transduction at lower temperatures. To test this, polymer thin films were cast from DMF solution and sandwiched between two gas diffusion electrodes. The polymer films were then exposed to 30% relative humidity and the conductivities were measured from room temperature to

150 ^{o}C. Gas diffusion electrodes were employed to allow for considerable gas flow over the sample in order to speed equilibration during measurement. The proton conductivities are shown in Figure 3.6. As anticipated, the proton conductivities of the phenolic polymers were enhanced by about two orders of magnitude, particularly in the lower temperature regime.

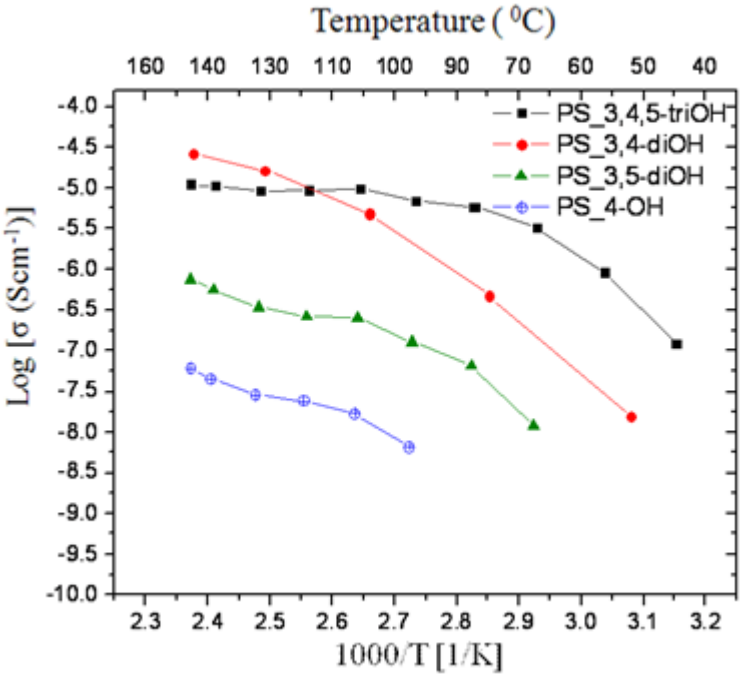

Figure 3.6. Proton conductivity of phenolic polymers with 30% relative humidity.

3.3 Summary

In summary, we have demonstrated that (*i*) phenolic systems can conduct protons under anhydrous conditions by forming a dynamic hydrogen bond network, akin to that observed in water, (*ii*) proton wires can be regenerated simply by rotating about the C-O bond, (*iii*) the 'single-site' hydrogen bond donor/acceptor feature in phenols facilitates

reorientational dynamics, and (*iv*) the proton conductivity of the best performing PS-3,4,5-triOH compares very well with the corresponding small molecules, pyrogallol. Perhaps, the most important conclusion is that while the classical search for functional groups involved acidic (-SO_3H, -H_2PO_3) or basic functional groups (imidazoles, triazoles)[1] to conduct protons, it is equally (if not more) important to consider dynamic hydrogen bonding systems for PT. In other words, reorientation should be considered as a crucial design parameter for protogenic groups in PT. Although other systems (*e.g.* phosphonic acid) can be envisioned to require minimal reorientation, the PT in these materials has not yet been examined in that context. Thus, we believe that our findings pave the way for the design of new protogenic groups with minimum reorientation barrier for efficient proton transport This design principle, in concert with nanostructuring strategies, will likely lead to proton transport materials with markedly advanced performance.

3.4 Experimental Details

3.4.1 General Materials and Methods

All the reagents were purchased from commercial sources and were used as received, unless otherwise noted. Poly(4-vinylphenol) (average Mw ca. 25,000) was obtained from Sigma Aldrich and was dried under vacuum at 120 ^{o}C for 24 h prior to use. Tetrahydrofuran (THF) was obtained from Fisher Scientific and was freshly distilled over sodium-benzophenone prior to use. Anhydrous dimethylformamide (DMF) and toluene were obtained from Sigma Aldrich and used as received. Pyrogallol (Sigma Aldrich, 99%) was recrystallized from xylenes, dried under vacuum at 50 ^{o}C and stored in a glove

box. Azobisisobutyronitrile (AIBN) was recrystallized from methanol and dried under vacuum prior to use.

^{1}H NMR spectra were recorded on a Bruker 400 MHz NMR spectrometer using the residual proton resonance of the solvent as the internal standard. Chemical shifts (δ) and coupling constants (*J*) are reported in parts per million (ppm) and Hertz, respectively. The following abbreviations are used for the peak multiplicities: s, singlet; d, doublet; t, triplet; m, multiplet; dd, doublet of doublet; bs, broad singlet; bm, broad multiplet. ^{13}C NMR spectra were proton decoupled and recorded on a Bruker 100 MHz NMR spectrometer using the carbon signal of the dueterated solvent as the internal standard. The molecular weights of the polymers were determined by gel permeation chromatography (GPC) using THF as eluent and toluene as the internal reference. PS standards were used for calibration and the output was received and analyzed using RI detector. Flash chromatography was performed using combiflash with normal phase Redi*sep R*f silica columns. Silica plates with F-254 indicator were used for analytical thin layer chromatography. FT-IR spectra were recorded on a Bruker Alpha FT-IR spectrometer. ATR-IR spectra were recorded on a Perkin Elmer Spectrum 100 equipped with ATR sampling. The polymer films were drop cast from DMF solution on to the silicon wafer and were dried on a hot plate at 160 ^{o}C for 3 days inside the glove box.

3.4.2 TGA and DSC Analysis

Polymer samples were dried under vacuum at 120 ^{o}C for 24 h and were used immediately for TGA and DSC analysis. Thermal stabilities of the polymers were investigated using a TA Instruments TGA 2950 thermogravimetric analyzer. The samples

(~ 10 mg) were heated from room temperature to 600 ^{o}C at a rate of 10 ^{o}C/min under a flow of nitrogen and at 1 ^{o}C/min under air. Glass transition temperature (T_g) of the polymers were obtained by differential scanning calorimeter (DSC) using TA instruments Dupont DSC 2910. The samples (~ 10 mg) were loaded into aluminum pans and were heated from room temperature to 260 ^{o}C with a rate of 10 ^{o}C/min under a flow of nitrogen (50 mL/min). Each sample was measured through two heating cycles and the data from the second heating cycle is considered.

3.4.3 Electrochemical Impedance Measurements

The impedance response of each polymer sample was measured from 0.1 Hz-10^7 Hz with a sinusoidal excitation voltage of 0.1 V_{rms} using a Solartron 1260 impedance/gain phase analyzer. The resistance (R) values were obtained by geometrically fitting a semicircular arc to the bulk response in the Z' vs. Z" plane and conductivities were derived from the equation ($\sigma = \ell/RA$), where ℓ and A are the thickness and the area of the polymer film, respectively. Conductivities lower than 10^{-9} S cm^{-1} are generally considered to be below the sensitivity of the instrument for the particular geometries used, and hence the absolute numbers below this value are not considered accurate.

Membrane preparation for vacuum measurements

Kapton tape with a hole of thickness 127 μm and an area of 0.0792 cm^2 was placed onto a gold coated electrode and the polymer films were drop cast from concentrated DMF solution onto the hole. Polymer film thickness and the contact area between the membrane and the electrode were determined by the dimensions of the hole and hence were held constant. Polymer films were prepared inside the glove box on a hot plate and

were annealed at 150 ^{o}C for 15 h prior to measurements. Films were then placed between two gold coated blocking electrodes and transferred immediately to a vacuum oven and the proton conductivities were characterized by impedance spectroscopy from 40 ^{o}C to 160 ^{o}C. The samples were initially heated from room temperature to 160 ^{o}C and were held at 160 ^{o}C (to ensure complete removal of the residual DMF) until the polymers displayed constant conductivity over at least 10 hours. The samples were then slowly cooled from 160 ^{o}C to room temperature and the conductivities during the cooling cycle are reported for all the polymers.

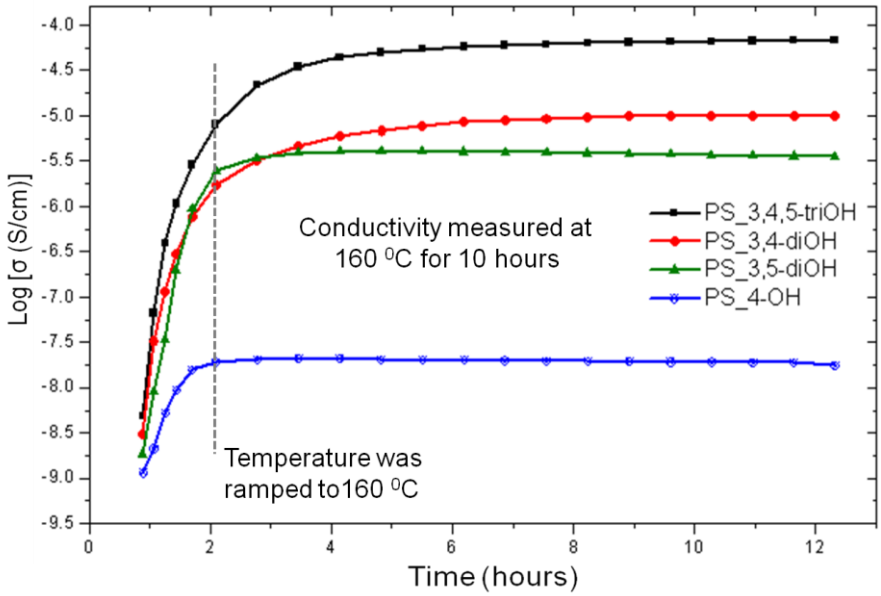

Figure 3.7 Proton conductivity of phenolic polymers (at 160 ^{o}C) as a function of time.

Membrane preparation for humidity measurements

A Teflon tape spacer with a hole of thickness 292 µm and an area of 0.0792 cm^2 was placed onto a Spectracarb 2050-A carbon gas diffusion electrode into which polymer films were drop cast from concentrated DMF solution and sandwiched with another gas

diffusion electrode. These membrane electrode assemblies were prepared on a hot plate and were annealed at 100 ^{o}C prior to measurements, then were clamped between two porous stainless steel disc electrodes (with 40 micron pores). This arrangement of electrodes was specifically designed to allow for considerable gas flow over the sample in order to speed equilibration during measurement. The samples were first analyzed via impedance spectroscopy while annealing for over 10 hours under vacuum up to 150 ^{o}C, following similar protocol described above. Then, the assemblies were transferred to an ESPEC SH-241 temperature/humidity chamber and were exposed to 30% relative humidity at room temperature for 12 hours. Directly after humidifying, the temperature was ramped up to 150 ^{o}C at a rate of 0.67 ^{o}C/min and impedance spectra were measured approximately every half hour (roughly every 20 ^{o}C).

Sample preparation for pyrogallol

Pyrogallol was melted inside the glove box and filled into a custom electrode assembly consisting of two brass electrodes inserted into a segment of PTFE tubing - the sample is confined between the electrodes in a cylindrical volume of length 0.3870 cm and area 0.0792 cm^2. This material was analyzed at high temperatures in the melt state using impedance spectroscopy, following a similar procedure described above for measurements under vacuum; only a short range of temperatures could be investigated, since the sample crystallized while cooling below 130 ^{o}C and has an immeasurably low conductivity in this state.

Activation energy (E_a) calculations

The activation energy is the minimum energy required for proton conduction through the polymer membrane. It was calculated using the Arrhenius equation ($\ln \sigma = \ln \sigma_o$ –

(E_a/RT)), where R is the universal gas constant and T is the temperature in Kelvin. The E_a was obtained from the slope of the linear fit of ln σ vs. 1/T. The pre-exponential factor (ln σ_o) was neglected.

3.4.4 Computational Methods

Density functional theory (LSDA)[22-24] as implemented in Gaussian03 and Gaussian Development Version was used to compute structures, energies and frequencies. PS-4-OH dimer was formed by optimizing with LSDA/6-311G(d,p).[25-26] The LSDA functional (level of theory) was used because it is known to capture π-π interactions with accuracy comparable to MP2.[15] The 6-311G(d,p) basis set was used because of our previous calculations finding that this basis set captures hydrogen bonding and proton addition in

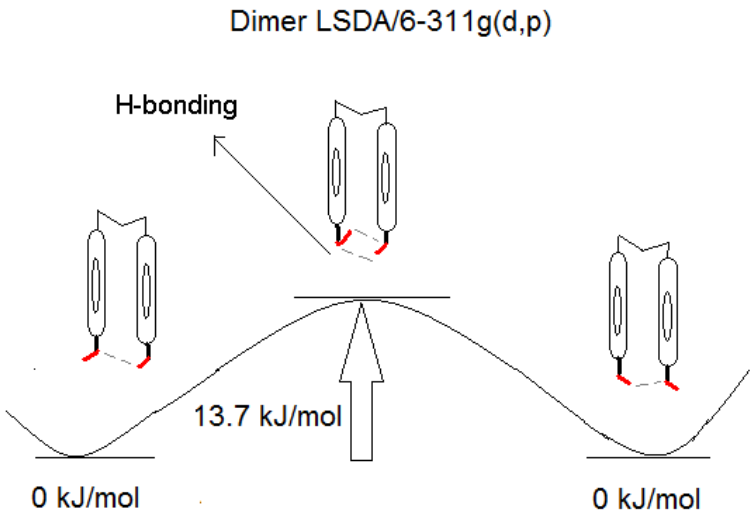

Figure 3.8 Structures of PS-4-OH dimer and the transition state.

organic and inorganic networks. The reoriented dimer structure was initialized by rotating the two OH groups in the PS-4-OH dimer to mimic the re-oriented structure; we

then optimized this initial structure. The transition state between the two minima was found using the quadratic synchronous transit (QST2). Frequency calculations were performed for each optimization to confirm classifications as minima and saddle points. Pentamers and protonated pentamers (formed by adding an extra proton) of PS-4-OH, PS-3,5-di-OH, PS-3,4-di-OH, and PS-3,4,5-tri-OH were initialized with LSDA/6-311G(d,p) by fixing the first and last carbons of the backbone atoms to mimic a polymer system; we then optimized these initial structures.

3.4.5 Polymer Synthesis

Synthesis of 3,4,5-tri(t-butoxycarbonyloxy) Benzaldehyde (1)

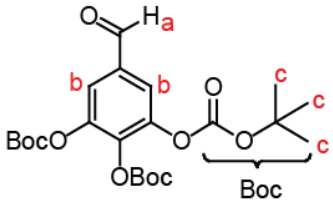

To a solution of 3,4,5-trihydroxy benzaldehyde (1.8 g, 10.5 mmol) in 70 mL THF was added *N*-*N*-diisopropylethylamine (DIPEA) (0.2 mL, 1.05 mmol), DMAP (64 mg, 0.53 mmol), and $(Boc)_2O$ (10.1 mL, 47.05 mmol) at room temperature under argon. The reaction mixture was continued to stir at room temperature for 3 h. THF was evaporated and the crude was taken up in ethyl acetate and washed with 1M NaOH and saturated NaCl solutions. The combined ethyl acetate layers were dried over Na_2SO_4, concentrated under reduced pressure and the crude was purified by column chromatography (SiO_2). The product was eluted with ethyl acetate/hexane (15:85 v/v) to afford the desired product (4.7 g, 98%) as colorless oil. ^{1}H NMR (400 MHz, $CDCl_3$) δ: 9.91 (s, 1H, a), 7.70

(s, 2H, b), 1.53 (s, 27H, c). ^{13}C NMR (100 MHz, $CDCl_3$) δ: 189.45, 150.08, 148.76, 144.66, 140.12, 133.75, 121.34, 84.93, 84.79, 27.65, 27.61.

Synthesis of 3,4,5-tri(t-butoxycarbonyloxy) Styrene (2)

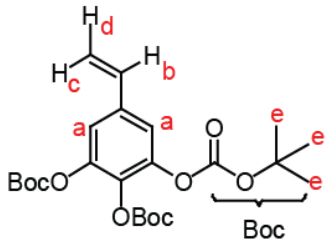

$MePPh_3Br$ (5.0 g, 13.94 mmol) and KO^tBu (1.56 g, 13.94 mmol) were taken in a 100 mL oven-dried schlenk flask and dried under vacuum for 30 min. The flask was cooled to 0 ^oC using ice bath and anhydrous THF (50 mL) was added under argon. The solution immediately turned yellow, indicating the formation of ylide. The reaction mixture was allowed to stir at 0 ^oC for 30 min and was then warmed to room temperature. A solution of compound **1** (4.22 g, 9.3 mmol) in 20 mL THF was added using syringe and the reaction mixture was continued to stir at room temperature for 12 h. The reaction was quenched by the addition of water and extracted with ethyl acetate. The combined ethyl acetate layers were dried over Na_2SO_4, concentrated under reduced pressure and the crude was purified by column chromatography (SiO_2). The product was eluted with ethyl acetate/hexane (15:85 v/v) to afford the desired product (2.96 g, 70%) as colorless oil. ^{1}H NMR (400 MHz, $CDCl_3$) δ: 7.18 (s, 2H, a), 6.65-6.58 (dd, *J* = 17.6, 10.9 Hz,1H, b), 5.71-5.67 (d, *J* = 17.6 Hz, 1H, c), 5.30-5.28 (d, *J* = 10.9 Hz, 1H, d), 1.53 (s, 27H, e). ^{13}C NMR (100 MHz, $CDCl_3$) δ: 150.36, 149.39, 143.78, 135.81, 134.86, 134.45, 117.85, 115.79, 84.00, 27.60, 27.56.

Synthesis of PS-3,4,5-triBoc Polymer

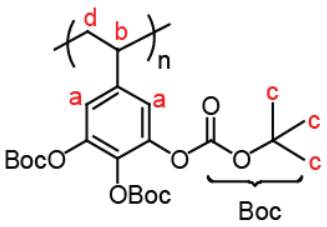

A solution of monomer **2** (2.5 g, 5.26 mmol) in 2.5 mL anhydrous toluene was taken in a 10 mL oven-dried schlenk flask under argon at room temperature. AIBN (9.1 mg, 0.06 mmol) was added and the reaction mixture was subjected to three freeze-pump-thaw cycles. It was stirred at room temperature for 5 min and transferred to an oil bath preheated to 90 ^{o}C. The polymerization was carried out with an argon inlet and the outlet connected to an oil bubbler. The polymerization was complete within 20 min. The polymer was diluted with THF and precipitated twice into hexane. The precipitate was filtered, washed several times with hexane, and dried under vacuum at 50 ^{o}C for 12 h to obtain the polymer (1.5 g, 60%) as white solid. GPC (THF) Mn: 60,000 g/mol; PDI: 1.5. ^{1}H NMR (400 MHz, $CDCl_3$) δ: 6.49 (bs, 2H, a, ArH), 1.74 (bs, 1H, b, -CH of polymer backbone), 1.40 (s, 27H, c, O-C(CH_3)$_3$), 1.00 (bs, 2H, d, -CH_2 of polymer backbone).

Synthesis of PS-3,4,5-triOH Polymer

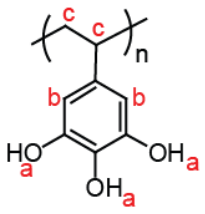

PS-3,4,5-triBoc (1.4 g, 3.09 mmol) was taken in 5 mL DCM at room temperature under argon and 5 mL trifluoro acetic acid (TFA) was added to it. The clear solution obtained was stirred at room temperature for 30 min, during which the solution initially turned turbid and finally a white precipitate was obtained. The precipitate was filtered,

washed thoroughly with DCM, and dried under vacuum at 50 ^{o}C for 24 h. The polymer (353 mg, 75%) was obtained as light brown powder. ^{1}H NMR (400 MHz, DMSO-d6) δ: 8.8-7.2 (2bs, 3H, a, -OH), 5.74 (bs, 2H, b, ArH), 2.2-0.5 (bm, 3H, c, -CH and -CH_2 of polymer backbone).

3,4-di(t-butoxycarbonyloxy) Benzaldehyde

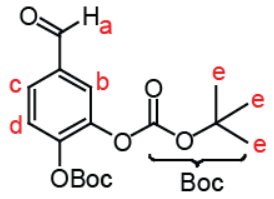

^{1}H NMR (400 MHz, $CDCl_3$) δ: 9.89 (s, 1H, a), 7.75 (d, *J* = 1.9 Hz, 1H, b), 7.73-7.70 (dd, *J* = 8.4, 1.9 Hz,1H, c), 7.40 (d, *J* = 8.4 Hz, 1H, d), 1.50 (s, 18H, e). ^{13}C NMR (100 MHz, $CDCl_3$) δ: 190.06, 150.27, 149.83, 147.29, 143.19, 134.55, 128.02, 123.90, 123.74, 84.50, 84.33, 27.49.

3,5-di(t-butoxycarbonyloxy) Benzaldehyde

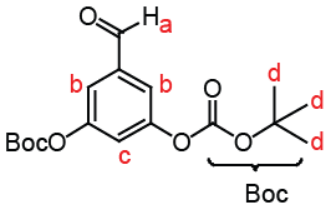

^{1}H NMR (400 MHz, $CDCl_3$) δ: 9.96 (s, 1H, a), 7.60 (d, *J* = 2.3 Hz, 2H, b), 7.33 (t, *J* = 2.3 Hz, 1H, c), 1.56 (s, 18H, d). ^{13}C NMR (100 MHz, $CDCl_3$) δ: 190.19, 152.17, 151.06, 138.15, 120.75, 119.56, 84.65, 27.79.

3,4-di(t-butoxycarbonyloxy) Styrene

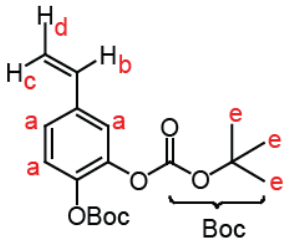

^{1}H NMR (400 MHz, $CDCl_3$) δ: 7.29-7.19 (m, 3H, a), 6.68-6.61 (dd, *J* = 17.8, 10.8 Hz, 1H, b), 5.71-5.67 (d, *J* = 17.8 Hz, 1H, c), 5.27-5.24 (d, *J* = 10.8 Hz, 1H, d), 1.55-1.54 (s, 18H, e). ^{13}C NMR (100 MHz, $CDCl_3$) δ: 150.74, 150.71, 142.59, 141.96, 136.41, 135.29, 124.21, 123.04, 120.51, 114.98, 83.77, 27.63.

3,5-di(t-butoxycarbonyloxy) Styrene

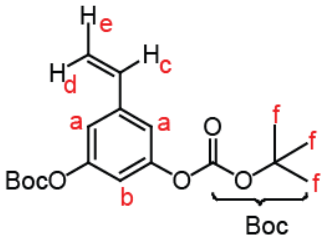

^{1}H NMR (400 MHz, $CDCl_3$) δ: 7.09-7.08 (d, *J* = 2.2 Hz, 2H, a), 6.98-6.97 (t, *J* = 2.2 Hz, 1H, b), 6.68-6.60 (dd, *J* = 17.6, 10.8 Hz, 1H, c), 5.76-5.71 (d, *J* = 17.6 Hz, 1H, d), 5.32-5.29 (d, *J* = 10.8 Hz, 1H, e), 1.55 (s, 18H, f). ^{13}C NMR (100 MHz, $CDCl_3$) δ: 151.54, 151.31, 139.79, 135.34, 116.28, 115.90, 114.01, 83.81, 27.69.

3,4,5-trimethoxy Styrene

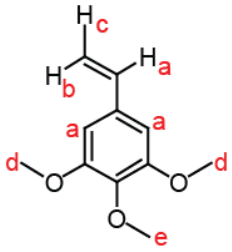

^{1}H NMR (400 MHz, $CDCl_3$) δ: 6.65-6.58 (dd, *J* = 17.6, 10.8 Hz, 1H and s, 2H, ArH, a), 5.66-5.62 (d, *J* = 17.6 Hz, 1H, b), 5.20-5.18 (d, *J* = 10.8 Hz, 1H, c), 3.85 (s, 6H, d), 3.82 (s, 3H, e). ^{13}C NMR (100 MHz, $CDCl_3$) δ: 153.29, 137.97, 136.76, 133.32, 113.24, 103.25, 60.88, 56.04.

PS-3,4-diBoc Polymer

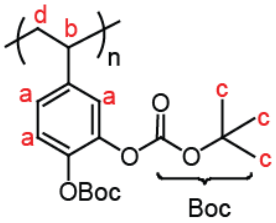

GPC (THF) Mn: 63,000 g/mol; PDI: 1.6. ^{1}H NMR (400 MHz, $CDCl_3$) δ: 7.1-6.2 (bm, 3H, a, ArH), 1.73 (bs, 1H, b, -CH of polymer backbone), 1.44 (s, 18H, c, O-C$(CH_3)_3$), 1.29 (bs, 2H, d, -CH_2 of polymer backbone).

PS-3,5-diBoc Polymer

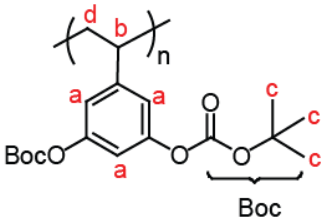

GPC (THF) Mn: 63,000 g/mol; PDI: 1.4. ^{1}H NMR (400 MHz, $CDCl_3$) δ: 6.9-6.1 (bm, 3H, a, ArH), 1.87 (bs, 1H, b, -CH of polymer backbone), 1.43 (s, 18H, c, O-C$(CH_3)_3$), 1.26 (bs, 2H, d, -CH_2 of polymer backbone).

PS-3,4,5-triOMe Polymer

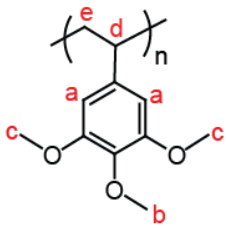

GPC (THF) Mn: 24,000; PDI; 1.34. ^{1}H NMR (400 MHz, $CDCl_3$) δ: 5.80-5.65 (bs, 2H, a, ArH,), 3.69 (bs, 3H, b, -OMe), 3,53 (bs, 6H, c, -OMe) 1.81 (bs, 1H, d, -CH of polymer backbone), 1.41 (bs, 2H, e, -CH_2 of polymer backbone).

PS-3,4-diOH Polymer

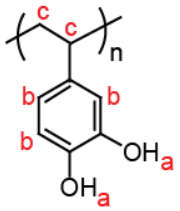

^{1}H NMR (400 MHz, DMSO-d6) δ: 8.36 (bs, 2H, a, -OH), 6.7-5.5 (bm, 3H, b, ArH), 2.2-0.5 (bm, 3H, c, -CH and -CH_2 of polymer backbone).

PS-3,5-diOH Polymer

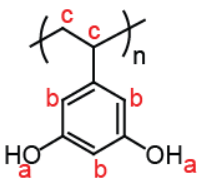

^{1}H NMR (400 MHz, DMSO-d6) δ: 8.69 (bs, 2H, a, -OH), 6.2-5.3 (2bs, 3H, b, ArH), 2.2-0.5 (bm, 3H, c, -CH and -CH_2 of polymer backbone).

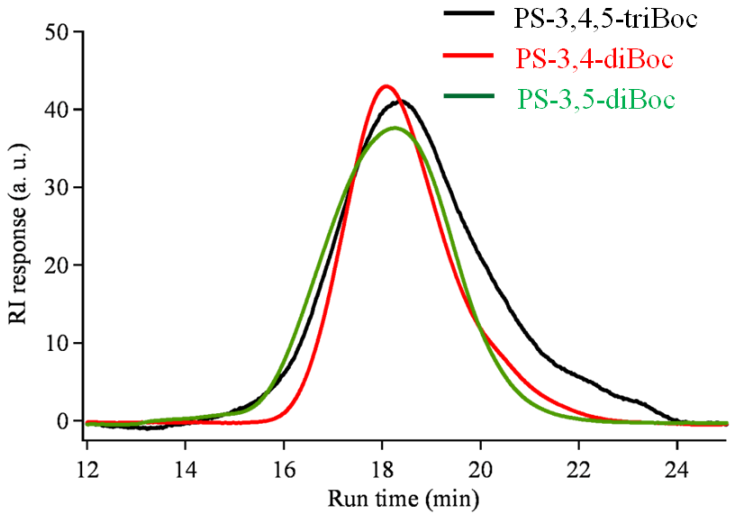

Figure 3.9 GPC (THF) traces of Boc protected phenolic polymers.

a)

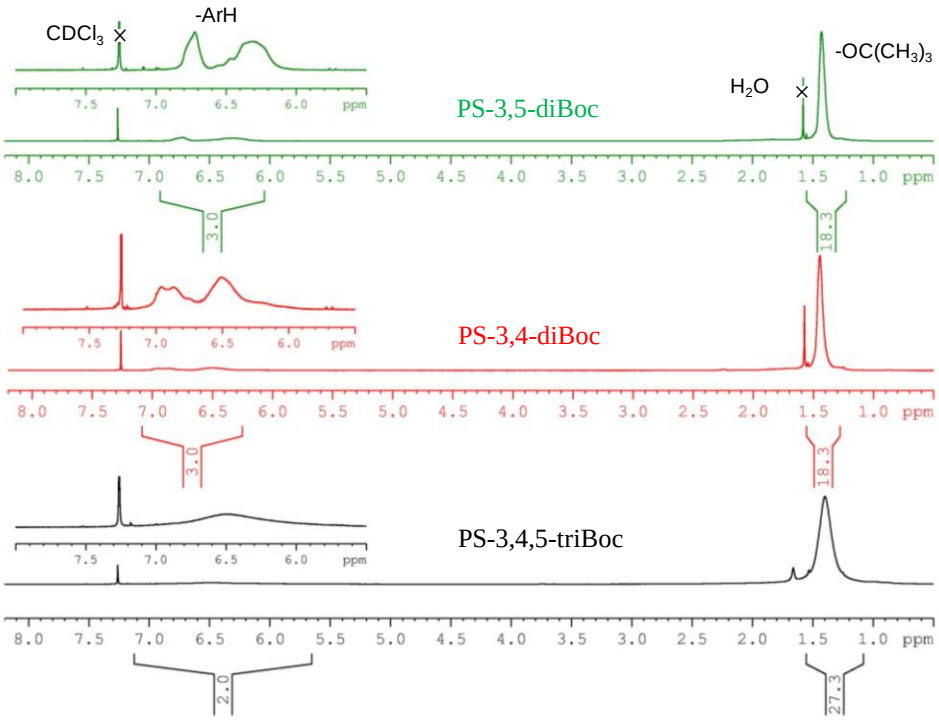

b)

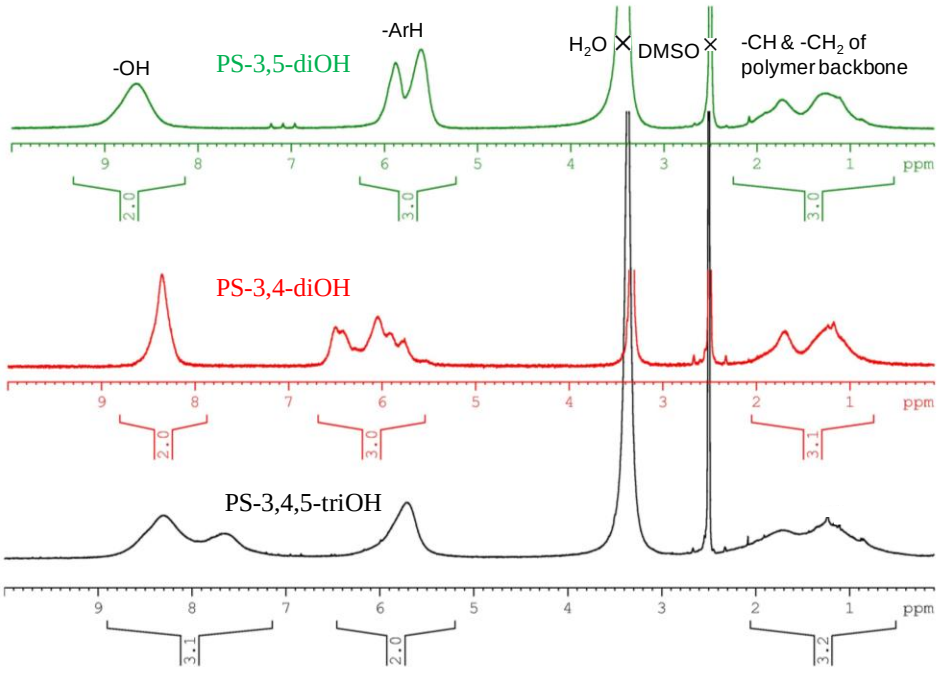

Figure 3.10 [1]H NMR spectra of (a) Boc protected phenolic polymers and (b) phenolic polymers.

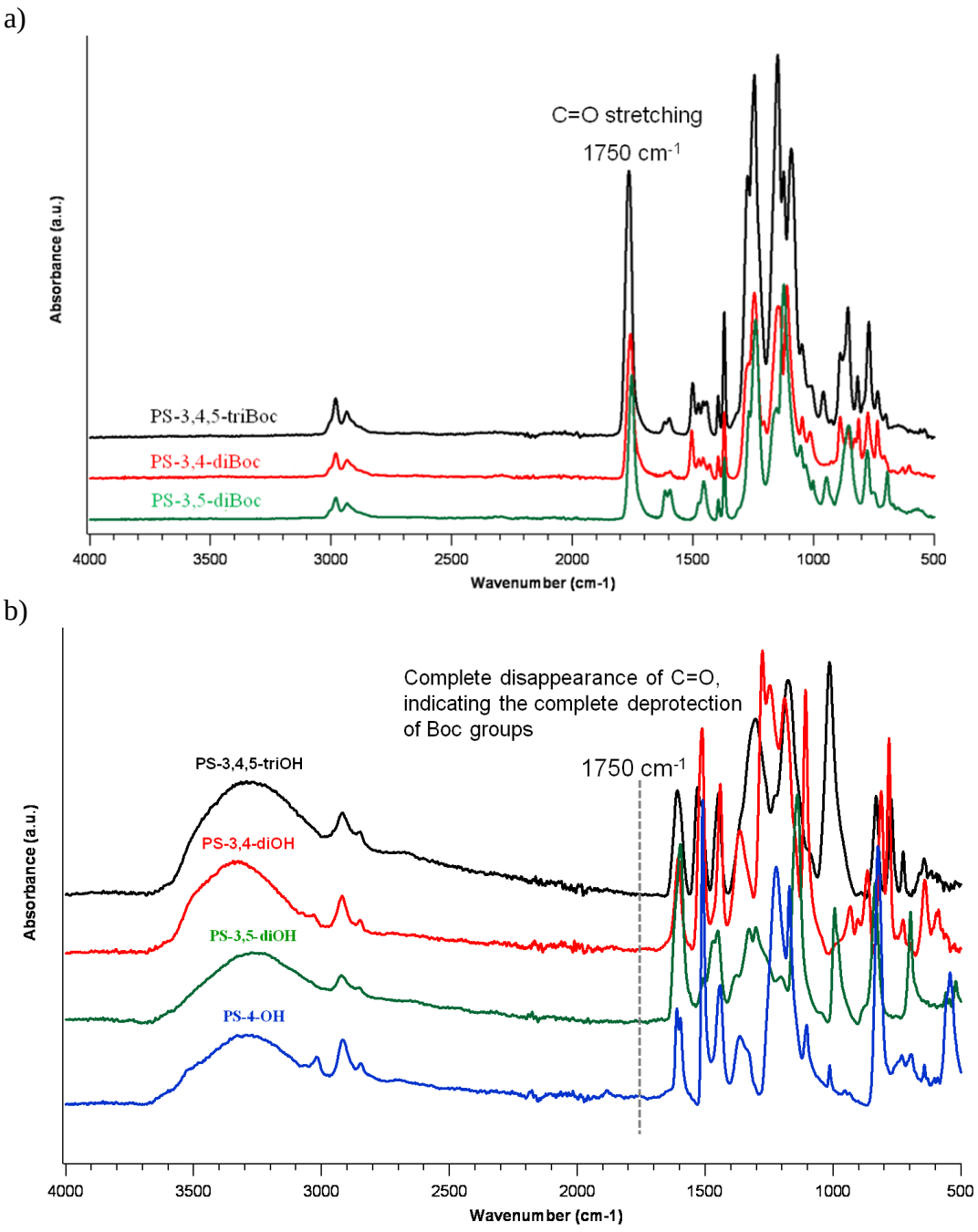

Figure 3.11 FTIR spectra of (a) Boc protected phenolic polymers and (b) phenolic polymers.

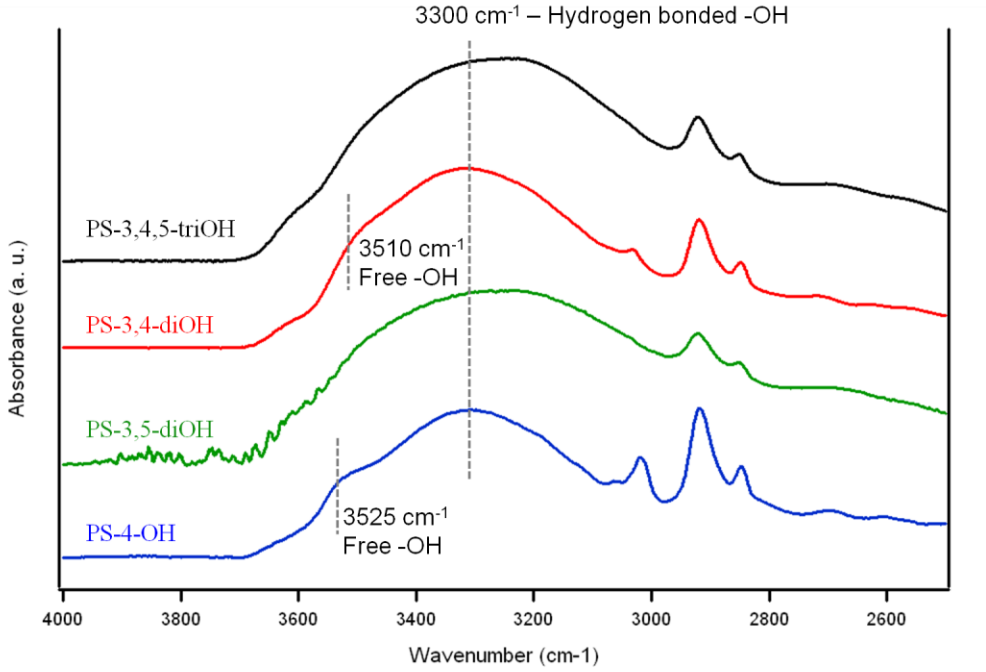

Figure 3.12 ATR-IR spectra of phenolic polymers (thin films).

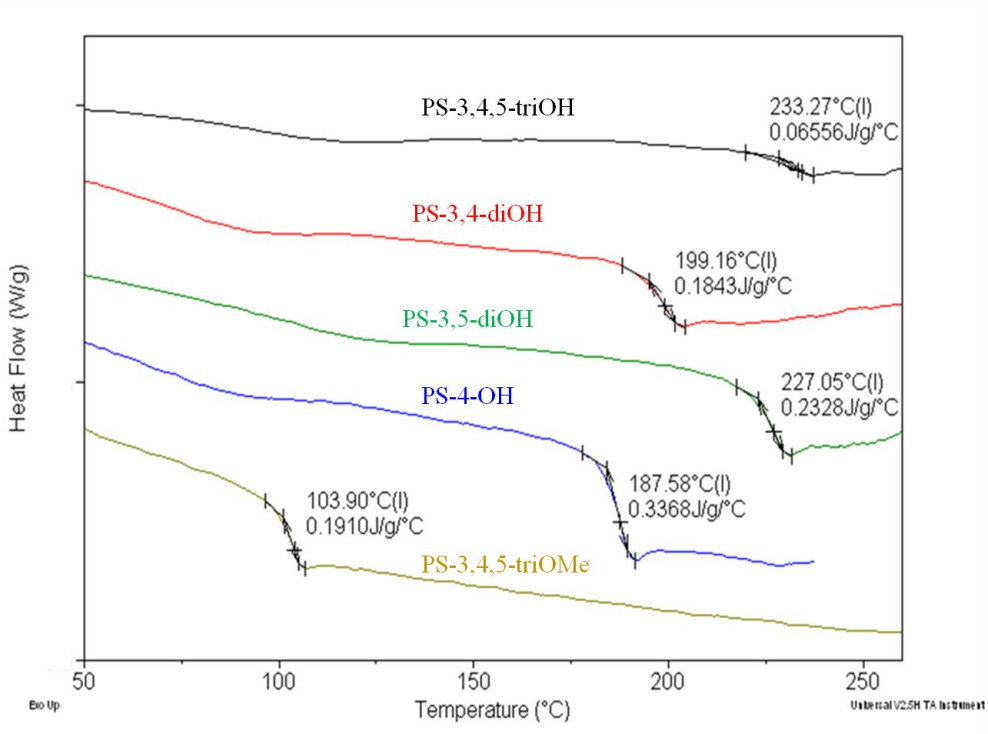

Figure 3.13 DSC traces of phenolic polymers.

a)

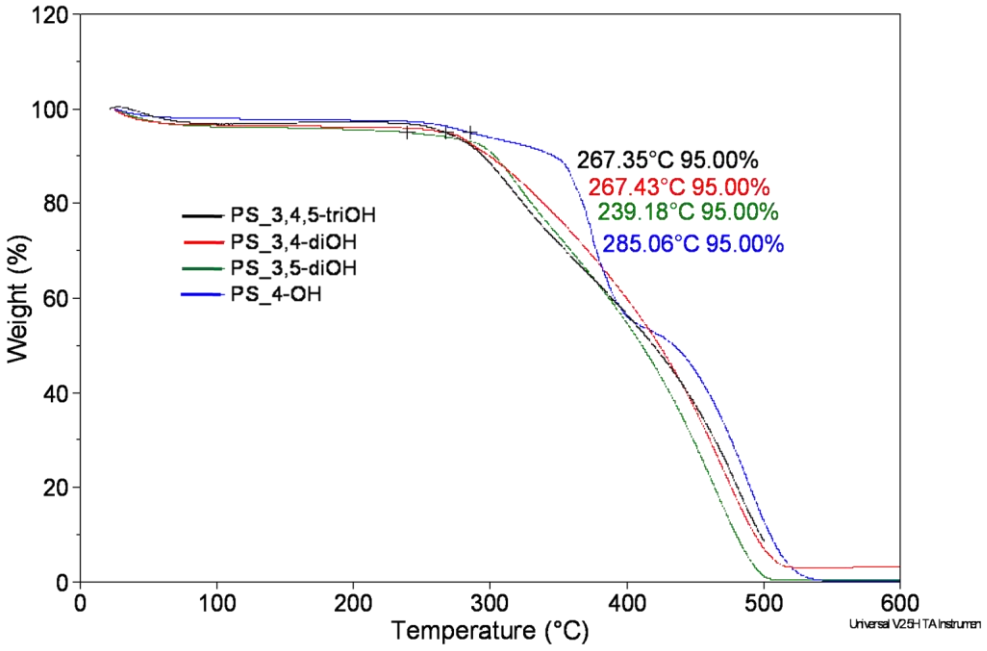

b)

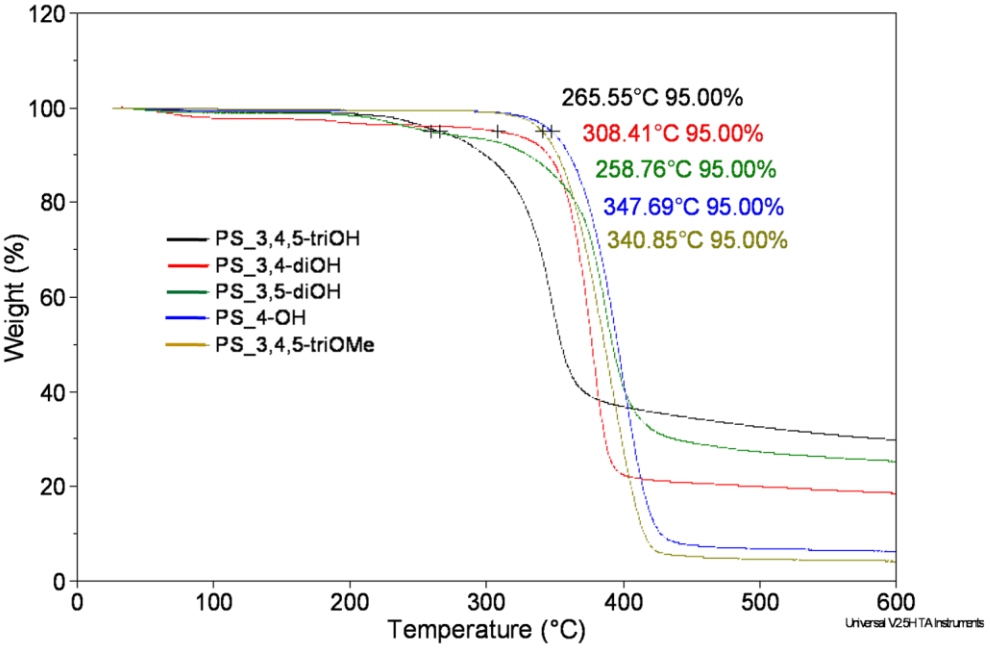

Figure 3.14 TGA traces of phenolic polymers (a) when heated under air at 1 ^{o}C/min and (b) when heated under nitrogen at 10 ^{o}C/min.

3.5 References

1. Kawada, A.; McGhie, A. R.; Labes, M. M., Protonic conductivity in imidazole single crystal. *J. Chem. Phys.* **1970**, *52*, 3121-3125.

2. Kreuer, K. D.; Fuchs, A.; Ise, M.; Spaeth, M.; Maier, J., Imidazole and pyrazole-based proton conducting polymers and liquids. *Electrochim. Acta* **1998**, *43*, 1281-1288.

3. Kreuer, K. D.; Paddison, S. J.; Spohr, E.; Schuster, M., Transport in proton conductors for fuel-cell applications: Simulations, elementary reactions, and phenomenology. *Chem. Rev.* **2004**, *104*, 4637-4678.

4. Zhou, Z.; Li, S. W.; Zhang, Y. L.; Liu, M. L.; Li, W., Promotion of proton conduction in polymer electrolyte membranes by 1H-1,2,3-triazole. *J. Am. Chem. Soc.* **2005**, *127*, 10824-10825.

5. Bozkurt, A.; Meyer, W. H., Proton conducting blends of poly(4-vinylimidazole) with phosphoric acid. *Solid State Ionics* **2001**, *138*, 259-265.

6. Martwiset, S.; Yavuzcetin, O.; Thorn, M.; Versek, C.; Tuominen, M.; Coughlin, E. B., Proton Conducting Polymers Containing 1H-1,2,3-Triazole Moieties. *J. Polym. Sci. Pol. Chem.* **2009**, *47*, 188-196.

7. Nagamani, C.; Versek, C.; Thorn, M.; Tuominen, M. T.; Thayumanavan, S., Proton Conduction in 1H-1,2,3-triazole Polymers: Imidazole-Like or Pyrazole-Like? *J. Polym. Sci. Pol. Chem.* **2010**, *48*, 1851-1858.

8. Persson, J. C.; Jannasch, P., Intrinsically proton-conducting benzimidazole units tethered to polysiloxanes. *Macromolecules* **2005**, *38*, 3283-3289.

9. Schuster, M. F. H.; Meyer, W. H.; Schuster, M.; Kreuer, K. D., Toward a new type of anhydrous organic proton conductor based on immobilized imidazole. *Chem. Mat.* **2004**, *16*, 329-337.

10. Bredas, J. L.; Poskin, M. P.; Delhalle, J.; Andre, J. M.; Chojnacki, H., Electronic-structure of hydrogen-bonded imidazole chains - Influence of the proton position *J. Phys. Chem.* **1984**, *88*, 5882-5887.

11. Daycock, J. T.; Jones, G. P.; Evans, J. R. N.; Thomas, J. M., Rotation of imidazole in solid state and its significance in deciding nature of charge migration in biological materials. *Nature* **1968**, *218*, 672-673.

12. Munch, W.; Kreuer, K. D.; Silvestri, W.; Maier, J.; Seifert, G., The diffusion mechanism of an excess proton in imidazole molecule chains: first results of an ab initio molecular dynamics study. *Solid State Ionics* **2001**, *145*, 437-443.

13. Markovitch, O.; Chen, H.; Izvekov, S.; Paesani, F.; Voth, G. A.; Agmon, N., Special pair dance and partner selection: Elementary steps in proton transport in liquid water. *J. Phys. Chem. B* **2008**, *112*, 9456-9466.

14. Fischbach, I.; Spiess, H. W.; Saalwachter, K.; Goward, G. R., Solid state NMR spectroscopic investigations of model compounds for imidazole-based proton conductors. *J. Phys. Chem. B* **2004**, *108*, 18500-18508.

15. Swart, M.; van der Wijst, T.; Guerra, C. F.; Bickelhaupt, F. M., pi-pi stacking tackled with density functional theory. *J. Mol. Model.* **2007**, *13*, 1245-1257.

16. Cheng, Q. Y.; Evangelista, F. A.; Simmonett, A. C.; Yamaguchi, Y.; Schaefer, H. F., Water Dimer Radical Cation: Structures, Vibrational Frequencies, and Energetics. *J. Phys. Chem. A* **2009**, *113*, 13779-13789.

17. Laage, D.; Hynes, J. T., A molecular jump mechanism of water reorientation. *Science* **2006**, *311*, 832-835.

18. Mukherjee, B.; Maiti, P. K.; Dasgupta, C.; Sood, A. K., Jump Reorientation of Water Molecules Confined in Narrow Carbon Nanotubes. *J. Phys. Chem. B* **2009**, *113*, 10322-10330.

19. Persson, J. C.; Jannasch, P., Self-conducting benzimidazole oligomers for proton transport. *Chem. Mat.* **2003**, *15*, 3044-3045.

20. Yu, S.; Zhang, H.; Xiao, L.; Choe, E. W.; Benicewicz, B. C., Synthesis of Poly (2,2 '-(1,4-phenylene)5,5 '-bibenzimidazole) (para-PBI) and Phosphoric Acid Doped Membrane for Fuel Cells. *Fuel Cells* **2009**, *9*, 318-324.

21. Woudenberg, R. C.; Yavuzeetin, O.; Tuorninen, M. T.; Coughlin, E. B., Intrinsically proton conducting polymers and copolymers containing benzimidazole moieties: Glass transition effects. *Solid State Ionics* **2007**, *178*, 1135-1141.

22. Hohenberg, P.; Kohn, W., Inhomogeneous electron gas. *Phys. Rev. B* **1964**, *136*, B864-B871.

23. Kohn, W.; Sham, L. J., Self-consistent equations including exchange and correlation effects. *Physical Review* **1965**, *140*, A1133-A1138.

24. Krishnan, R.; Binkley, J. S.; Seeger, R.; Pople, J. A., Self-consistent molecular-orbital methods .20. Basis set for correlated wave-functions. *J. Chem. Phys.* **1980**, *72*, 650-654.

25. McLean, A. D.; Chandler, G. S., Contracted gaussian-basis sets for molecular calculations .1. 2nd row atoms, Z=11-18. *J. Chem. Phys.* **1980**, *72*, 5639-5648.

26. Vosko, S. H.; Wilk, L.; Nusair, M., Accurate spin-dependent electron liquid correlation energies for local spin-density calculations - A critical analysis. *Can. J. Phys.* **1980**, *58*, 1200-1211.

CHAPTER 4

PHENOL-BASED TWO-DIMENSIONAL BIARYL PROTON CONDUCTING POLYMERS

4.1 Introduction

Proton transporting polymers that can selectively and efficiently transfer protons play a pivotal role in the overall operation of a hydrogen fuel cell. Polymers that can conduct protons under anhydrous conditions are particularly sought after for applications in moderate to high temperature hydrogen fuel cells. Polymers based on *N*-heterocycles such as imidazole, triazole and benzimidazole have been widely studied to develop efficient anhydrous proton conducting polymers.[1-8] We have also recently introduced a new class of functional groups, phenols, for anhydrous proton transport.[9] A majority of the polymers that have been studied so far for anhydrous PT are based on linear polymer architecture such as polyacrylate, polysiloxane, and polystyrene. Both intra-chain and inter-chain proton transport are important for long range proton transport. We thought that a molecular architecture that presents PT moieties in orthogonal planes would be interesting as it allows for greater inter-chain interactions along with intra-chain interactions among PT moieties, thereby enhancing the net proton transport (Figure 4.1).

Biaryl would be an interesting scaffold for the proposed molecular design because (i) the steric interactions between the ortho hydrogen atoms is very well known to lead to a twist in the phenyl rings,[10-11] thereby inducing the two-dimensionality at the molecular level (ii) both the phenyl rings of the biaryl scaffold can be functionalized with PT moieties, thus providing an interesting two-dimensional spatial disposition of the PT

moieties (iii) a polymerizable double bond can be easily introduced onto one of the phenyl rings to generate a biaryl monomer, which could be easily polymerized similar to that of styrene. We chose to introduce phenols as the proton transporting moieties on the biaryl architecture. A space-filling model of a pentahydroxy biaryl compound, energy minimized using MM2 calculations, supports the presumed two-dimensional spatial disposition of the phenolic moieties (Figure 4.1). The dihedral angle between the phenyl rings was found to be 55 degrees. In this work, we report the synthesis and characterization, thermal properties, and proton conductivity of biaryl phenolic polymers. To further investigate if the biaryl architecture provides any advantage over the styrenic architecture, the proton conductivities of the biaryl and styrenic hydroxy polymers shown in Chart 4.1 are compared.

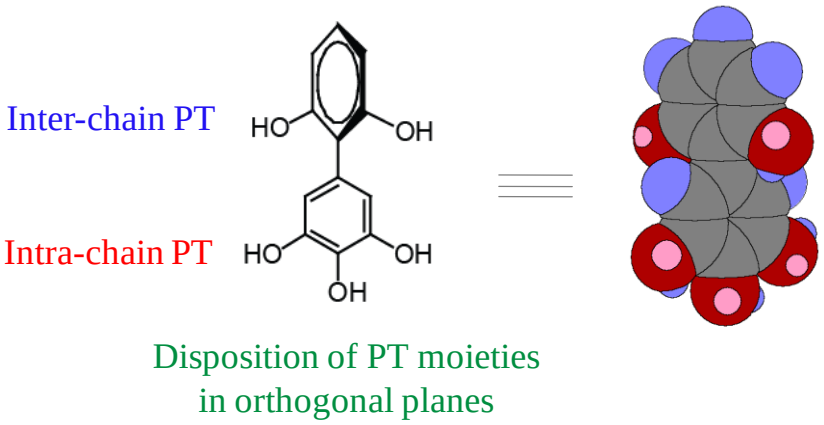

Figure 4.1 Space filling model of biphenyl-3,4,5,2',6'-pentaol illustrating the two-dimensional disposition of proton transporting -OH moieties.

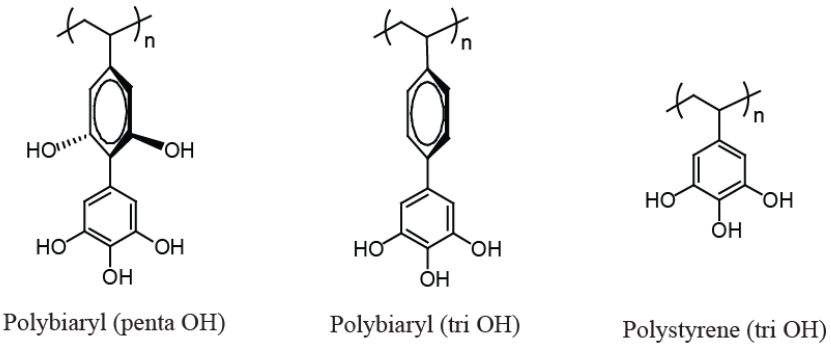

Chart 4.1 Structures of biaryl and styrenic hydroxy polymers.

4.2. Results and Discussion

4.2.1 Synthesis and Characterization

Boc protected biaryl monomers were obtained by coupling the appropriately functionalized top and bottom phenyl rings via Stille coupling reaction, followed by subsequent reduction, oxidation, deprotection, and protection steps. The synthetic Schemes for the biaryl monomers are shown in Schemes 4.1 and 4.2. The monomers were polymerized via free radical polymerization with AIBN as the initiator (Scheme 4.3). Monomer: AIBN ratio as well as the solvent was optimized to get a good control over polymerization. GPC chromatograms of the Boc-protected biaryl polymers are shown in Figure 4.2. All the polymers exhibit unimodal distribution. The Boc groups were further deprotected using TFA/DCM to obtain the corresponding biaryl hydroxy polymers. The polymers were obtained in good yield and ^{1}H NMR of the polymers indicated the complete deprotection of Boc groups. The polymers were also characterized by FTIR spectroscopy (Figure 4.3). Polybiaryl (penta Boc) and polybiaryl (tri Boc) polymers exhibit a peak at ~1750 cm^{-1}, characteristic of the C=O stretch of Boc

protecting groups. The peak at 1750 cm^{-1} has completely disappeared in polybiaryl (penta OH) and polybiaryl (tri OH) polymers, confirming the complete deprotection of Boc protecting groups. These polymers also exhibit a broad band at around 3000-3600 cm^{-1}, with a maximum at ~3400 cm^{-1} characteristic of hydrogen bonded O-H stretch. The molecular weight details of the polymers are summarized in Table 4.1. The synthesis, thermal properties, and proton conductivity of polystyrene (tri OH) polymer is discussed in our previous report.[9]

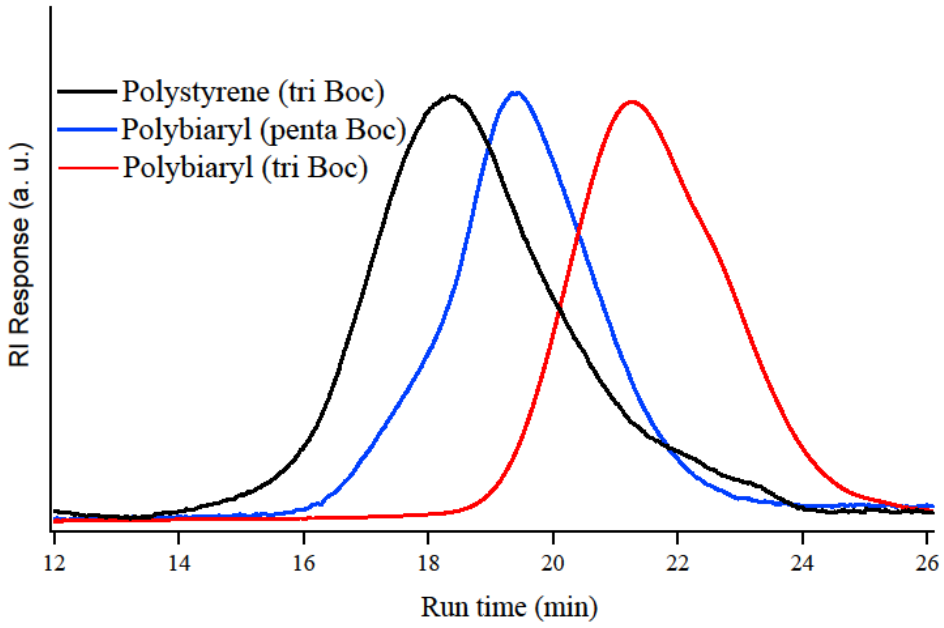

Figure 4.2 GPC (THF) chromatograms of Boc protected biaryl polymers.

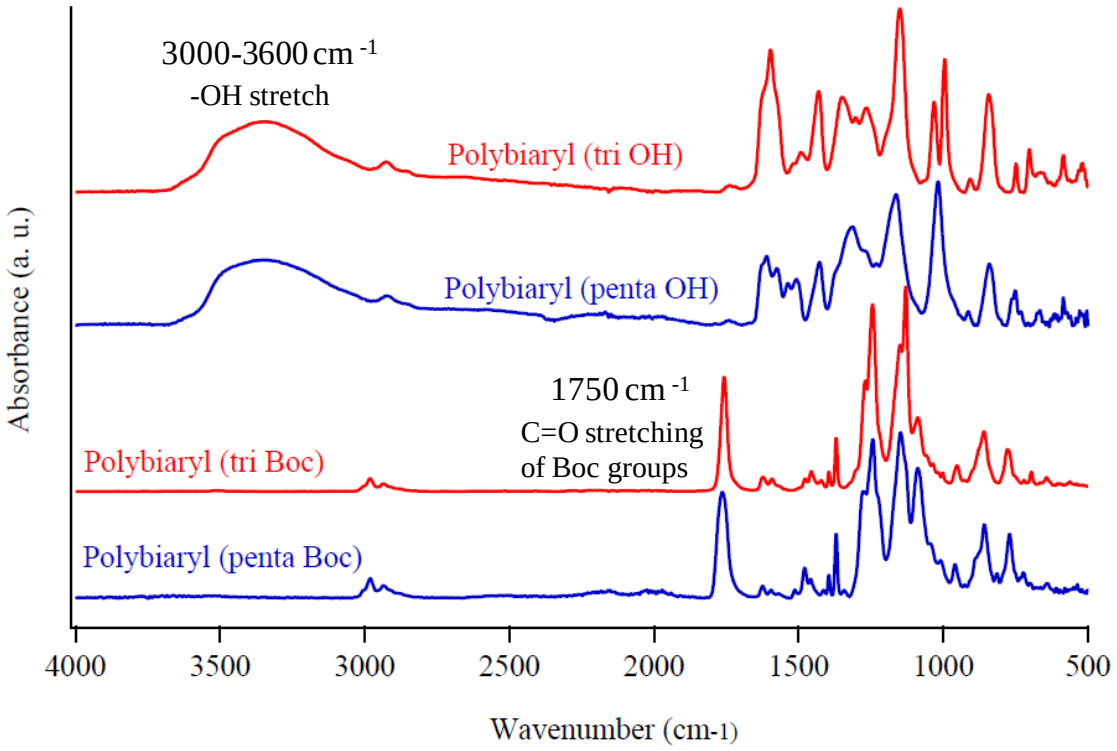

Figure 4.3 FTIR spectra of biaryl polymers.

4.2.2 Thermal Analyses

Since proton conductivity measurements were carried out under variable temperature conditions and the conductivity could be affected by the glass transition temperature (T_g) of polymers, it is necessary that we investigate the thermal properties of biaryl hydroxy polymers. The thermal stability of polymers was determined by thermogravimetric analysis (TGA) under nitrogen atmosphere. Since phenol based polymers are susceptible to oxidation, the polymers were also analyzed for thermo-oxidative stability i.e. the thermal stability of polymers was examined under air atmosphere. The thermal and

thermo-oxidative stabilities of polymers are shown in Table 4.1 and Figure 4.8. The decomposition temperatures are reported at 5% weight loss. All polymers were found to be stable up to atleast 220 ^{o}C both under nitrogen and air atmosphere.

Table 4.1 Polymer details, thermal stability ($T_{d,5\%}$, under nitrogen), thermo-oxidative stability ($T_{d,5\%}$, under air), and glass transition temperature (T_g) of biaryl polymers.

Polymer	Mn[a] (g/mol)	PDI	Polymer	Mn[b] (g/mol)	$T_{d,5\%}$ [c] (^{o}C)	$T_{d,5\%}$ [d] (^{o}C)	T_g [e] (^{o}C)
Polybiaryl (penta Boc)	37,000	1.56	Polybiaryl (penta OH)	12,500	347	223	309
Polybiaryl (tri Boc)	11,600	1.71	Polybiaryl (tri OH)	5,000	318	248	217
Polystyrene (tri Boc)	60,000	1.5	Polystyrene (tri OH)	20,000	265	267	233

[a] Estimated by GPC (THF) using PS standards

[b] Estimated based on the complete deprotection of Boc groups, which was confirmed by both ^{1}H NMR and FT-IR (Figure 4.3)

[c] Temperature at 5% weight loss when heated under nitrogen at 10 ^{o}C/min

[d] Temperature at 5% weight loss when heated under air at 1 ^{o}C/min

[e] Obtained from DSC on the second heating cycle

The glass transition temperatures (T_g values) of polymers were determined by differential scanning calorimetry (DSC) and are shown in Table 4.1 and Figure 4.9. The glass transition temperature steadily increases with increasing number of -OH groups. This is expected because the hydrogen bonding interactions among hydroxyl groups

along the polymer chains would increase with increasing number of –OH groups, leading to increased polymer chain interactions and hence the T_g. Polybiaryl (penta OH) with maximum number of –OH moieties exhibits the highest T_g of 309 ^oC. Although polybiaryl (tri OH) and polystyrene (tri OH) have same number of -OH groups, the former exhibits slightly lower T_g compared to the later one. This might be due to the lower molecular weight of polybiaryl (tri OH) since T_g is known to be dependent on the molecular weight of polymers.

4.2.3 Proton Conductivity

The proton conductivity of biaryl hydroxy polymers is shown in Figure 4.4 In general, bulk proton conductivity is known to be influenced by several factors such as the nature of the PT moiety (for eg. imidazole, triazole, phenol etc.), variations in the polymer architecture, T_g of polymers, and charge carrier density (density of proton transporting moieties).[3,12,5,13] Since -OH is the proton transporting moiety in all the polymers, the effect of the nature of PT moiety can be neglected. The weight fraction of -OH groups contained in each polymer was calculated by dividing the product of the equivalent weight of -OH unit (17 g/mol) and the number of -OH units per polymer repeat unit by the equivalent weight of the polymer repeat unit. The charge carrier density for each polymer is shown in Table 4.2.

Unlike *N*-heterocycle-based proton conducting polymers, the proton conductivity in phenol-based polymers as a function of temperature follow an Arrhenius-type behavior over the entire temperature range investigated here. The proton conductivity can be

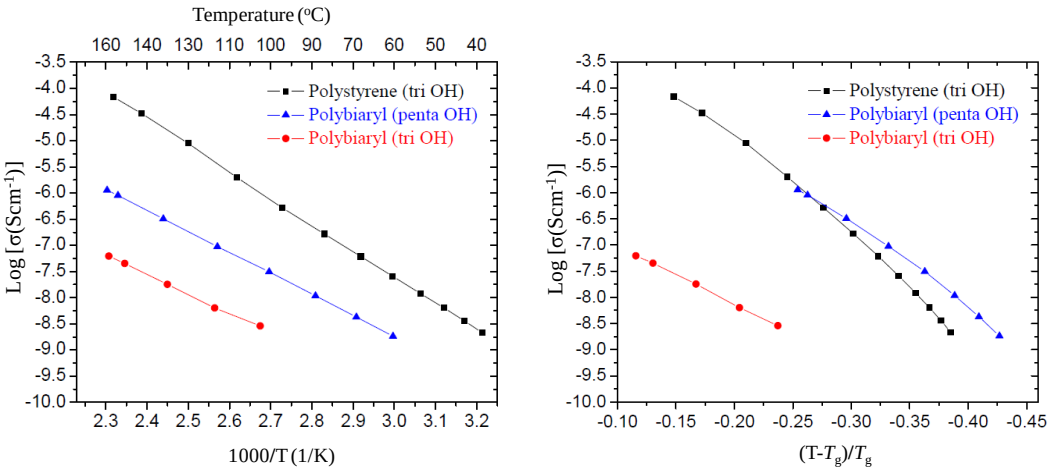

Figure 4.4 Proton conductivity (left) and normalized proton conductivity (right) of biaryl and styrenic hydroxy polymers.

Table 4.2 Charge carrier density, apparent activation energy (E_a), and glass transition temperature (T_g) of phenolic polymers.

Polymer	weight fraction of -OH units	Log [σ (Scm^{-1})] at 140 °C	E_a /kJ mol^{-1}	T_g (°C)
Polybiaryl (penta OH)	32	-6.4	77	309
Polybiaryl (tri OH)	22	-7.6	74	217
Polystyrene (tri OH)	33	-4.5	94	233

described by Equation (4.1), where σ_o is a pre-exponential factor, R is a universal gas constant, and T is the temperature in Kelvin. The conductivity plots were fitted by Arrhenius equation (4.1) and the activation energies (E_a) were computed from the slope of the linear fit of log (σ) versus 1/T and are shown in Table 4.2.

$$\sigma = \sigma_o \exp(-E_a/RT) \qquad (4.1)$$

Polybiaryl (penta OH) and polybiaryl (tri OH) have similar polymer architecture. In addition, both polymers also present similar E_a values of 74-77 kJ/mol. Thus, the proton transport is equally feasible in both these polymers. Nonetheless, polybiaryl (tri OH) exhibits poor proton conducting ability, and its proton conductivity is lower by an order of magnitude compared to polybiaryl (penta OH). This might be due to the lack of -OH groups in one of the biaryl rings of polybiaryl (tri OH), resulting in lower weight fraction of the proton conducting -OH moieties. The reduced proton carrier density might impede -OH groups from forming continuous hydrogen bond pathway, thereby adversely affecting the overall proton transport.

Polybiaryl (penta OH) and polystyrene (tri OH) have similar -OH weight fractions. The E_a for proton transfer in polybiaryl (penta OH) is 17 kJ/mol lower than that in polystyrene (tri OH). Thus, the proton transfer in polybiaryl (penta OH) is more facilitated compared to polystyrene (tri OH). Although polybiaryl (penta OH) presents lower E_a for proton transfer, it is surprising that its net proton conductivity is almost two orders of magnitude lower than that of polystyrene (tri OH) over the entire temperature range. This might be, in part, due to the variations in polymer architecture and/or the differences in T_g values of polymers.

To eliminate the effect of T_g on proton conductivity, log (σ) is plotted against reduced temperature. Reduced temperature is defined as $[(T-T_g)/T_g]$, where all temperatures are considered in Kelvin and the term is known to take into account the differences in T_g values of polymers. The normalized conductivity versus reduced temperature plot is shown in Figure 4.4b. Considering that polybiaryl (penta OH) and polystyrene (triOH) have similar proton carrier densities, the differences in their proton conductivities in log

(σ) versus reduced temperature plots can now be solely ascribed to the variations in biaryl versus styrenic polymer architectures. The normalized proton conductivities of polybiaryl (penta OH) and polystyrene (tri OH) converge with each other with the difference being less than an order magnitude over the entire temperature range. Thus, the biaryl architecture does not seem to provide any obvious advantages over the styrenic polymers in terms of proton conductivity.

To further confirm this, we also synthesized another set of polymers shown in Chart 2 and investigated their thermal and proton conducting properties. polybiaryl (tetra OH) and polybiaryl (di OH) polymers were synthesized following similar synthetic protocols described above for polybiaryl (penta OH) and polybiaryl (tri OH), respectively. The synthetic Schemes for the biaryl monomers are shown in Schemes 4.3 and 4.4. The synthesis, thermal and proton conducting properties of polystyrene (di OH) are described in our previous paper.[9] The polymer details and thermal properties are shown in Table 4.3 and Figures 4.8 and 4.9. All polymers are stable up to atleast 230 ^{o}C. Polybiaryl (tetra OH) with the maximum number of -OH moieties exhibits the highest T_g of 294 ^{o}C.

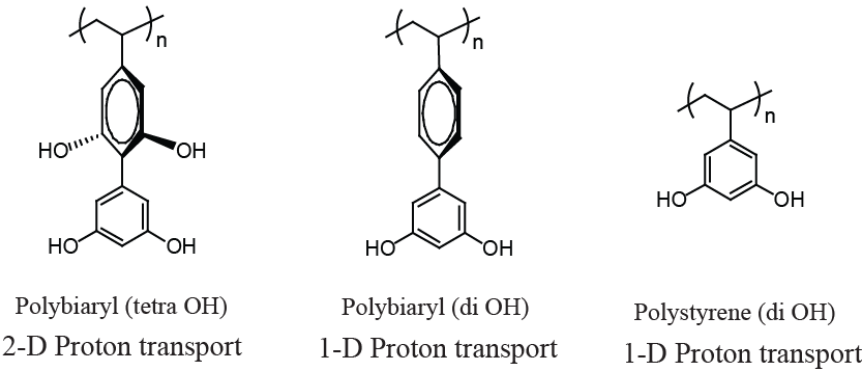

Chart 4.2 Structures of biaryl and styrenic hydroxy polymers.

Table 4.3 Polymer details, thermal stability ($T_{d,5\%}$, under nitrogen), thermo-oxidative stability ($T_{d,5\%}$, under air), and glass transition temperature (T_g) of biaryl polymers.

Polymer	Mn[a] (g/mol)	PDI	Polymer	Mn[b] (g/mol)	$T_{d,5\%}$ [c] (^oC)	$T_{d,5\%}$ [d] (^oC)	T_g [e] (^oC)
Polybiaryl (tetra Boc)	37,000	1.6	Polybiaryl (tetra OH)	14,000	364	274	294
Polybiaryl (di Boc)	15,000	1.8	Polybiaryl (di OH)	7,600	339	287	216
Polystyrene (di Boc)	64,000	1.4	Polystyrene (di OH)	25,000	258	239	227

[a] Estimated by GPC (THF) using PS standards

[b] Estimated based on the complete deprotection of Boc groups, which was confirmed by both ^{1}H NMR and FT-IR (Figure 4.7)

[c] Temperature at 5% weight loss when heated under nitrogen at 10 ^{o}C/min

[d] Temperature at 5% weight loss when heated under air at 1 ^{o}C/min

[e] Obtained from DSC on the second heating cycle

The conductivity and normalized conductivity plots are shown in Figure 4.5a and 4.5b, respectively. It can be seen from Figure 4.5a that the proton conductivity of polybiaryl (tetra OH) is slightly lower than that of polystyrene (di OH) in the higher temperature range and the difference is less than an order of magnitude over the entire temperature range. On the otherhand, the normalized proton conductivity of polybiaryl (tetra OH) is about 1-2 orders of magnitude higher compared to polystyrene (di OH). Since polybiaryl (tetra OH) and polybiaryl (di OH) have similar charge carrier densities

(27 and 25, respectively), the differences in their normalized proton conductivities can be ascribed to the variations in polymer architecture. Thus, given a constant charge carrier density and similar T_g values, the biaryl architecture might prove advantageous over the styrenic polymers, especially in the lower temperature range. Nevertheless, considering that the placement of hydroxyl groups in both rings of the biaryl hydroxy polymers is always accompanied by a corresponding increase in T_g, the advantage of the biaryl architecture, if any, on the net proton conductivity is not substantial.

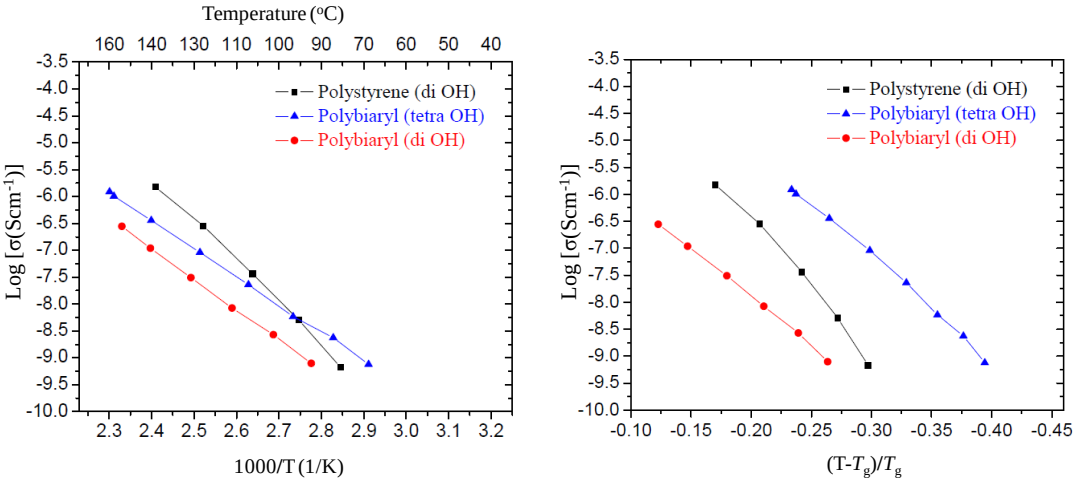

Figure 4.5 Proton conductivity (left) and normalized proton conductivity (right) of biaryl and styrenic hydroxy polymers.

4.3 Summary

A series of biaryl and styrene-based hydroxy polymers with varying number of hydroxyl groups have been successfully synthesized and characterized. The biaryl architecture is observed to enhance the thermal stability of phenol-based polymers. Incorporation of proton transporting -OH moieties on both phenyl rings of the biaryl scaffold increases the T_g of biaryl polymers. The proton conductivities of the biaryl and

styrenic polymers are compared to elucidate the role of biaryl architecture on proton transport. The disposition of -OH moieties in orthogonal planes in biaryl polymers does provide low E_a for proton transport compared to the styrenic hydroxy polymers. Despite low E_a for proton transport, the biaryl architecture did not result in an increase in the net proton conductivity compared to the styrenic polymers over the temperature range investigated here. This might be due to the accompanying increase in T_g since the normalized proton conductivities of polybiaryl (penta OH) and polybiaryl (tetra OH) are either comparable or slightly higher than that of the corresponding styrenic polymers. Thus, the simplicity of molecular design, ease of synthesis, and lower T_g values of phenol-based styrene polymers make the styrenic polymer architecture preferable over the analogous biaryl architecture.

4.4 Experimental Details

4.4.1 General Materials and Methods

All chemicals were purchased from commercial sources and were used as received, unless otherwise noted. Tetrahydrofuran (THF) was obtained from Fisher Scientific and was freshly distilled over sodium-benzophenone prior to use. Anhydrous dimethylformamide (DMF) and toluene were obtained from Sigma Aldrich and used as received. Azobisisobutyronitrile (AIBN) was recrystallized from methanol and dried under vacuum prior to use. Compounds 1,[14] 2,[15] 13,[16] and 14[16] were synthesized following reported procedures. The synthesis and characterization of polystyrene (tri OH) and polystyrene (di OH) are described in our previous report.[9]

^{1}H NMR spectra were recorded on a Bruker 400 MHz NMR spectrometer using the residual proton resonance of the solvent as the internal standard. Chemical shifts (δ) and coupling constants (J) are reported in parts per million (ppm) and Hertz, respectively. The following abbreviations are used for the peak multiplicities: s, singlet; d, doublet; t, triplet; q, quartet; m, multiplet; dd, doublet of doublet; bs, broad singlet; bm, broad multiplet. ^{13}C NMR spectra were proton decoupled and recorded on a Bruker 100 MHz NMR spectrometer using the carbon signal of the dueterated solvent as the internal standard. The molecular weights of the polymers were determined by gel permeation chromatography (GPC) using THF as eluent and toluene as the internal reference. PS standards were used for calibration and the output was received and analyzed using RI detector. Flash chromatography was performed using combiflash with normal phase Redi*sep R*f silica columns. Silica plates with F-254 indicator were used for analytical thin layer chromatography. FT-IR spectra were recorded on a Bruker Alpha FT-IR spectrometer.

4.4.2 TGA and DSC Analysis

Polymer samples were dried under vacuum at 120 ^{o}C for 24 h and were used immediately for TGA and DSC analysis. Thermal stabilities of the polymers were investigated using a TA Instruments TGA 2950 thermogravimetric analyzer. The samples (~ 10 mg) were heated from room temperature to 600 ^{o}C at a rate of 10 ^{o}C/min under a flow of nitrogen and at 1 ^{o}C/min under air. Glass transition temperature (T_g) of the polymers were obtained by differential scanning calorimeter (DSC) using TA instruments Dupont DSC 2910. The samples (~ 10 mg) were loaded into aluminum pans and were

heated from room temperature to 320 ^{o}C with a rate of 10 ^{o}C/min under a flow of nitrogen (50 mL/min). Each sample was measured through two heating cycles and the data from the second heating cycle is considered.

4.4.3 Electrochemical Impedance Measurements

The impedance response of each polymer sample was measured from 0.1 Hz-10^{7} Hz with a sinusoidal excitation voltage of 0.1 V_{rms} using a Solartron 1260 impedance/gain phase analyzer. The resistance (R) values were obtained by geometrically fitting a semicircular arc to the bulk response in the Z' vs. Z" plane and conductivities were derived from the equation ($\sigma = \ell/RA$), where ℓ and A are the thickness and the area of the polymer film, respectively. Conductivities lower than 10^{-9} S/cm are generally considered to be below the sensitivity of the instrument for the particular geometries used, and hence the absolute numbers below this value are not considered accurate.

4.4.4 Membrane Preparation for Vacuum Measurements

Kapton tape with a hole of thickness 127 μm and an area of 0.0792 cm^{2} was placed onto a gold coated electrode and the polymer films were drop cast from concentrated DMF solution onto the hole. Polymer film thickness and the contact area between the membrane and the electrode were determined by the dimensions of the hole and hence were held constant. Polymer films were prepared inside the glove box on a hot plate and were annealed at 150 ^{o}C for 15 h prior to measurements. Films were then placed between two gold coated blocking electrodes and transferred immediately to a vacuum oven and the proton conductivities were characterized by impedance spectroscopy from 40 ^{o}C to

160 ^{o}C. The samples were initially heated from room temperature to 160 ^{o}C and were held at 160 ^{o}C (to ensure complete removal of the residual DMF) until the polymers displayed constant conductivity over at least 10 hours. The samples were then slowly cooled from 160 ^{o}C to room temperature and the conductivities during the cooling cycle are reported for all the polymers.

4.4.5 Activation Energy (E_a) Calculations

The activation energy is the minimum energy required for proton conduction through the polymer membrane. It was calculated using the Arrhenius equation ($\ln \sigma = \ln \sigma_o - (E_a/RT)$), where R is the universal gas constant and T is the temperature in Kelvin. The E_a was obtained from the slope of the linear fit of $\ln \sigma$ vs. 1/T. The pre-exponential factor ($\ln \sigma_o$) was neglected.

4.4.6 Synthetic Schemes for Monomers

Biaryl (penta Boc) monomer 9

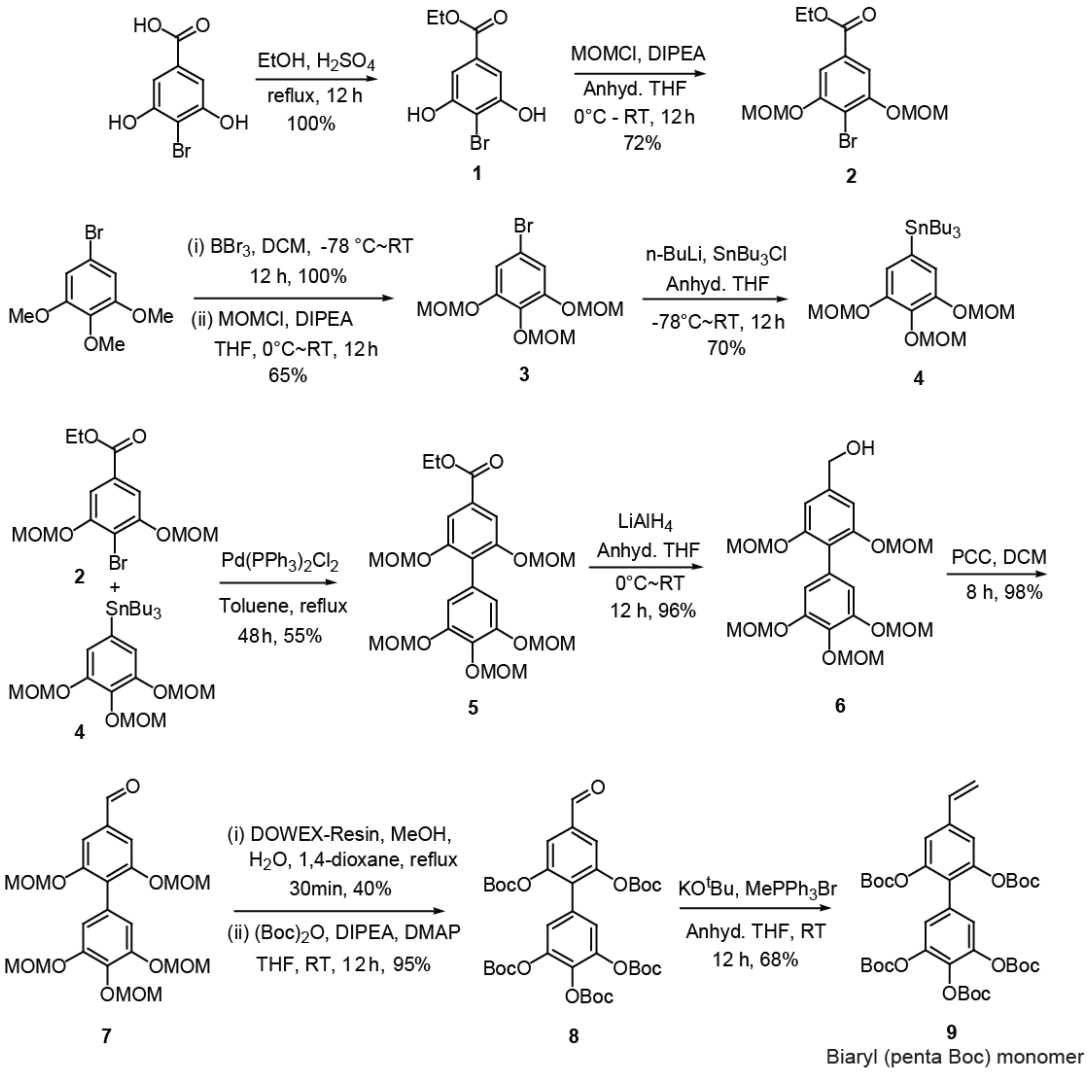

Scheme 4.1 Synthesis of biaryl (penta Boc) monomer **9**.

Biaryl (tri Boc) monomer 12

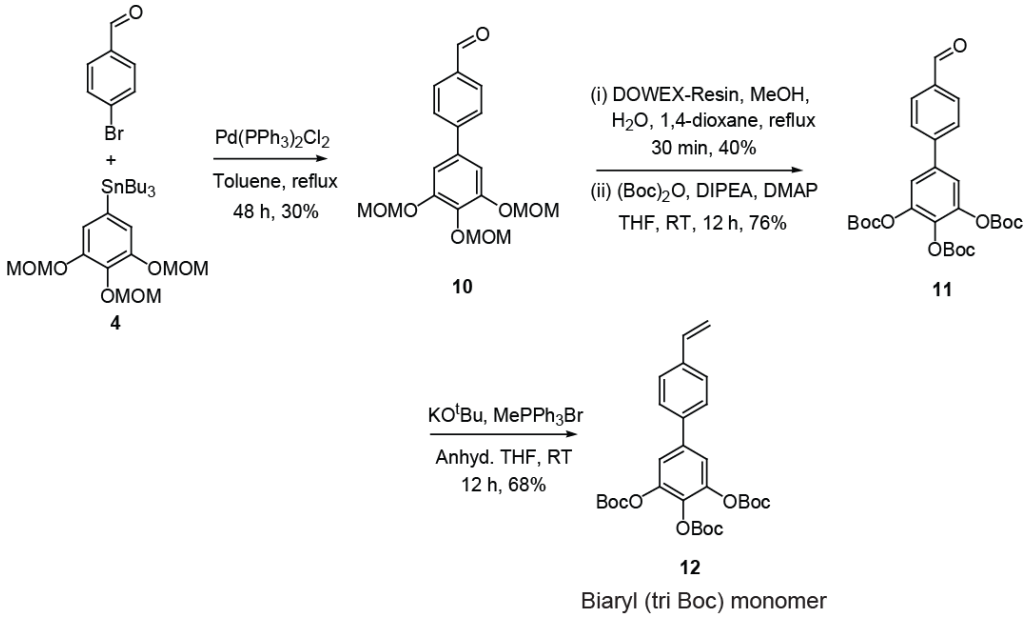

Scheme 4.2 Synthesis of biaryl (tri Boc) monomer **12**.

Biaryl (di Boc) monomer 22

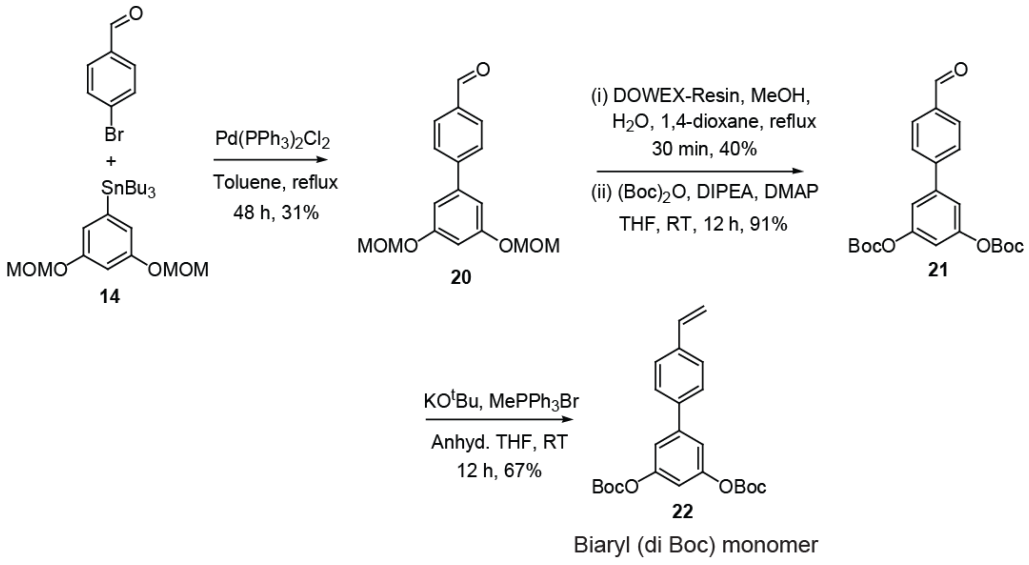

Scheme 4.3 Synthesis of biaryl (di Boc) monomer **22**.

Biaryl (tetra Boc) monomer 19

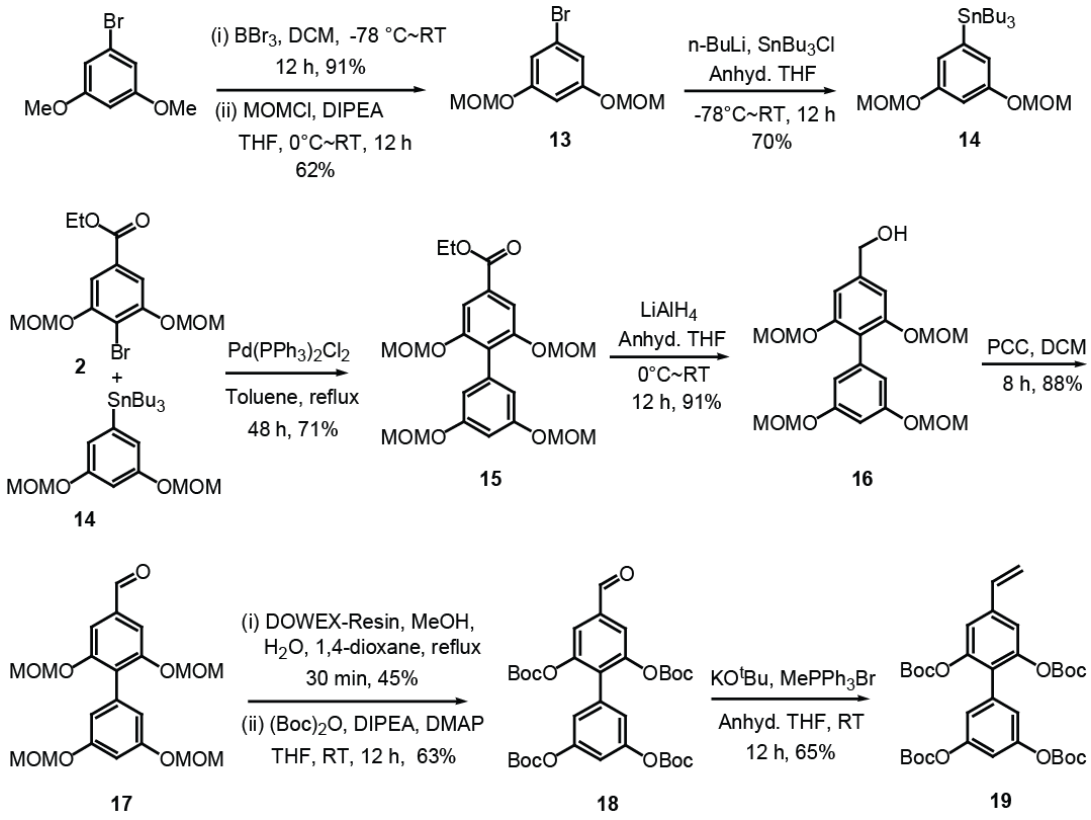

Scheme 4.4 Synthesis of biaryl (tetra Boc) monomer **19**.

4.4.7 General Procedures for Monomer Syntheses

Compounds **1**[1], **2**[2], **13**[3], and **14**[3] were synthesized following reported procedures.

Procedure 1 for deprotection of –OMe group using BBr_3

A solution of the appropriate methoxy benzene (1.0 equiv) in dichloromethane (DCM) at RT under argon was cooled to -78 ^{o}C for 30 min, and boron tribromide (1.5 equiv per methoxy group) was added at -78 ^{o}C. The reaction mixture was stirred at -78 ^{o}C

for 30 min and was slowly warmed to RT and continued to stir at RT for overnight. The reaction mixture was then cooled to -78 ^{o}C and the excess BBr_3 was quenched with saturated NH_4Cl solution. The precipitate was filtered, and washed twice with excess DCM. The DCM and aqueous layers were separated, and the DCM layer was concentrated. The aqueous layer was extracted twice with ethyl acetate and the combined organic layers were dried over Na_2SO_4, concentrated under reduced pressure and the crude was purified by column chromatography (SiO_2).

Procedure 2 for protection of phenolic hydroxyl group as methoxymethyl ether (MOM)

A solution of the appropriate hydroxy benzene (1.0 equiv) in dry THF under argon was cooled to 0 ^{o}C. *N*,*N*-diisopropylethylamine (DIPEA) (1.5 equiv per hydroxyl group) and chloromethyl methyl ether (MOMCl) (1.5 equiv per hydroxyl group) were added and the reaction was slowly warmed to room temperature (RT) and continued to stir at RT. The progress of the reaction was monitored using thin layer chromatography (TLC). The reaction is usually complete in about 12 h. After complete disappearance of the starting material, the reaction was cooled to 0 ^{o}C and quenched with saturated NH_4Cl. The organic and aqueous layers were separated and the organic layer was concentrated. The aqueous layer was extracted thrice with ethyl acetate and the combined organic layers were dried over Na_2SO_4, concentrated under reduced pressure and the crude was purified by column chromatography (SiO_2).

Procedure 3 for conversion of bromo benzene to the aromatic tributyltin

A solution of the appropriate bromo benzene (1.0 equiv) in dry THF at RT under argon was cooled to -78 ^{o}C for 30 min, and *n*-BuLi (2.0 equiv) was added. The mixture was stirred at -78 ^{o}C for 1 h and tributyltin chloride (1.5 equiv) was added. The reaction was slowly warmed to RT and stirred for overnight. The reaction mixture was then cooled to 0 ^{o}C and quenched with saturated NH_4Cl solution. The organic and aqueous layers were separated and the organic layer was concentrated. The aqueous layer was extracted twice with ethyl acetate and the combined organic layers were dried over Na_2SO_4, concentrated under reduced pressure and the crude was purified by column chromatography (SiO_2).

Procedure 4 for Stille coupling reaction

The appropriate tributyltin (1.0 equiv), bromo benzene (1.2 equiv), and $PdCl_2(PPh_3)_2$ (0.05 equiv) were dissolved in toluene under argon at RT. The reaction mixture was degassed for 1 h with an argon inlet/outlet and the reaction mixture was then refluxed for 48 h. After evaporating the solvent, the resultant mixture was extracted twice with ethyl acetate and water. The combined organic layers were dried over Na_2SO_4, concentrated under reduced pressure, and the crude was purified by column chromatography (SiO_2).

Procedure 5 for the reduction of ester with $LiAlH_4$

A solution of $LiAlH_4$ (2.0 equiv) in dry THF at RT under argon was cooled to 0 ˚C. The appropriate biaryl ester compound (1.0 equiv) in dry THF was then added and the reaction mixture was slowly warmed to RT and stirred for about 12 h. The progress of the reaction was monitored using thin layer chromatography (TLC). After complete

disappearance of the biaryl ester compound, the reaction was cooled to 0 ˚C and quenched with saturated NH_4Cl solution. The precipitate was filtered and washed with ethyl acetate. The filtrate was concentrated, and extracted thrice with ethyl acetate and water. The combined organic layers were dried over Na_2SO_4, concentrated under reduced pressure, and the crude was purified by column chromatography (SiO_2).

Procedure 6 for the oxidation of benzyl alcohol to aldehyde using PCC

To a stirring solution of the appropriate benzyl alcohol (1.0 equiv) in DCM at RT, was added pyridinium chloro chromate (PCC) (1.2 equiv). The mixture was exposed to air while stirring and the progress of the reaction was monitored using thin layer chromatography (TLC). The reaction is usually complete within 2-8 h depending on the scale of the reaction. After complete disappearance of the benzyl alcohol, the crude was concentrated under reduced pressure and purified by column chromatography (SiO_2).

Procedure 7 for the deprotection of MOM group using DOWEX resin

The appropriate MOM-protected biaryl aldehyde (1.0 equiv) was dissolved in a mixture of (MeOH: H_2O: 1,4-dioxane) (1.0:0.5:0.1 v/v) at RT under argon. DOWEX resin (4.0 equiv w.r.t each MOM group) was added and the solution was refluxed. The progress of the reaction was monitored for every 10 min using thin layer chromatography (TLC). If the reaction is not complete within 30 min, then an additional amount of DOWEX resin (1.0 equiv) was added each time until the starting material was completely disappeared. The mixture was filtered and the resin was washed with MeOH. The filtrate

was concentrated under reduced pressure and the crude was taken to the next step without further characterization.

Procedure 8 for Boc-protection

The appropriate biaryl hydroxy aldehyde (1.0 equiv) was dissolved in THF at RT under argon. The reaction mixture was cooled to 0˚C and *N*,*N*-Diisopropylethylamine (1.5 equiv per hydroxyl group), $(Boc)_2O$ (1.5 equiv per hydroxyl group), and 4-Dimethylaminopyridine (DMAP) (0.05 equiv) were added. The reaction mixture was then warmed to RT and continued to stir at RT for overnight. THF was evaporated and the crude was taken up in ethyl acetate and washed twice with 1M NaOH and saturated NaCl solutions. The combined ethyl acetate layers were dried over Na_2SO_4, concentrated under reduced pressure and the crude was purified by column chromatography (SiO_2).

Procedure 9 for Wittig reaction

$MePPh_3Br$ (1.5 equiv) and KO^tBu (1.5 equiv) were taken in an oven-dried schlenk flask at RT and dried under vacuum for 30 min. The flask was cooled to 0 ^oC using ice bath and anhydrous THF (50 mL) was added under argon. The solution immediately turned yellow, indicating the formation of ylide. The reaction mixture was allowed to stir at 0 ^oC for 30 min and was then warmed to room temperature. A solution of the appropriate Boc-protected biaryl aldehyde (1.0 equiv) in anhydrous THF was added using syringe and the reaction mixture was continued to stir at room temperature for 12 h. The reaction was quenched by the addition of water and extracted thrice with ethyl acetate.

The combined ethyl acetate layers were dried over Na_2SO_4, concentrated under reduced pressure and the crude was purified by column chromatography (SiO_2).

Synthesis of Compound 3

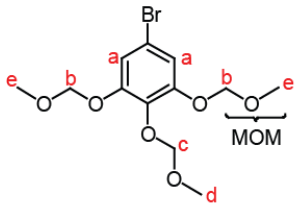

3

According to general procedure 1, 5-bromo-1,2,3-trimethoxybenzene (10.0 g, 40.5 mmol) was treated with boron tribromide (BBr_3) (45.6 g, 182.1 mmol). The product was eluted with ethyl acetate/hexane (80:20 v/v) to afford 5-bromo-1,2,3-trimethoxybenzene (8.2 g, 100%) as yellow oil, which was carried to the next step without further characterization. According to general procedure 2, 5-bromo-1,2,3-trimethoxybenzene (8.2 g, 40.2 mmol) was treated with *N*,*N*-diisopropylethylamine (23.4 g, 181.0 mmol) and MOMCl (14.6 g, 181.0 mmol). The product was eluted with ethyl acetate/hexane (25:75 v/v) to afford compound **3** (8.8 g, 65%) as colorless oil. ^{1}H NMR (400 MHz, $CDCl_3$) δ: 7.01 (s, 2H, a), 5.17 (s, 4H, b), 5.10 (s, 2H, c), 3.60 (s, 3H, d), 3.49 (s, 6H, e).^{13}C NMR (100 MHz, $CO(CD_3)_2$) δ: 152.81, 137.08, 116.23, 114.10, 98.95, 96.00, 57.13, 56.46. FAB/MS *m/z* 337.024 $[M+H]^+$ (expected m/z=337.02).

Synthesis of compound 4

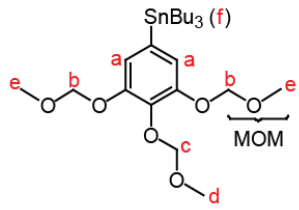

4

According to general procedure 3, compound **3** (8.8 g 26.0 mmol) was treated with 1.6 M n-BuLi/hexane (32.5 mL, 52.0 mmol) and $SnBu_3Cl$ (12.7 g, 39.0 mmol) to afford compound **4** (10.0 g, 70%) as yellow oil. The product was eluted with ethyl acetate/hexane (3:97 v/v). The tributyl stannane is not very stable and hence was used immediately in next steps. ^{1}H NMR (400 MHz, $CDCl_3$) δ: 6.92 (s, 2H, a), 5.19 (s, 4H, b), 5.15 (s, 2H, c), 3.62 (s, 3H, d), 3.51 (s, 6H, e), 1.58-0.89 (m, 27H,f).

Synthesis of compound 5

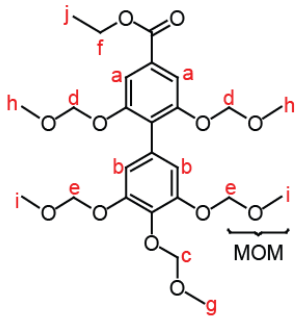

5

According to general procedure 4, compound **2** (6.4 g, 18.3 mmol) was treated with compound **4** (8.36 g, 15.3 mmol) and $PdCl_2(PPh_3)_2$ (0.536 g, 0.8 mmol) to afford compound **5** (5.5 g, 55%) as white solid. The product was eluted with ethyl acetate/hexane (20:80 v/v). ^{1}H NMR (400 MHz, $CDCl_3$) δ: 7.52 (s, 2H, a), 6.89 (s, 2H, b), 5.20 (s, 2H, c), 5.19 (s, 4H, d), 5.12 (s, 4H, e), 4.40-4.37 (q, *J* = 7.10 Hz, 2H, f), 3.66 (s, 3H, g), 3.48 (s, 6H, h), 3.37 (s, 6H, i), 1.40-1.38 (t, *J* = 7.10 Hz, 3H, j). ^{13}C NMR (100 MHz, $CDCl_3$) δ: 166.16, 155.09, 150.54, 135.88, 131.09, 129.39, 126.20, 113.24, 110.07, 98.68, 95.64, 94.83, 61.35, 57.22, 56.34, 56.26, 14.51; FAB/MS *m/z* 527.206 [M+H] (expected m/z=527.20).

Synthesis of compound 6

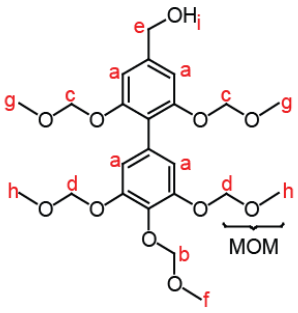

6

According to general procedure 5, compound **5** (5.4 g, 10.3 mmol) was treated with $LiAlH_4$ (0.78 g, 20.6 mmol) to afford compound **6** (4.8 g, 96%) as white solid. The product was eluted with ethyl acetate/hexane (25:75 v/v). ^{1}H NMR (400 MHz, $CDCl_3$) δ: 6.88 (s, 4H, a), 5.19 (s, 2H, b), 5.18(s, 4H, c), 5.08 (s, 4H, d), 4.69-4.67 (d, *J* = 6.10 Hz, 2H, e), 3.66 (s, 3H, f), 3.48 (s, 6H, g), 3.38 (s, 6H, h), 1.77 (t, *J* = 6.10 Hz, 1H, i). ^{13}C NMR (100 MHz, $CDCl_3$) δ: 155.43, 150.45, 142.23, 135.56, 130.03, 120.85, 113.57, 107.47, 98.69, 95.65, 94.81, 65.45, 57.21, 56.24; FAB/MS *m/z* 485.192 $[M+H]^+$ (expected m/z=485.19).

Synthesis of compound 7

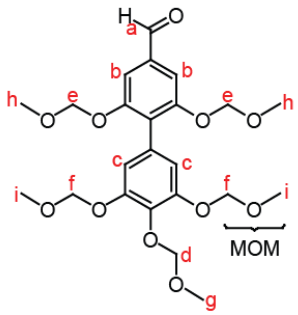

7

According to general procedure 6, compound **6** (4.3g, 9.0 mmol) was treated with PCC (2.3 g, 10.7 mmol) to afford compound 7 (4.2 g, 98%) as light yellow solid. The product was eluted with ethyl acetate/hexane (25:75 v/v). ^{1}H NMR (400 MHz, $CDCl_3$) δ: 9.94 (s, 1H, a) 7.38 (s, 2H, b), 6.89 (s, 2H, c), 5.21 (s, 2H, d), 5.19 (s, 4H, e), 5.14 (s, 4H, f), 3.67 (s, 3H, g), 3.49 (s, 6H, h), 3.40 (s, 6H, i). ^{13}C NMR (100 MHz, $CDCl_3$) δ: 191.59, 155.83, 150.62, 136.93, 136.00, 129.06, 127.60, 113.08, 109.86, 98.66, 95.63, 94.78, 57.23, 56.36, 56.26; FAB/MS *m/z* 483.178 $[M+H]^+$ (expected m/z=483.17).

Synthesis of compound 8

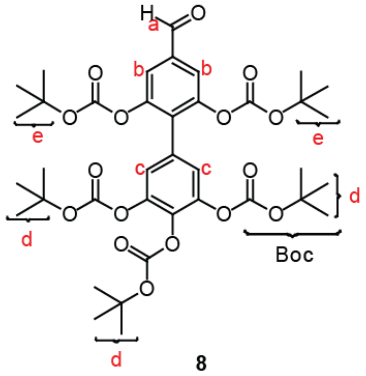

8

According to general procedure 7, compound **7** (4.2 g, 8.7 mmol) was treated with DOWEX resin to afford 0.9 g (40%) of the crude penta hydroxy biaryl aldehyde. The hydroxyl groups were further protected with Boc according to general procedure 8 to obtain compound **8** (2.5 g, 95%) as white solid. The product was eluted with ethyl acetate/hexane (10:90 v/v). ^{1}H NMR (400 MHz, $CDCl_3$) δ: 9.98 (s, 1H, a), 7.65 (s, 2H, b), 7.18 (s, 2H, c), 1.54-1.53 (m, 27H, d), 1.35 (s, 18H, e). ^{13}C NMR (100 MHz, $CDCl_3$) δ: 189.79, 150.79, 149.98, 149.93, 149.03, 143.76, 137.20, 135.53, 133.65, 128.35, 122.09, 121.38, 84.81, 84.03, 83.95, 27.72, 27.37.

Synthesis of compound 9

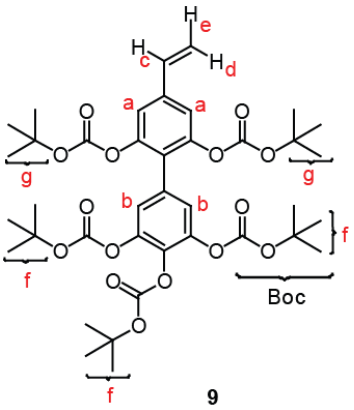

9

According to general procedure 9, compound **8** (2.5 g, 3.3 mmol) was reacted with $MePPh_3Br$ (1.8 g, 5.0 mmol) and KO^tBu (0.6 g, 5.0 mmol) to afford compound **9** (1.7 g, 68%) as white solid. The product was eluted with ethyl acetate/hexane (8:92 v/v). ^1H NMR (400 MHz, $CDCl_3$) δ: 7.17 (s, 2H, a), 7.15 (s, 2H, b), 6.70-6.62 (dd, 17.56, 10.92 Hz, 1H, c), 5.80-5.75 (d, 17.56 Hz, 1H, d), 5.36-5.33 (d, 10.92 Hz, 1H, e), 1.54-1.52 (m, 27H, f), 1.35-1.33 (s, 18H, g). ^{13}C NMR (100 MHz, $CDCl_3$) δ: 151.14, 150.03, 149.27, 149.11, 143.57, 139.45, 135.09, 135.00, 129.40, 126.73, 122.33, 118.13, 116.36, 84.18, 83.84, 83.75, 27.74, 27.41.

Synthesis of compound 10

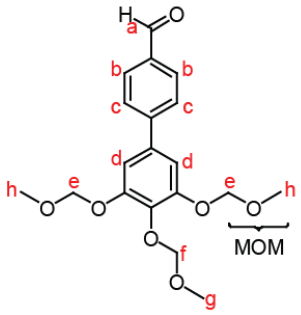

10

According to general procedure 4, compound **4** (4.8 g, 8.8 mmol) was reacted with 4-bromobenzaldehyde (2.0 g, 10.5 mmol) and $PdCl_2(PPh_3)_2$ (0.35 g, 0.5 mmol) to afford compound **10 (**0.8 g, 30%) as light yellow solid. ^{1}H NMR (400 MHz, $CDCl_3$) δ: 10.04 (s, 1H, a), 7.93-7.91 (d, 2H, *J* = 8.41 Hz, b), 7.71-7.69 (d, 2H, *J* = 8.41 Hz, c), 7.13 (s, 2H, d), 5.28 (s, 4H, e), 5.21 (s, 2H, f), 3.65 (s, 3H, g), 3.54 (s, 6H, h). ^{13}C NMR (100 MHz, $CDCl_3$) δ: 192.01, 151.60, 146.83, 137.03, 136.16, 135.33, 130.34, 127.78, 109.73, 98.71, 95.58, 57.37, 56.49; FAB/MS *m/z* 363.144 $[M+H]^+$ (expected m/z=363.13).

Synthesis of compound 11

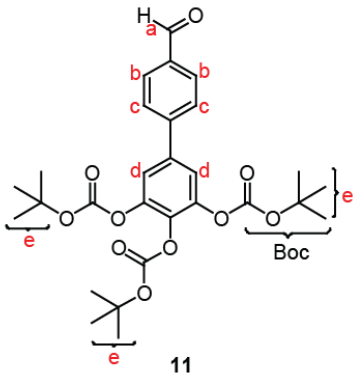

11

According to general procedure 7, compound **10** (0.9 g, 2.5 mmol) was treated with DOWEX resin to yield 0.5 g of the trihydroxy biaryl aldehyde. The hydroxyl groups were further protected as Boc according to general procedure 8 to obtain compound **11** (0.8 g, 76%) as white solid. The product was eluted with ethyl acetate/hexane (5:95 v/v). ^{1}H NMR (400 MHz, $CDCl_3$) δ: 10.05 (s, 1H, a), 7.95-7.93 (d, 2H, *J* = 8.44 Hz, b), 7.71-7.69 (d, 2H, *J* = 8.44 Hz, c), 7.43 (s, 2H, d), 1.57 (s, 27H, e). ^{13}C NMR (100 MHz, $CDCl_3$) δ: 191.91, 150.45, 149.46, 145.02, 144.29, 137.87, 135.81, 135.41, 130.44, 127.94, 119.40, 84.42, 27.75.

Synthesis of biaryl (tri Boc) monomer 12

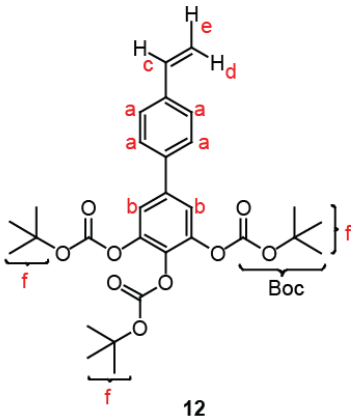

12

According to general procedure 9, compound **11** (0.93 g, 1.75 mmol) was reacted with $MePPh_3Br$ (0.94 g, 2.63 mmol) and KO^tBu (0.30 g, 2.63 mmol) to afford the biaryl (tri Boc) monomer **11** (0.73 g, 79%) as white solid. The product was eluted with ethyl acetate/hexane (10:90 v/v). ^1H NMR (400 MHz, $CDCl_3$) δ: 7.51-7.44 (m, 4H, a), 7.36 (s, 2H, b), 6.77-6.70 (dd, *J* = 17.56, 10.92 Hz, 1H, c), 5.81-5.76 (d, *J* = 17.56 Hz, 1H, d), 5.29-5.27 (d, *J* = 10.92 Hz, 1H, e), 1.57-155 (m, 27H, f). ^{13}C NMR (100 MHz, $CDCl_3$) δ: 150.53, 149.62, 144.04, 139.05, 138.50, 137.39, 136.36, 134.47, 127.40, 126.83, 118.88, 114.51, 84.19, 27.76, 27.72.

Synthesis of compound 15

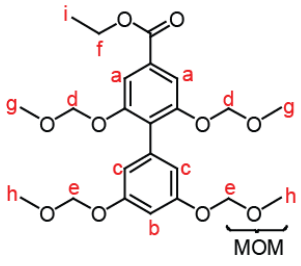

15

According to general procedure 4, compound **2** (10.2 g, 29.1 mmol) was reacted with compound **4** (11.8 g, 24.2 mmol) and $PdCl_2(PPh_3)_2$ (0.9 g, 1.2 mmol) to afford compound **15** (8.0 g, 71%) as white solid. The product was eluted with ethyl acetate/hexane (20:80 v/v). ^{1}H NMR (400 MHz, $CDCl_3$) δ: 7.53 (s, 2H, a), 6.74 (t, *J* = 2.28 Hz, 1H, b), 6.71 (d, *J* = 2.28 Hz, 2H, c), 5.17 (s, 4H, d), 5.12 (s, 4H, e), 4.40-4.37 (q, 7.14 Hz, 2H, f), 3.48 (s, 6H, g), 3.37 (s, 6H, h), 1.41-1.39 (t, *J* = 7.14 Hz, 3H, i). ^{13}C NMR (100 MHz, $CDCl_3$) δ: 166.18, 157.84, 155.09, 135.60, 131.24, 126.48, 112.25, 110.11, 104.17, 94.82, 61.37, 56.34, 56.18, 14.52; FAB/MS *m/z* 467.184 $[M+H]^+$ (expected m/z=467.18).

Synthesis of compound 16

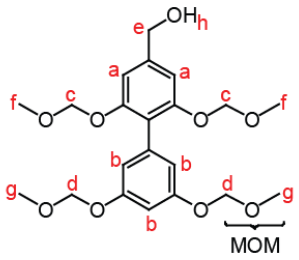

16

According to general procedure 5, compound **15** (8.0 g, 17.1 mmol) was treated with $LiAlH_4$ (1.9g, 51.0mmol) to afford compound **16** (6.6 g, 91%) as white solid. The product was eluted with ethyl acetate/hexane (25:85 v/v). ^{1}H NMR (400 MHz, $CDCl_3$) δ: 6.90 (s, 2H, a), 6.72 (m, 3H, b), 5.16 (s, 4H, c), 5.08 (s, 4H, d), 4.69-4.68 (d, *J* = 6.18 Hz, 2H, e), 3.48 (s, 6H, f), 3.37 (s, 6H, g), 1.72 (t, *J* = 6.18 Hz, 1H, h). ^{13}C NMR (100 MHz, $CDCl_3$) δ: 157.72, 155.34, 142.37, 136.20, 121.00, 112.60, 107.43, 103.78, 94.78, 94.74, 65.31, 56.18, 56.11; FAB/MS *m/z* 425.173 $[M+H]^+$ (expected m/z=425.17).

Synthesis of compound 17

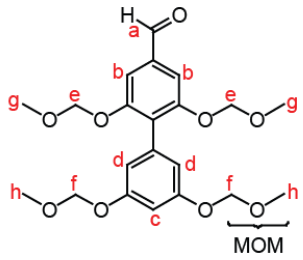

17

According to general procedure 6, compound **16** (6.6 g, 15.4 mmol) was treated with PCC (4.0 g, 18.5 mmol) to afford compound **17** (5.7 g, 88%) as light yellow solid. The product was eluted with ethyl acetate/hexane (20:80 v/v). ^{1}H NMR (400 MHz, $CDCl_3$) δ: 9.95 (s, 1H, a) 7.39 (s, 2H, b), 6.76 (t, *J* = 2.28 Hz, 1H, c), 6.71 (d, *J* = 2.28 Hz, 2H, d), 5.17 (s, 4H, e), 5.14 (s, 4H, f), 3.49 (s, 6H, g), 3.39 (s, 6H, h). ^{13}C NMR (100 MHz, $CDCl_3$) δ: 191.61, 157.90, 155.82, 137.06, 135.27, 127.84, 112.04, 109.88, 104.35, 94.81, 94.75, 56.34, 56.18; FAB/MS *m/z* 423.159 $[M+H]^+$ (expected m/z=423.15).

Synthesis of compound 18

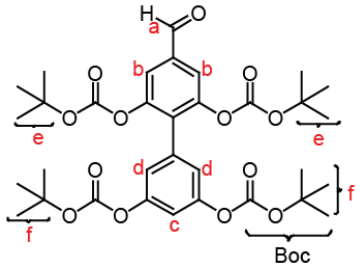

18

According to general procedure 7, compound **17** (5.7 g, 13.5 mmol) was treated with DOWEX resin to yield 1.5 g of the tetrahydroxy biaryl aldehyde. The hydroxyl groups were further protected as Boc according to general procedure 8 to obtain compound **18** (2.2 g, 63%) as white solid. The product was eluted with ethyl acetate/hexane (12:88 v/v). ^{1}H NMR (400 MHz, $CDCl_3$) δ: 9.98 (s, 1H, a), 7.65 (s, 2H, b), 7.14 (t, *J* = 2.27 Hz,1H,

c), 7.06 (d, *J* = 2.27 Hz, 2H, d) 1.54 (s, 18H, e), 1.33 (s, 18H, f).[13]C NMR (100 MHz, $CDCl_3$) δ: 189.80, 151.27, 151.03, 150.78, 149.90, 137.23, 133.96, 132.53, 121.38, 120.20, 115.44, 84.60, 83.90, 27.81, 27.36.

Synthesis of biaryl (tetra Boc) monomer 19

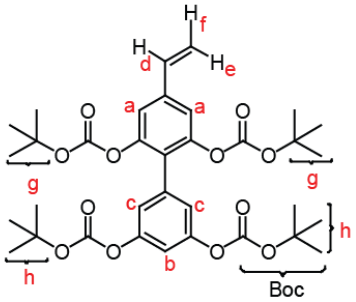

19

According to general procedure 9, compound **18** (2.2 g, 3.4 mmol) was reacted with $MePPh_3Br$ (1.9 g, 5.1 mmol) and KO^tBu (0.6 g, 5.1 mmol) to afford the biaryl (tetra Boc) monomer **16** (1.4 g, 65%) as white solid. The product was eluted with ethyl acetate/hexane (10:90 v/v). [1]H NMR (400 MHz, $CDCl_3$) δ: 7.15 (s, 2H, a), 7.09 (t, *J* = 2.13 Hz,1H, b), 7.05 (d, *J* = 2.13 Hz, 2H, c), 6.70-6.63 (dd, *J* = 17.56, 10.87 Hz, 1H, d), 5.80-5.76 (d, *J* = 17.56 Hz, 1H, e), 5.36-5.34 (d, *J* = 10.87 Hz, 1H, f), 1.54 (s, 18H, g), 1.31 (s, 18H, h). [13]C NMR (100 MHz, $CDCl_3$) δ: 151.11, 149.24, 139.45, 135.09, 133.54, 127.04, 120.51, 118.12, 116.37, 114.77, 83.96, 83.69, 27.83, 27.39.

Synthesis of compound 20

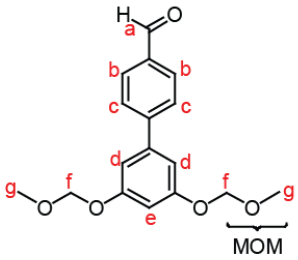

20

According to general procedure 4, compound **14** (5.0 g, 10.3 mmol) was reacted with 4-bromobenzaldehyde (2.3 g, 12.3 mmol) and $PdCl_2(PPh_3)_2$ (0.35 g, 0.5 mmol) to afford compound **20** (2.4 g, 31%) as light yellow solid. The product was eluted with ethyl acetate/hexane (12:88 v/v). ^{1}H NMR (400 MHz, $CDCl_3$) δ: 10.04 (s, 1H, a), 7.94-7.92 (d, 2H, *J* = 8.44 Hz, b), 7.73-7.71 (d, 2H, *J* = 8.44 Hz, c), 6.97 (d, *J* = 2.27 Hz, 2H, d), 6.81-6.80 (t, *J* = 2.27 Hz, 1H, e), 5.22 (s, 4H, f), 3.51 (s, 6H, g). ^{13}C NMR (100 MHz, $CDCl_3$) δ: 191.98, 158.85, 146.84, 142.02, 135.53, 130.29, 127.87, 109.01, 104.85, 94.65, 56.25; FAB/MS *m/z* 303.115 $[M+H]^+$ (expected m/z=303.11).

Synthesis of compound 21

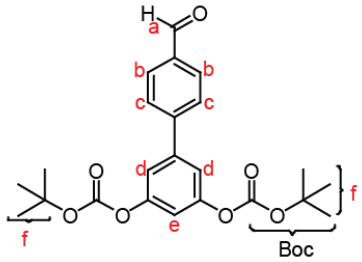

21

According to general procedure 7, compound **20** (2.4 g, 7.9 mmol) was reacted with DOWEX resin to yield 0.6 g of dihydroxy biaryl aldehyde. The hydroxyl groups were further protected as Boc groups according to general procedure 8 to obtain compound **21** (1.0 g, 91%) as white solid. The product was eluted with ethyl acetate/hexane (5:95 v/v). ^{1}H NMR (400 MHz, $CDCl_3$) δ: 10.06 (s, 1H, a), 7.96-7.94 (d, 2H, *J* = 8.41 Hz, b), 7.73-7.71 (d, 2H, *J* = 8.41 Hz, c), 7.33 (d, *J* = 2.17 Hz, 2H, d), 7.15 (t, *J* = 2.17 Hz, 1H, e), 1.57 (s, 18H, f). ^{13}C NMR (100 MHz, $CDCl_3$) δ: 191.92, 151.97, 151.37, 145.38, 141.88, 135.88, 130.43, 127.97, 117.73, 114.85, 84.26, 27.83.

Synthesis of compound 22

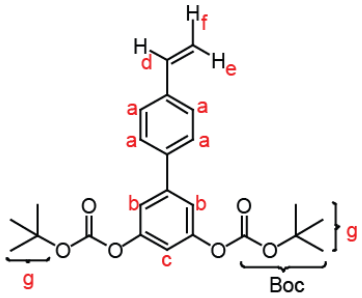

22

According to general procedure 9 for Wittig reaction, compound **19** (1.3 g, 3.14 mmol) was reacted with $MePPh_3Br$ (1.68 g, 4.71 mmol) and KO^tBu (0.53 g, 4.71 mmol). The product was eluted with ethyl acetate/hexane (10:90 v/v) to afford the desired product (0.87 g, 67%) as white solid. ^1H NMR (400 MHz, $CDCl_3$) δ: 7.53-7.46 (m, 4H, a), 7.28 (d, 2.17 Hz, 2H, b), 7.08 (t, 2.17 Hz, 1H, c), 6.78-6.71 (dd, *J* = 17.56, 10.87 Hz,1H, d), 5.82-5.77 (d, *J* = 17.56 Hz, 1H, e), 5.30-5.27 (d, *J* = 10.87 Hz, 1H, f), 1.58-157 (m, 18H, g). ^{13}C NMR (100 MHz, $CDCl_3$) δ: 151.80, 151.47, 142.98, 138.84, 137.48, 136.36, 127.42, 126.83, 117.23, 114.51, 113.68, 84.02, 27.84.

4.4.8 General Procedures for Polymer Syntheses

All the Boc-protected biaryl monomers were polymerized via free radical polymerization with AIBN as the initiator. The Boc groups were then deprotected using trifluoroacetic acid (TFA) to obtain the corresponding biaryl phenolic polymers.

Procedure 10 for polymerization

A solution of the appropriate Boc-protected biaryl monomer in anhydrous THF was taken in a 10 mL oven-dried schlenk flask under argon at room temperature. AIBN was added and the schlenk flask was sealed and subjected to three freeze-pump-thaw cycles. The reaction mixture was stirred at RT for 5 min and the schlenk flask was then transferred to an oil bath preheated to 70 ^{o}C. After the polymerization was complete, the polymer was diluted with THF and precipitated twice into large excess of hexane. The white precipitate was filtered, and was washed with either isopropanol or methanol to get rid of the residual monomer. The white powder obtained was dried under vacuum at 40 ^{o}C for 24 h to obtain the final polymers as white solids.

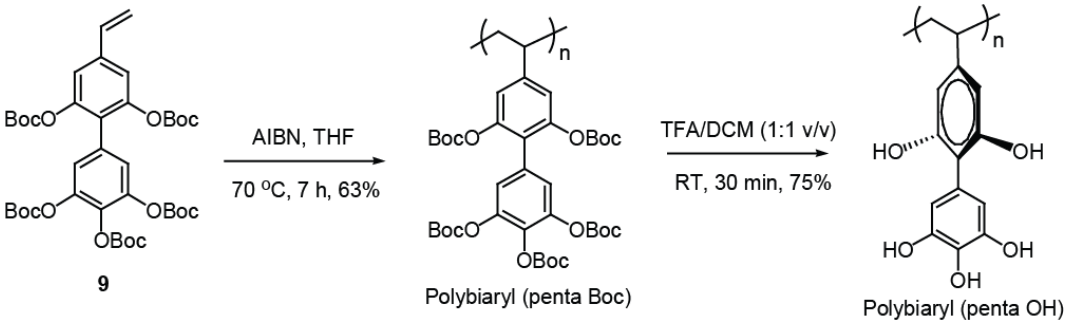

Scheme 4.5 Synthesis of polybiaryl (penta OH) polymer.

Procedure 11 for the deprotection of Boc groups using TFA

The appropriate Boc-protected biaryl polymer was taken in 5 mL DCM at RT under argon and 5 mL trifluoro acetic acid (TFA) was added to it. The clear solution obtained was stirred at RT for 30 min, during which the solution initially turned turbid and finally

a precipitate was obtained. An additional 10 mL DCM was added and the solution was centrifuged. The precipitate obtained was washed thrice with excess DCM and was dried under vacuum at 40 ^{0}C for 24 h to obtain the corresponding biaryl phenolic polymer.

Polybiaryl (Penta Boc)

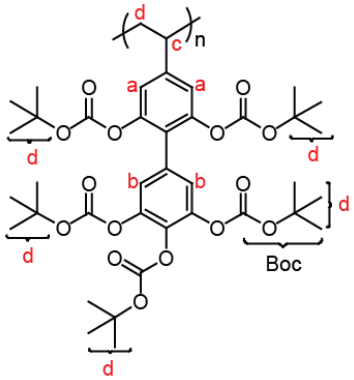

According to general procedure 10, monomer **9** (1.35 g, 1.778 mmol) was reacted with AIBN (2.93 mg, 0.018 mmol) in THF (4.0 mL) for 7 h. The white precipitate was washed with excess isopropanol to obtain the polymer (0.85 g, 63%) as a white solid. GPC (THF) Mn: 37,000 g/mol; PDI: 1.56. ^{1}H NMR (400 MHz, $CDCl_3$) δ: 7.06 (bs, 2H, a, ArH), 6.62 (bs, 2H, b, ArH), 2.34 (bs, 1H, c, -CH of polymer backbone), 1.44-1.23 (2bs, 47H, d, O-C$(CH_3)_3$, and -CH_2 of polymer backbone).

Polybiaryl (tetra Boc)

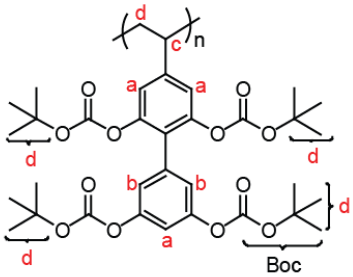

According to general procedure 10, monomer **19** (1.30 g, 2.016 mmol) was reacted with AIBN (2.93 mg, 0.020 mmol) in THF (2.6 mL) for 20 h. The white precipitate was

washed with excess isopropanol to obtain the polymer (0.87 g, 67%) as a white solid. GPC (THF) Mn: 37,000 g/mol; PDI: 1.68. ^{1}H NMR (400 MHz, $CDCl_3$) δ: 7.06-6.92 (2bs, 3H, a, ArH), 6.47 (bs, 2H, b, ArH), 2.34 (bs, 1H, c, -CH of polymer backbone), 1.45-1.23 (2bs, 38H, d, O-C$(CH_3)_3$, and -CH_2 of polymer backbone).

Polybiaryl (tri Boc)

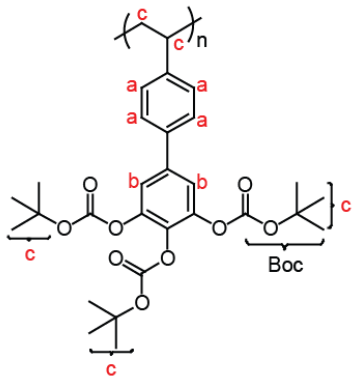

According to general procedure 10, monomer **12** (0.65 g, 1.230 mmol) was reacted with AIBN (20.2 mg, 0.123 mmol) in THF (1.3 mL) for 42 h. The white precipitate was washed with hexane to obtain the polymer (0.58 g, 89%) as a white solid. GPC (THF) Mn: 11,600 g/mol; PDI: 1.71. ^{1}H NMR (400 MHz, $CDCl_3$) δ: 7.43-7.16 (bs, a, 4H, ArH), 6.82-6.59 (bs, 2H, b, ArH), 1.55-1.39 (bm, 30H, c, O-C$(CH_3)_3$, -CH of polymer backbone, and -CH_2 of polymer backbone).

Polybiaryl (di Boc)

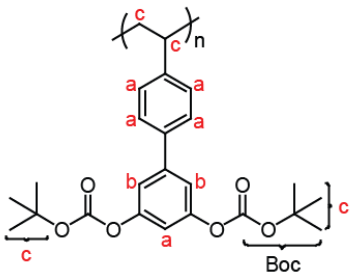

According to general procedure 10, monomer **22** (0.80 g, 1.941 mmol) was reacted with AIBN (31.9 mg, 0.194 mmol) in THF (3.2 mL) for 2 days. The white precipitate was washed with excess methanol to obtain the polymer (0.58 g, 72%) as a white solid. GPC (THF) Mn: 15,000 g/mol; PDI: 1.84. ^{1}H NMR (400 MHz, $CDCl_3$) δ: 7.16-6.98 (bm, 5H, a, ArH), 6.54 (bm, 2H, b, ArH), 1.53-1.43 (bm, 21H, c, O-C(CH_3)$_3$, -CH of polymer backbone, and -CH_2 of polymer backbone).

Polybiaryl (Penta OH)

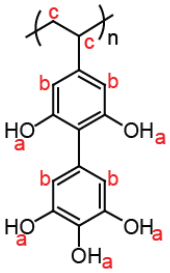

According to general procedure 11, polybiaryl (penta Boc) (0.77 g, 1.013 mmol) was reacted with TFA/DCM (1:1 v/v) to obtain the polybiaryl (penta OH) (0.25 g, 95%) as a dark brown solid. ^{1}H NMR (400 MHz, DMSO-d6) δ: 8.53-7.93 (2bs, 5H, a, -OH), 6.25-5.95 (2bs, 4H, b, ArH), 2.2-0.8 (bs, 3H, c, -CH and -CH_2 of polymer backbone).

Polybiaryl (tetra OH)

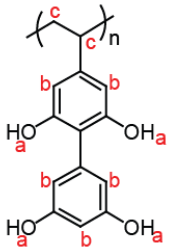

According to general procedure 11, polybiaryl (tetra Boc) (0.80 g, 1.241 mmol) was reacted with TFA/DCM (1:1 v/v) to obtain the polybiaryl (tetra OH) (0.30 g, 99%) as a

light brown solid. ^{1}H NMR (400 MHz, DMSO-d6) δ: 8.89-8.09 (2bs, 4H, a, -OH), 6.19-5.84 (bm, 5H, b, ArH), 2.2-0.8 (bs, 3H, c, -CH and -CH_2 of polymer backbone).

Polybiaryl (triOH)

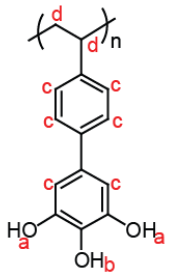

According to general procedure 11, polybiaryl (tri Boc) (0.52 g, 1.984 mmol) was reacted with TFA/DCM (1:1 v/v) to obtain the polybiaryl (tetra OH) (0.185 g, 82%) as a dark brown solid. ^{1}H NMR (400 MHz, DMSO-d6) δ: 8.83 (s, 2H, a, -OH), 8.16 (s, 1H, b, -OH), 7.6-6.0 (2bs, 6H, c, ArH), 2.2-0.8 (bs, 3H, d, -CH and -CH_2 of polymer backbone).

Polybiaryl (diOH)

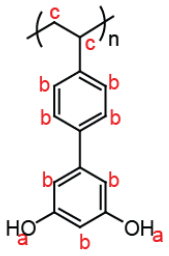

According to general procedure 11, polybiaryl (di Boc) (0.55 g, 1.334 mmol) was reacted with TFA/DCM (1:1 v/v) to obtain the polybiaryl (di OH) (0.19 g, 67%) as a light brown solid. ^{1}H NMR (400 MHz, DMSO-d6) δ: 9.23 (s, 2H, a, -OH), 7.33-6.17 (bm, 7H, b, ArH), 2.2-0.8 (bs, 3H, c, -CH and -CH_2 of polymer backbone).

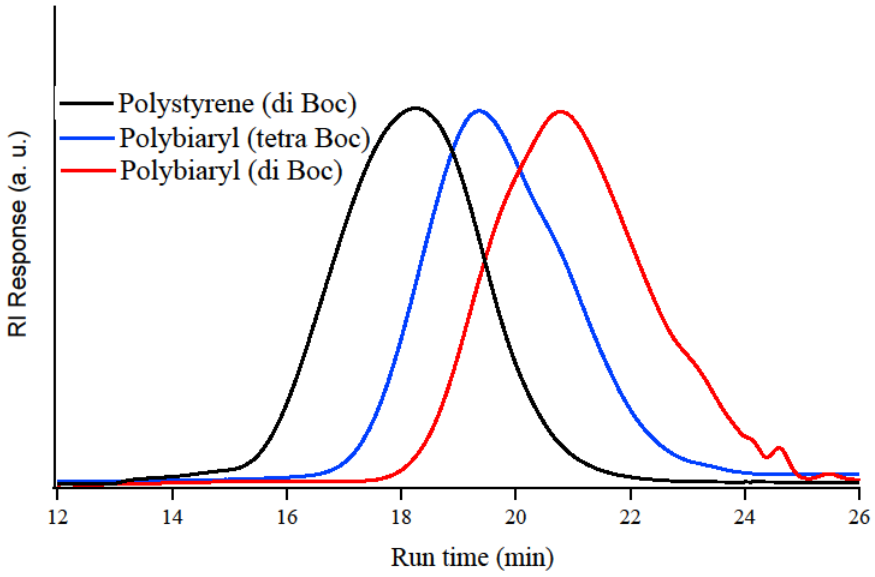

Figure 4.6 GPC (THF) traces of Boc protected phenolic biaryl polymers.

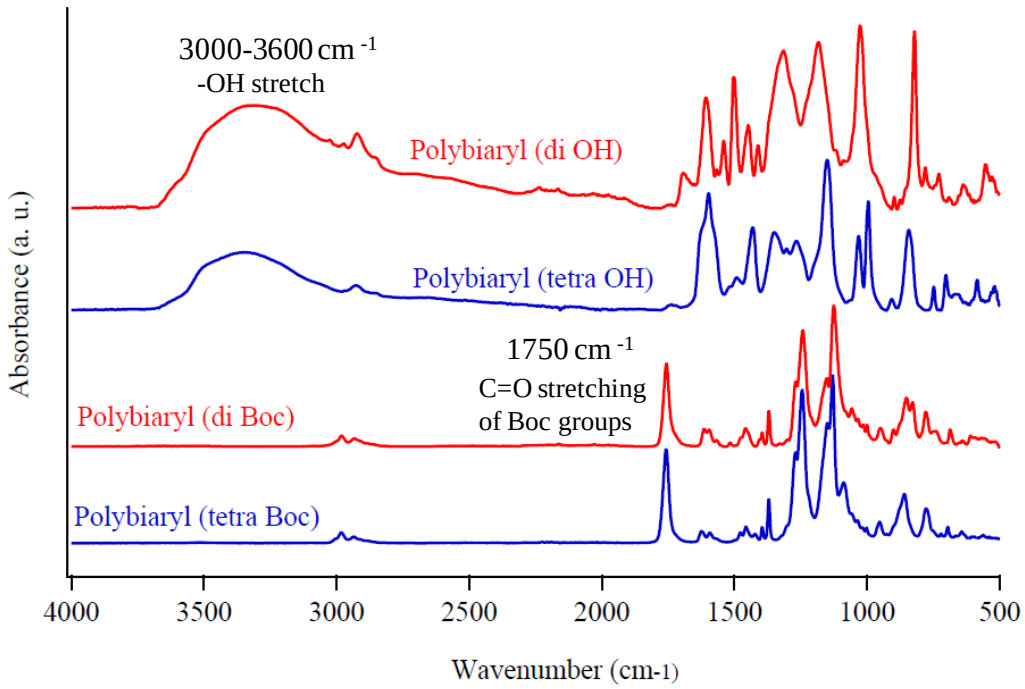

Figure 4.7 FTIR spectra of biaryl polymers.

a)

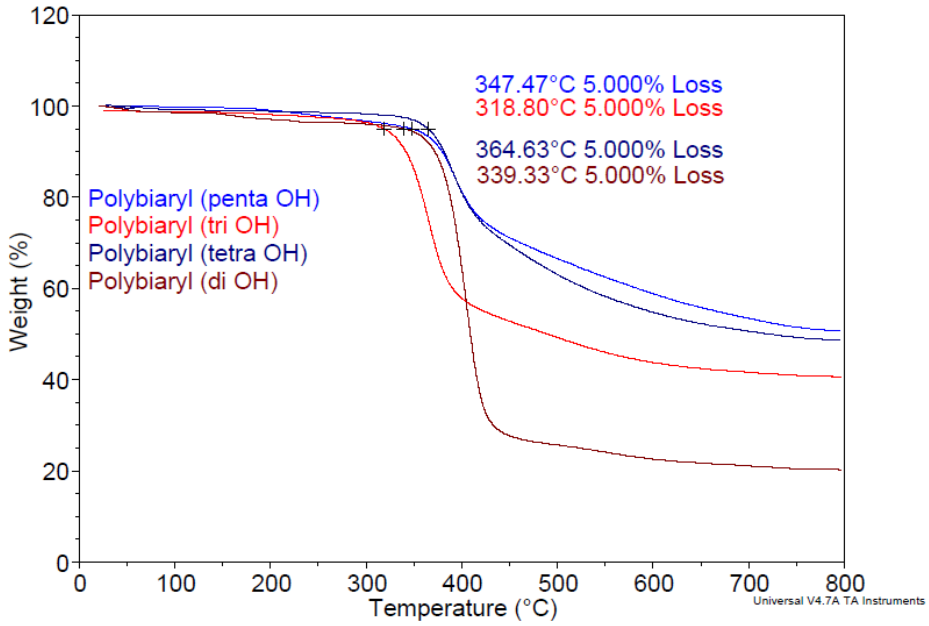

b)

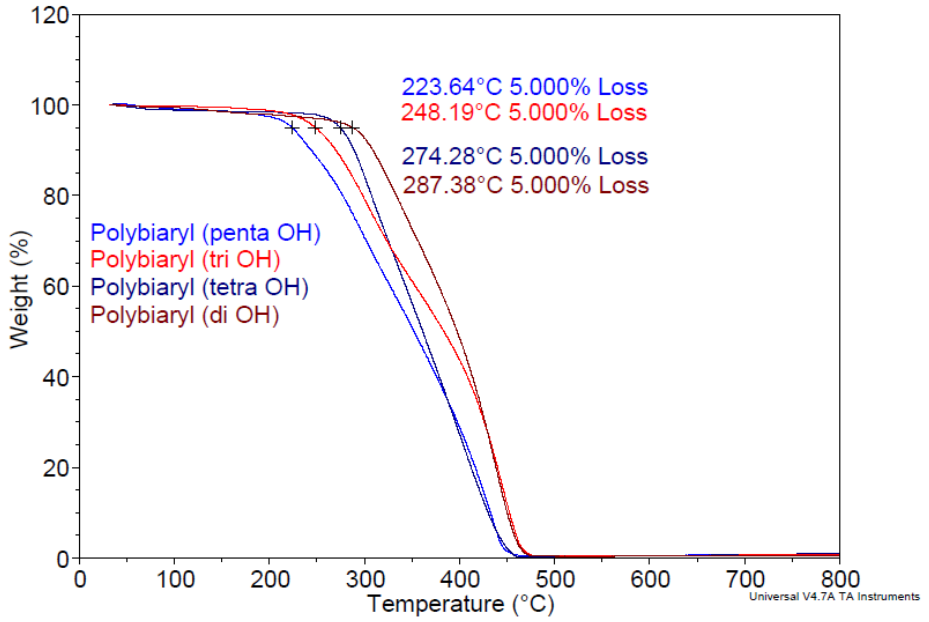

Figure 4.8 TGA traces of phenolic polymers (a) when heated under nitrogen at 10 ^{o}C/min and (b) when heated under air at 1 ^{o}C/min.

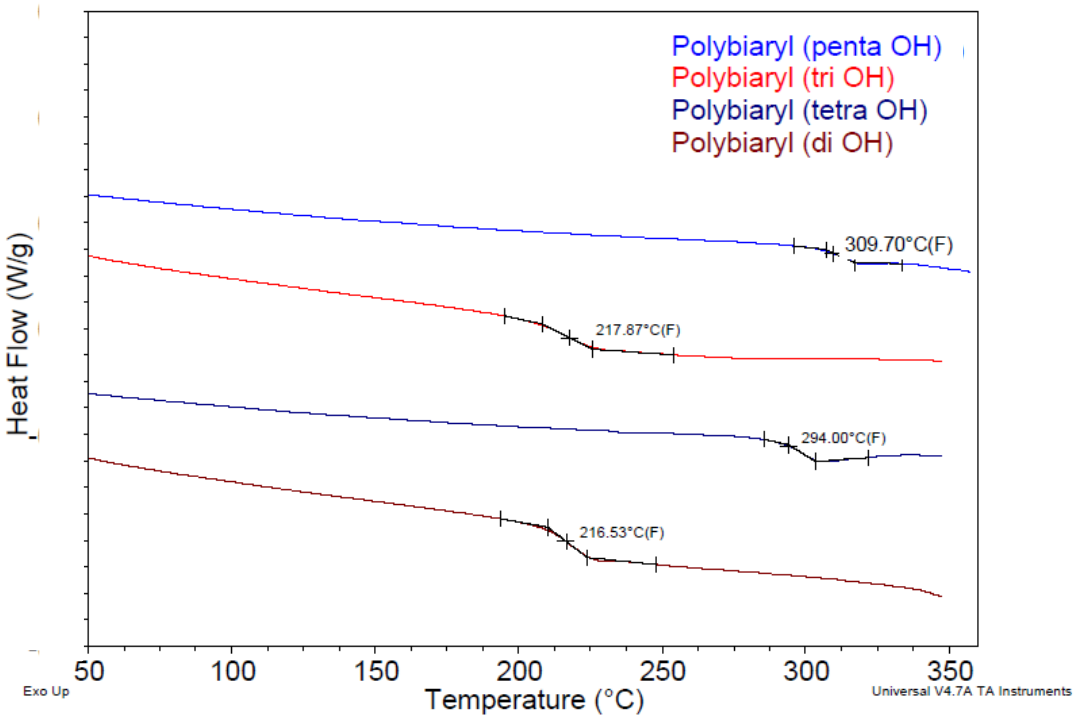

Figure 4.9 DSC traces of biaryl polymers.

4.5 References

1. Celik, S. U.; Bozkurt, A., Proton conduction promoted by 1H-1,2,3-benzotriazole in non-humidified polymer membranes. *Electrochim. Acta* **2011**, *56*, 5961-5965.

2. Chen, Y. B.; Thorn, M.; Christensen, S.; Versek, C.; Poe, A.; Hayward, R. C.; Tuominen, M. T.; Thayumanavan, S., Enhancement of anhydrous proton transport by supramolecular nanochannels in comb polymers. *Nat. Chem.* **2010**, *2*, 503-508.

3. Granados-Focil, S.; Woudenberg, R. C.; Yavuzcetin, O.; Tuominen, M. T.; Coughlin, E. B., Water-free proton-conducting polysiloxanes: A study on the effect of heterocycle structure. *Macromolecules* **2007**, *40*, 8708-8713.

4. Kreuer, K. D., On the development of proton conducting polymer membranes for hydrogen and methanol fuel cells. *J. Membr. Sci.* **2001**, *185*, 29-39.

5. Nagamani, C.; Versek, C.; Thorn, M.; Tuominen, M. T.; Thayumanavan, S., Proton conduction in 1*H*-1,2,3-triazole polymers: Imidazole-like or pyrazole-like? *J. Polym. Sci. Pol. Chem.* **2010**, *48*, 1851-1858.

6. Schuster, M. E.; Meyer, W. H., Anhydrous proton-conducting polymers. *Ann. Rev. Mater. Res.* **2003**, *33*, 233-261.

7. Schuster, M. F. H.; Meyer, W. H.; Schuster, M.; Kreuer, K. D., Toward a new type of anhydrous organic proton conductor based on immobilized imidazole. *Chem. Mat.* **2004**, *16*, 329-337.

8. Wang, J. T. W. W. J. T. W.; Hsu, S. L. C., Enhanced high-temperature polymer electrolyte membrane for fuel cells based on polybenzimidazole and ionic liquids. *Electrochim. Acta* **2011**, *56*, 2842-2846.

9. Nagamani, C.; Viswanathan, U.; Versek, C.; Tuominen, M. T.; Auerbach, S. M.; Thayumanavan, S., Importance of dynamic hydrogen bonds and reorientation barriers in proton transport. *Chem. Commun.* **2011**, *47*, 6638-6640.

10. Grein, F., Twist angles and rotational energy barriers of biphenyl and substituted biphenyls. *J. Phys. Chem. A* **2002**, *106*, 3823-3827.

11. Leroux, F., Atropisomerism, biphenyls, and fluorine: A comparison of rotational barriers and twist angles. *Chembiochem* **2004**, *5*, 644-649.

12. Martwiset, S.; Yavuzcetin, O.; Thorn, M.; Versek, C.; Tuominen, M.; Coughlin, E. B., Proton Conducting Polymers Containing 1H-1,2,3-Triazole Moieties. *J. Polym. Sci. Pol. Chem.* **2009**, *47*, 188-196.

13. Zhou, Z.; Li, S. W.; Zhang, Y. L.; Liu, M. L.; Li, W., Promotion of proton conduction in polymer electrolyte membranes by 1H-1,2,3-triazole. *J. Am. Chem. Soc.* **2005**, *127*, 10824-10825.

14. Bharathi, P.; Zhao, H. D.; Thayumanavan, S., Toward globular macromolecules with functionalized interiors: Design and synthesis of dendrons with an interesting twist. *Org. Lett.* **2001**, *3*, 1961-1964.

15. Sivanandan, K.; Aathimanikandan, S. V.; Arges, C. G.; Bardeen, C. J.; Thayumanavan, S., Probing every layer in dendrons. *J. Am. Chem. Soc.* **2005**, *127*, 2020-2021.

16. Azagarsamy, M. A.; Sokkalingam, P.; Thayumanavan, S., Enzyme-Triggered Disassembly of Dendrimer-Based Amphiphilic Nanocontainers. *J. Am. Chem. Soc.* **2009**, *131*, 14184-14185.

CHAPTER 5

SYNTHESIS OF POLYSTYRENE-b-POLY (3,4-DIHYDROXY STYRENE) BLOCK COPOLYMERS

5.1 Introduction

A number of polymers based on *N*-heterocycles are studied for use as anhydrous proton transporting polymers in high temperature polymer electrolyte membrane fuel cells (PEMFCs).[1-7] A majority of these proton transporting polymers are homopolymers in which the organization of the proton transporting moieties is poorly controlled. In the case of hydrous proton transporting sulfonated polymers, it has been very well established that the block copolymers with self-assembled ordered proton conducting nanostructures provide enhanced proton conductivity compared to the corresponding random copolymers. [8-13] The increase in proton conductivity is attributed to the ordered contiguous pathway available for proton transport through water channels in self-assembled nanostructures. The enhancement of proton conductivity via nano-confinement has also been demonstrated in the case of anhydrous proton transport.[14] While sulfonated block copolymers have been extensively investigated, there are very limited reports on anhydrous proton transporting block copolymers. Moreover, the effect of nanoscale morphology on proton transport has not been investigated in anhydrous proton transporting materials.

One of the reasons for limited studies on anhydrous proton transporting block copolymers is the lack of a viable synthetic pathway, restricting easy access to these polymers. The synthesis and self-assembly properties of poly (styrene-b-4-hydroxy

styrene) (PS-b-PS(4-OH)) block copolymers have been well studied, and show that PS-b-PS(4-OH) block copolymers display great propensity to form self-assembled nanostructures.[15-18] It has also been shown in Chapter 3 that poly(4-hydroxy styrene) can conduct protons under anhydrous conditions.[19] Considering that PS-b-PS(4-OH) block copolymers are synthetically easily accessible, and phenols can conduct protons under anhydrous conditions, we thought that PS-b-PS(4-OH) block copolymers will be suitable candidates to investigate the effect of morphology on proton transport.

Although poly (4-hydroxy styrene) can conduct protons under anhydrous conditions, its proton conductivity is not substantial. Hence, we focused on poly (3,4-dihydroxystyrene)-b- polystyrene (PS(3,4-diOH)-b-PS) block copolymers instead of poly PS-b-PS(4-OH). The synthesis of PS(3,4-diOH)-b-PS has not been reported, and initial efforts to synthesize PS(3,4-diOH)-b-PS block copolymers via nitroxide mediated polymerization (NMP) initiated by 2,2,5-trimethyl-4-phenyl-3-azahexane-3-oxy (TIPNO), following similar synthetic procedures reported for PS-b-PS(4-OH),[17] were either not successful or resulted in broader molecular weight distribution. Hence, our initial focus has been on developing a viable synthetic pathway to easily access PS(3,4-diOH)-b-PS block copolymers. The synthesis of PS(3,4-diOH)-b-PS block polymers of varying molecular weights and block ratios via anionic polymerization is discussed in this Chapter. The self-assembly and proton transport characteristics of the block copolymers will be the focus of future work.

5.2 Results and Discussion

PS-b-PS(4-OH) block copolymers can be obtained through the deacetylation of poly(styrene-b-4-acetoxy styrene) (PS-b-PS(4-OAc)) block copolymers. The synthesis of PS-b-PS(4-OAc) block copolymers via NMP polymerization of styrene and 4-acetoxy styrene is well established.[17] Synthetic procedures for the removal of acetoxy groups (deacetylation) after polymerization have also been well studied and optimized.[16-17] Thus, PS(3,4-diOH)-b-PS block copolymers can be easily obtained by deacetylation of the precursor poly(3,4-diacetoxystyrene)-b-styrene (PS(3,4-diOAc)-b-PS) block copolymers. Hence, we initially attempted to synthesize PS(3,4-diOAc)-b-PS block copolymers via NMP. The polymerization of 3,4-diacetoxy styrene in both xylenes and toluene resulted in a broad molecular weight distribution. Attempts to grow 3,4-diacetoxy styrene block from the polystyrene macroinitiator were also not successful. The polymerizations resulted in either bimodal or broad molecular weight distributions. This might be due to

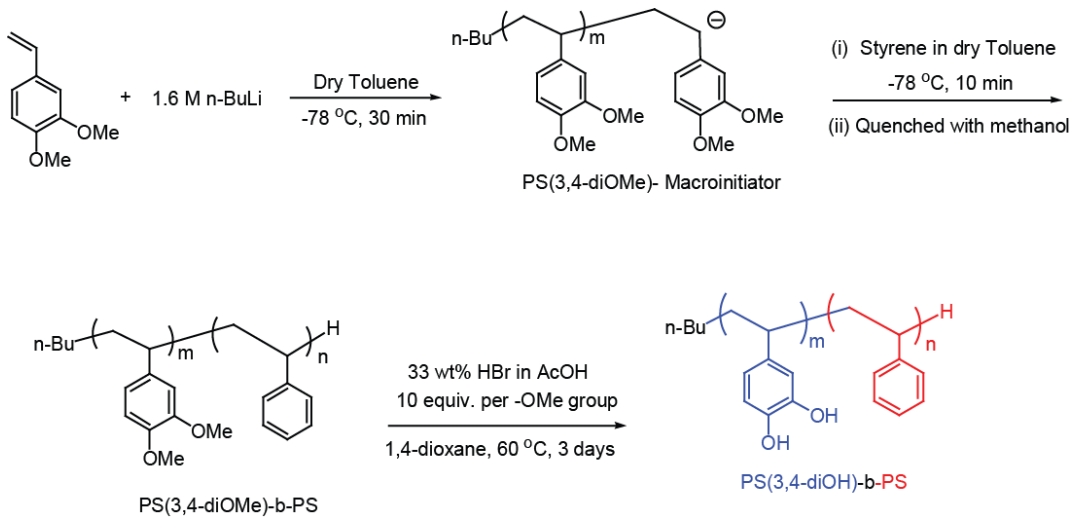

Scheme 5.1 Synthesis of PS(3,4-diOH)-b-PS block copolymers via anionic polymerization.

the differences in the solubility of PS and PS(3,4-diOAc) blocks since acetoxy groups are polar. Thus, the synthesis of PS(3,4-diOH)-b-PS block copolymers was pursued via anionic polymerization. Acetoxy groups are not stable under basic conditions employed in anionic polymerization. Hence, 3,4-dimethoxy styrene was used as a precursor monomer for 3,4-dihydroxy styrene instead of 3,4-diacetoxy styrene. The synthetic scheme for anionic polymerization of 3,4-dimethoxy styrene and styrene monomers is shown in Scheme 5.1.

Table 5.1 The polymerization and molecular weight details of poly(3,4-dimethoxystyrene)-b-polystyrene block copolymers.

Trial	3,4-diOMe Styrene v/ mL	1.6 M n-BuLi v/ mL	PS(3,4-diOMe) macroinitiator		Styrene	PS(3,4-diOMe)-b-PS		PS(3,4-diOMe) weight fraction	PS weight fraction
			Mn g/mol	PDI		Mn g/mol	PDI		
1	0.8	0.20	13,100	1.45	1.0	88,200	1.45	0.15	0.85
2	1.0	0.20	18,400	1.48	0.5	55,500	1.42	0.33	0.67
3	1.5	0.20	20,300	1.49	0.4	45,800	1.50	0.44	0.56

5.2.1 Synthesis of Poly(3,4-dimethoxystyrene)-b-Polystyrene Block Copolymers

A series of poly(3,4-dimethoxystyrene)-b-styrene block copolymers with different molecular weights and varying block ratios were synthesized. The polymerization of 3,4-dimethoxy styrene at room temperature did not result in any polymer. The solution of a mixture of 3,4-dimethoxy styrene and n-BuLi in toluene displays orange color at -78 ^{o}C. However, the orange color disappeared when the solution was warmed to room temperature. The orange color is a characteristic of 3,4-dimehtoxy styrene anion, and therefore the disappearance of color is an indication that 3,4-dimehtoxy styrene anion is

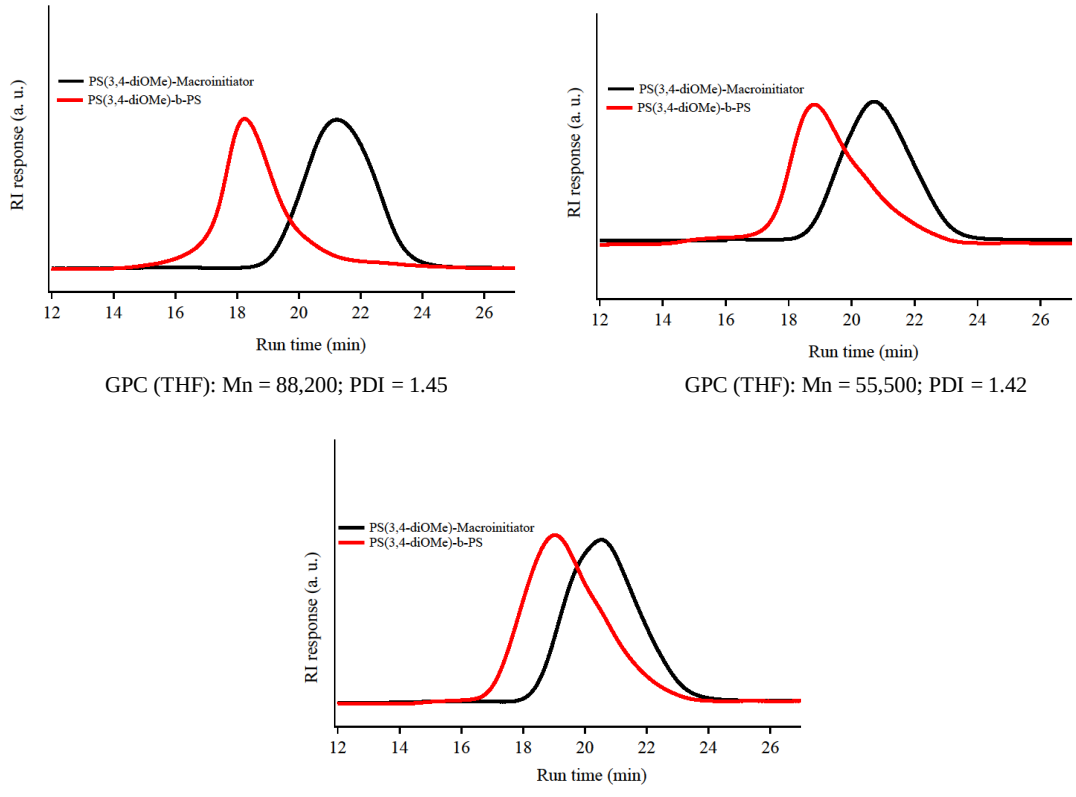

GPC (THF): Mn = 88,200; PDI = 1.45

GPC (THF): Mn = 55,500; PDI = 1.42

GPC (THF): Mn = 45,800; PDI = 1.50

Figure 5.1 GPC (THF) chromatograms of PS(3,4-diOMe)-b-PS block copolymers of varying molecular weights.

not stable at room temperature. Thus, the polymerization was carried out at -78 ^{o}C.

The polymerization and molecular weight details of poly(3,4-dimethoxystyrene)-b-polystyrene block copolymers are shown in Table 5.1. Poly(3,4-dimethoxy styrene) with different molecular weights was obtained by varying the monomer : initiator ratio. The volume of n-BuLi initiator was kept constant, and the amount of 3,4-dimethoxy styrene monomer was increased gradually from 0.8 to 1.5 mL. As expected, the molecular weight increases with increasing moles of 3,4-dimethoxy styrene monomer. The molecular weight of the block copolymers was controlled by varying the amount of styrene added in the second step of polymerization. Three block copolymers of different molecular weights and varying block ratios of poly(3,4-dimethoxy styrene) and polystyrene were obtained. The GPC chromatograms of the block copolymers are shown in Figure 5.1. All polymers display unimodal distribution. Thus, a fine control over the molecular weight and block ratios was obtained by tuning the monomer: initiator ratio, as well as the relative amounts of styrene and 3,4-dimethoxy styrene monomers.

Table 5.2 Details of poly(3,4-dihydroxystyrene)-b-polystyrene block copolymers.

Trial	PS(3,4-diOMe)	PS(3,4-diOH)	PS	PS(3,4-diOH)-b-PS	PS(3,4-diOH) weight fraction	PS weight fraction
	Mn	Mn	Mn	Mn		
1	13,100	10,900	75,100	86,000	0.13	0.87
2	18,400	15,300	37,100	52,400	0.30	0.70
3	20,300	16,800	25,500	42,300	0.40	0.60

5.2.2 Synthesis of Poly(3,4-dihydroxystyrene)-b-Polystyrene Block Copolymers

PS(3,4-diOH)-b-PS block copolymers were obtained from the demethylation of PS(3,4-diOMe)-b-PS block copolymers. Boron tribromide (BBr_3) is widely employed for the demethylation of -OMe groups in small molecules. The use of BBr_3 for the deprotection of -OMe groups is also reported in case of random copolymers.[20-22] However, the purification process in the case of polymers is very tedious. Initial attempts for the removal of -OMe groups in PS(3,4-diOMe)-b-PS block copolymers using BBr_3 did not result in pure polymers. The polymers obtained were bluish in color indicating the incomplete removal of BBr_3 reagent from the polymer. Acidification of the polymer solution, followed by thorough washing with various solvents did not result in the complete removal of BBr_3. Unlike random copolymers, block copolymers present a high local density of -OH groups. Due to the presence of high density of -OH groups, particularly in ortho position to each other, the electron deficient boron atom might be strongly coordinating with the -OH groups, making it difficult to completely remove from the polymeric system.

To overcome the purification problem with the use of BBr_3, the removal of -OMe groups was carried out with HBr solution in acetic acid. The polymers were obtained as off-white solids and ^{1}H NNMR indicated the polymers to be pure. A series of PS(3,4-diOH)-b-PS copolymers with varying molecular weights and block ratios were obtained in good yields. The details of the block copolymers are summarized in Table 5.2. The molecular weights of the polymers were estimated based on the complete removal of -OMe groups, which was confirmed by ^{1}H NMR. The ^{1}H NMR spectra of PS(3,4-diOMe)-b-PS and PS(3,4-diOH)-b-PS block copolymers are shown in Figure 5.2. The

complete removal of -OMe groups is evident from the complete disappearance of peaks at 3.5-3.8 ppm, corresponding to -OMe groups and a concomitant appearance of the peak at 8.4 ppm corresponding to the -OH groups.

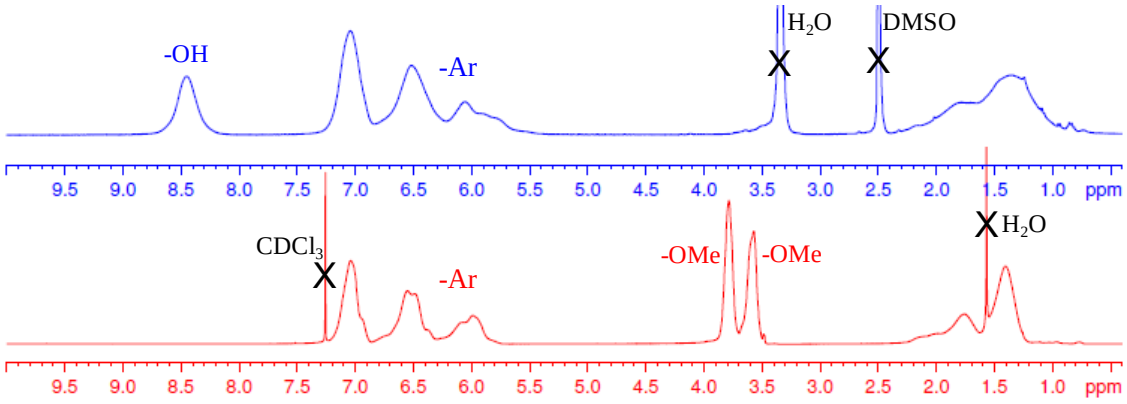

Figure 5.2 ^{1}HNMR spectra of PS(3,4-diOMe)-b-PS (red) and PS(3,4-diOH)-b-PS (blue) block copolymers.

5.3 Summary

The synthesis of a series of PS(3,4-diOH)-b-PS block copolymers has been demonstrated via anionic polymerization. The control over the molecular weight of the block copolymers was achieved by varying the monomer: initiator ratio as well as the relative moles of 3,4-dimethoxy styrene and styrene monomers. It has also been shown that the -OMe protecting groups in polymers can be removed with great ease and purity by using HBr solution instead of BBr_3. The synthetic route developed here will provide a facile access to a series of PS(3,4-diOH)-b-PS block copolymers. The self-assembly and proton transport characteristics of these block copolymers are the focus of future work. It

will provide an opportunity to systematically evaluate the correlation between nanoscale morphology and proton transport in anhydrous systems.

5.4 Experimental Details

5.4.1 General Materials and Methods

Styrene was purchased from Sigma Aldrich and passed through neutral alumina to remove the inhibitor. 1.6 M n-BuLi was purchased from and used as received from a fresh bottle. Toluene was obtained from Fisher Scientific and freshly distilled over sodium-benzophenone prior to use. ^{1}H NMR (400 MHz) and ^{13}C NMR (100 MHz) spectra were recorded on a Bruker 400 MHz NMR spectrometer using the residual proton and carbon resonance of the solvent, respectively as internal standards. Chemical shifts (δ) and coupling constants (J) are reported in parts per million (ppm) and Hertz, respectively. The following abbreviations are used for the peak multiplicities: s, singlet; d, doublet; t, triplet; q, quartet; m, multiplet; dd, doublet of doublet; bs, broad singlet; bm, broad multiplet. The molecular weights of the polymers were determined by gel permeation chromatography (GPC) using THF as eluent and toluene as the internal reference. PS standards were used for calibration and the output was received and analyzed using RI detector. All polymerizations were carried out under an argon atmosphere in schlenk flasks.

5.4.2 Synthetic Procedures

Synthesis of 3,4-dimethoxy styrene

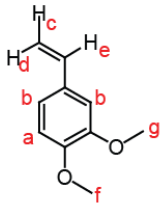

$MePPh_3Br$ (5.0 g, 13.94 mmol) and KO^tBu (1.56 g, 13.94 mmol) were taken in a 100 mL oven-dried schlenk flask and dried under vacuum for 30 min. The flask was cooled to 0 ^oC using ice bath and anhydrous THF (50 mL) was added under argon. The solution immediately turned yellow, indicating the formation of ylide. The reaction mixture was allowed to stir at 0 ^oC for 30 min and was then warmed to room temperature. A solution of 3,4-dimethoxy benzaldehyde (1.55 g, 9.3 mmol) in 20 mL THF was added using syringe and the reaction mixture was continued to stir at room temperature for 12 h. The reaction was quenched by the addition of water and extracted with ethyl acetate. The combined ethyl acetate layers were dried over Na_2SO_4, concentrated under reduced pressure and the crude was purified by column chromatography (SiO_2). The product was eluted with ethyl acetate/hexane (15:85 v/v) to afford the desired product (1.15 g, 75%) as colorless oil. ^1H NMR (400 MHz, $CDCl_3$) δ: 6.80-6.86 (m, 2H, b), 6.66-6.68 (m, 1H, a), 6.51-6.58 (dd, *J* = 17.47, 10.85 Hz, 1H, e), 5.50-5.55 (d, *J* = 17.47 Hz, 1H, d), 5.03-5.06 (d, *J* = 10.85 Hz, 1H, c), 3.76 (s, 3H, f), 3.73 (s, 3H, g). ^{13}C NMR (100 MHz, $CDCl_3$) δ: 148.62, 148.60, 136.13, 130.27, 119.02, 111.23, 110.67, 108.18, 55.33, 55.26.

Synthesis of poly(3,4-dimethoxystyrene)-b-polystyrene

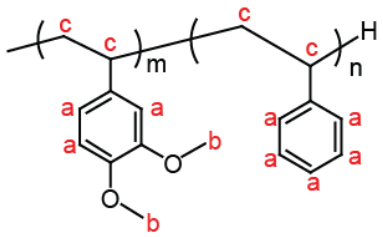

PS(3,4-diOMe)-b-PS

Anhydrous Toluene (7.0 mL) was added via syringe to a degassed oven dried schlenk flask at room temperature, followed by 3,4-dimethoxy styrene. The reaction mixture was subjected to one vacuum/argon cycle and cooled to -78 ^{o}C (dry ice/acetone bath). The flask was held at -78 ^{o}C for 30 min and n-BuLi (0.2 mL, 1.6 M in hexanes) was added via syringe. With the addition of –BuLi, the solution changed from colorless to yellow to dark orange. The polymerization of 3,4-diemthoxy styrene was continued at -78 ^{o}C for 30 min. An aliquot of the reaction mixture was taken out using an oven dried and degassed syringe and quenched with ice cold methanol. The white precipitate obtained was washed twice with methanol, centrifuged, dried under vacuum, and analyzed for molecular weight and PDI through GPC.

To the above mixture of poly(3,4-dimethoxy styrene) macroinitiator, a degassed solution of styrene (0.5 mL in 7.0 mL anhydrous Toluene) was added via syringe and the reaction mixture was stirred at -78 ^{o}C for 10 min. The reaction mixture was quenched by pouring into a 100 mL round bottom flask containing 60 mL of ice cold methanol. The white precipitate obtained was filtered, washed twice with excess methanol, and dried under vacuum to obtain the block copolymers in 60-70% yield. ^{1}H NMR (400 MHz, $CDCl_3$) δ: 7.0-5.9 (bs, 8H, a, -ArH), 3.8-3.5 (2s, 6H, b, -OMe groups), 2.1-1.2 (bs, 6H, c, -CH and -CH_2 of polymer backbone).

Synthesis of poly(3,4-dihydroxystyrene)-b-polystyrene

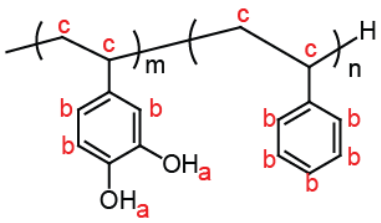

PS(3,4-diOH)-b-PS

The methoxy groups of poly(3,4-diemthoxystyrene)-b-polystyrene block copolymers were deprotected using HBr. Poly(3,4-diemthoxystyrene)-b-polystyrene (1.0 equiv) was dissolved in 1,4-dioxane (6.0 mL) and a solution of 33wt% HBr in AcOH (10 equiv. per -OMe group) was added at room temperature under argon. The reaction mixture was stirred at 60 ^{o}C for 3 days. The reaction mixture was concentrated using rotary evaporator and poured into excess water. The off-white powder obtained was centrifuged and washed thrice with excess water. The gummy off-white solid obtained was triturated with excess hexane and diethyl ether to obtain the poly(3,4-dihoxystyrene)-b-polystyrene block copolymers as off-white solids in 70-80% yield. ^{1}H NMR (400 MHz, DMSO-d6)δ: 8.4 (bs, 2H, a, -OH), 7.2-5.6(bs, 8H, b, -ArH), 2.2.-0.8 (bs, 6H, c, -CH and -CH_2 of polymer backbone).

5.5 References

1. Celik, S. U.; Bozkurt, A., Proton conduction promoted by 1H-1,2,3-benzotriazole in non-humidified polymer membranes. *Electrochim. Acta* **2011**, *56*, 5961-5965.

2. Granados-Focil, S.; Woudenberg, R. C.; Yavuzcetin, O.; Tuominen, M. T.; Coughlin, E. B., Water-free proton-conducting polysiloxanes: A study on the effect of heterocycle structure. *Macromolecules* **2007**, *40*, 8708-8713.

3. Kreuer, K. D.; Fuchs, A.; Ise, M.; Spaeth, M.; Maier, J., Imidazole and pyrazole-based proton conducting polymers and liquids. *Electrochim. Acta* **1998**, *43*, 1281-1288.

4. Martwiset, S.; Yavuzcetin, O.; Thorn, M.; Versek, C.; Tuominen, M.; Coughlin, E. B., Proton Conducting Polymers Containing 1H-1,2,3-Triazole Moieties. *J. Polym. Sci. Pol. Chem.* **2009**, *47*, 188-196.

5. Schuster, M. E.; Meyer, W. H., Anhydrous proton-conducting polymers. *Ann. Rev. Mater. Res.* **2003**, *33*, 233-261.

6. Schuster, M. F. H.; Meyer, W. H.; Schuster, M.; Kreuer, K. D., Toward a new type of anhydrous organic proton conductor based on immobilized imidazole. *Chem. Mat.* **2004**, *16*, 329-337.

7. Wang, J. T. W. W. J. T. W.; Hsu, S. L. C., Enhanced high-temperature polymer electrolyte membrane for fuel cells based on polybenzimidazole and ionic liquids. *Electrochim. Acta* **2011**, *56*, 2842-2846.

8. Elabd, Y. A.; Hickner, M. A., Block Copolymers for Fuel Cells. *Macromolecules* **2011**, *44*, 1-11.

9. Hickner, M. A.; Ghassemi, H.; Kim, Y. S.; Einsla, B. R.; McGrath, J. E., Alternative polymer systems for proton exchange membranes (PEMs). *Chem. Rev.* **2004**, *104*, 4587-4611.

10. Kishimoto, K.; Suzawa, T.; Yokota, T.; Mukai, T.; Ohno, H.; Kato, T., Nano-segregated polymeric film exhibiting high ionic conductivities. *J. Am. Chem. Soc.* **2005**, *127*, 15618-15623.

11. Lee, H. C.; Lim, H.; Su, W. F.; Chao, C. Y., Novel Sulfonated Block Copolymer Containing Pendant Alkylsulfonic Acids: Syntheses, Unique Morphologies, and Applications in Proton Exchange Membrane. *J. Polym. Sci. Pol. Chem.* **2011**, *49*, 2325-2338.

12. Schmidt-Rohr, K.; Chen, Q., Parallel cylindrical water nanochannels in Nafion fuel-cell membranes. *Nat. Mater.* **2008**, *7*, 75-83.

13. Takamuku, S.; Jannasch, P., Fully Aromatic Block Copolymers for Fuel Cell Membranes with Densely Sulfonated Nanophase Domains. *Macromol. Rapid Commun.* **2011**, *32*, 474-480.

14. Chen, Y. B.; Thorn, M.; Christensen, S.; Versek, C.; Poe, A.; Hayward, R. C.; Tuominen, M. T.; Thayumanavan, S., Enhancement of anhydrous proton transport by supramolecular nanochannels in comb polymers. *Nat. Chem.* **2010**, *2*, 503-508.

15. Cho, A. S.; Wang, L.; Dowuona, E.; Zhou, H. Y.; Nguyen, S. T.; Broadbelt, L. J., 4-Acetoxystyrene Nitroxide-Mediated Controlled Radical Polymerization: Comparison with Styrene. *J. Appl. Polym. Sci.* **2010**, *118*, 740-750.

16. Deokar, S.; Ghadage, R. S.; Rajan, C. R.; Ponrathnam, S., Facile synthesis of poly(4-hydroxy styrene) from polystyrene. *J. Appl. Polym. Sci.* **2004**, *91*, 3192-3201.

17. Quinn, J. D.; Register, R. A., Microphase Separation in Block-Random Copolymers of Styrene, 4-Acetoxystyrene, and 4-Hydroxystyrene. *J. Polym. Sci. Pt. B-Polym. Phys.* **2009**, *47*, 2106-2113.

18. Rajan, M.; Agarwal, U. S.; Bailly, C.; George, K. E.; Lemstra, P. J., Diblock and triblock copolymers of styrene and acetoxymethylstyrene by one-pot ATRP. *J. Polym. Sci. Pol. Chem.* **2005**, *43*, 575-583.

19. Nagamani, C.; Viswanathan, U.; Versek, C.; Tuominen, M. T.; Auerbach, S. M.; Thayumanavan, S., Importance of dynamic hydrogen bonds and reorientation barriers in proton transport. *Chem. Commun.* **2011**, *47*, 6638-6640.

20. Clas, S. D.; Eisenberg, A., Synthesis and bulk physical properties of styrene-alkoxide ionomers. 1. Sodium salts of polystyrene-co-4-hydroxystyrene. *J. Polym. Sci. Pt. B-Polym. Phys.* **1986**, *24*, 2743-2756.

21. Westwood, G.; Horton, T. N.; Wilker, J. J., Simplified polymer mimics of cross-linking adhesive proteins. *Macromolecules* **2007**, *40*, 3960-3964.

22. Yang, Z.; Pelton, R., The synthesis of poly(3,4-dihydroxystyrene) and poly (sodium 4-styrenesulfonate)-co-(3,4-dihydroxystyrene). *Macromol. Rapid Commun.* **1998**, *19*, 241-246.

CHAPTER 6

SUMMARY AND FUTURE DIRECTIONS

6.1 Summary

Proton transporting polymers play a critical role in the operation of a hydrogen fuel cell. The proton conductivity in polymers is influenced by several factors such as the nature of the proton transport moiety, polymer architecture, charge carrier density, and glass transition temperature (T_g). The design and development of polymer with a delicate balance among various synergistic and competing factors to provide appreciable proton conductivities is a challenging task. In this dissertation, the proton transport characteristics of two diverse classes of functional groups - *N*-heterocycles and phenols have been investigated and efforts have been made to develop the molecular design criteria for the design and development of efficient proton transporting functional groups and polymers.

In Chapter 1, a detailed discussion about the hydrous and anhydrous proton transporting polymers is presented. The interesting features as well as the limitations of the state-of-the art PFSA based polymers, particularly Nafion, are discussed. The effect of various factors on the proton transport characteristics of anhydrous proton transporting polymers is also discussed in detail.

In Chapter 2, structurally analogous polymers based on *N*-heterocycles (triazole, imidazole, and pyrazole) and benz-*N*-heterocycles (benzotriazole, benzimidazole, and benzopyrazole) are employed to probe the most probable proton conduction pathway in 1*H*-1,2,3-triazole polymers. 1*H*-1,2,3-triazole polymers have access to both *imidazole*-

like and *pyrazole-like* pathways to conduct protons. It has been shown that the *imidazole-like* pathway makes a significant contribution for the proton transport in 1*H*-1,2,3-triazole polymers, while contribution from the *pyrazole-like* pathway is negligible. Polymers containing benz-*N*-heterocycles exhibited higher proton conductivity than those with the corresponding *N*-heterocycles. Pyrazole-like functional groups, *i.e*. the molecules with two nitrogen atoms adjacent to each other, were found not to be good candidates for PT applications.

Chapter 3 introduces a new class of proton transporting functional groups, phenols. Reorientation has been well recognized to be the rate-limiting step for the Grotthuss proton transport in polymers. The 'two-site' hydrogen bond donor/acceptor feature in *N*-heterocycles is expected to hinder the reorientational dynamics, thereby adversely affecting the overall proton transport. Unlike the case of *N*-heterocycles, the hydrogen bond donor/acceptor reorientation in phenols can happen on a single -OH moiety. This 'single site' hydrogen bond donor/acceptor feature in phenols is shown to facilitate the reorientational dynamics of Grotthuss proton transport.

In Chapter 4, the proton transport characteristics of phenol-based biaryl polymers in which the -OH groups are presented in orthogonal planes have been investigated and compared with the analogous phenol-based styrene polymers. The two-dimensional disposition of -OH moieties in biaryl polymers does result in lower apparent activation energies (E_a) for proton transport. However, the lower E_a values did not translate into a net increase in proton conductivity due to the accompanying increase in glass transition temperature (T_g). Thus, the simplicity of molecular design, ease of synthesis, and lower

T_gs pf phenol-based styrenic polymer makes the styrenic architecture preferable over the analogous biaryl architecture.

Finally, in Chapter 5, the synthetic route allowing facile access to poly (styrene-b-3,4-dihydroxy styrene) block copolymers has been outlined. A series of poly (styrene-b-3,4-dihydroxy styrene) block copolymers with varying molecular weights and block ratios were achieved via anionic polymerization.

6.2 Future Directions

Block copolymers are known to provide access to a rich landscape of morphologies by simply tuning the relative volume fractions of the constituent blocks (Figure 6.1).[1] While the role of nanoscale morphology on proton conductivity has been well established in the case of hydrous proton conducting polymers, it has received limited attention in the

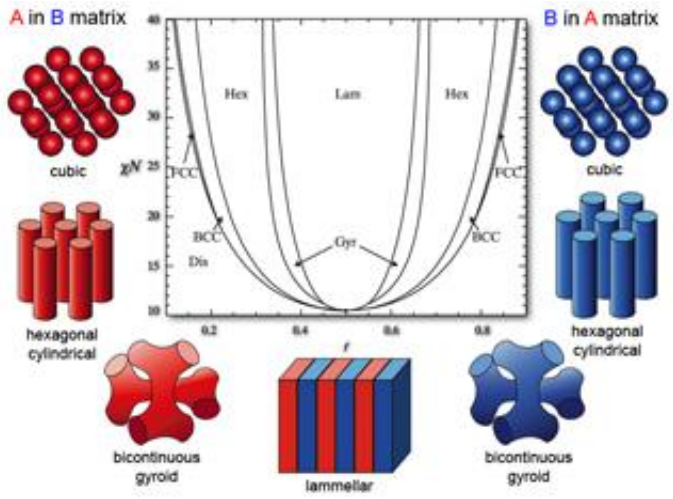

Figure 6.1 Various morphologies provided by block copolymers (taken from www.physics.nyu.edu/pine/research/nanocopology.html).

case of anhydrous proton transporting systems. Considering the great demand for efficient anhydrous proton conducting polymers in hydrogen fuel cells, it is imperative to develop a systematic understanding of the relationship between molecular structure and morphology, and the morphology and proton conductivity.

Poly (styrene-b-hydroxy styrene) block copolymers would be an interesting platform to systematically investigate the effect of nanoscale morphology on proton transport because (i) it has been shown in Chapter 3 that the reorientational dynamics in phenol-based polymers are facile,[2] and (ii) the synthetic route allowing facile access to poly (styrene-b-3,4-dihydroxy styrene) block copolymers has already been outlined in Chapter 5. The facile reorientational dynamics in phenols, combined with nano-confinement of proton transporting functionalities will likely lead to proton transport materials with markedly advanced performance.

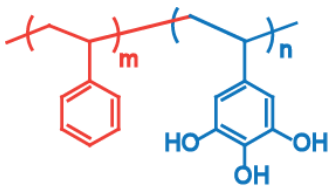

Poly(styrene-b-3,4,5-trihydroxy styrene)

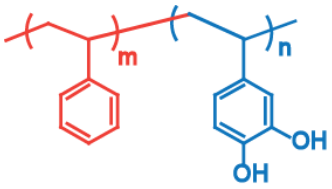

Poly(styrene-b-3,4-dihydroxy styrene)

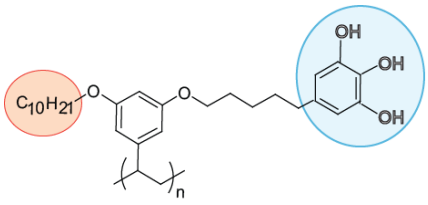

Styrene based amphiphilic comb polymer with 3,4,5-trihydroxy benzene as the proton transporting functionality

Figure 6.2 Structures of proton transporting block copolymers and amphiphilic comb polymers.

Amphiphilic comb polymers are another interesting class of polymers which have the potential to form self-assembled structures. The effect of nano-confinement on proton transport has already been demonstrated in styrene based comb polymers with *N*-heterocycles as the proton transport functionalities.[3] Considering that the reorientational dynamics in phenols, unlike the case of *N*-heterocycles, are facile amphiphilic comb polymers bearing phenols as proton transporting groups would also be interesting candidates for anhydrous proton transport. The structures of proton conducting block and amphiphilic comb polymers are shown in Figure 6.2.

6.3 References

1. Burke, S.; Eisenberg, A., Physico-chemical investigation of multiple asymmetric amphiphilic diblock copolymer morphologies in solution. *High Perform. Polym.* **2000**, *12*, 535-542.

2. Nagamani, C.; Viswanathan, U.; Versek, C.; Tuominen, M. T.; Auerbach, S. M.; Thayumanavan, S., Importance of dynamic hydrogen bonds and reorientation barriers in proton transport. *Chem. Commun.* **2011**, *47*, 6638-6640.

3. Chen, Y. B.; Thorn, M.; Christensen, S.; Versek, C.; Poe, A.; Hayward, R. C.; Tuominen, M. T.; Thayumanavan, S., Enhancement of anhydrous proton transport by supramolecular nanochannels in comb polymers. *Nat. Chem.* **2010**, *2*, 503-508.

APPENDIX

ELECTROCHEMICAL IMPEDANCE SPECTROSCOPY

A.1 Sample Preparation for Impedance Spectroscopy Measurements

Electrochemical impedance spectroscopy (EIS) is the most commonly employed technique to determine the proton conductivity of polymer electrolytes.[1-3] For impedance measurements, the polymer samples were drop cast from appropriate solvents and analyzed by ac impedance spectroscopy (IS). A schematic of a sample holder used for IS measurements is shown in Figure A.1. Kapton tape with a hole of thickness 127 μm and an area of 0.0792 cm^2 was placed onto a gold coated electrode and the polymer films were drop cast from concentrated solution onto the hole. Polymer film thickness and the contact area between the membrane and the electrode were determined by the dimensions of the hole and hence were held constant. Polymer films were annealed at 150 ^oC for

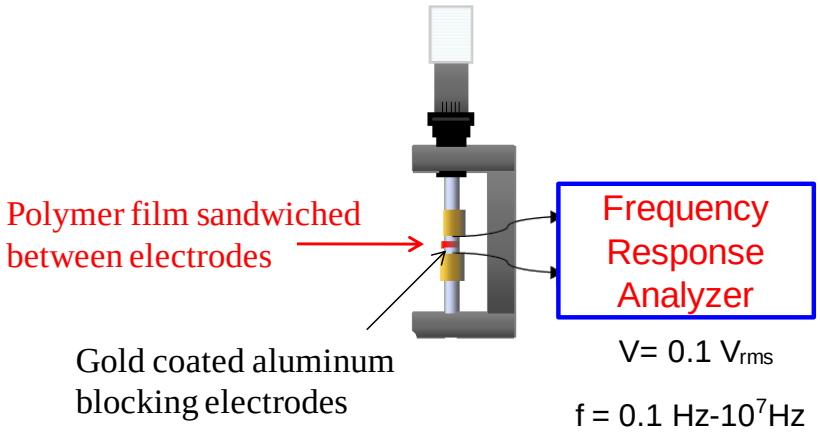

Figure A.1 Schematic representation of the sample holder used for ac impedance measurements.

about 15 h prior to measurements. Films were then placed between two gold coated aluminum blocking electrodes and transferred immediately to a vacuum oven and the proton conductivities were characterized by IS in the desired temperature range. The samples were initially heated from room temperature to the maximum temperature and were held at that temperature (to ensure complete removal of the residual solvent) for at least 10 hours. The samples were then slowly cooled to room temperature and the conductivities during the cooling cycle are reported for all the polymers reported in this thesis.

A.2 Experimental Data Analysis

The impedance response of each polymer sample was measured from 0.1 Hz-10^7 Hz with a sinusoidal excitation voltage of 0.1 V_{rms} using a Solartron 1260 impedance/gain phase analyzer. The data obtained was analyzed using Zview software. The

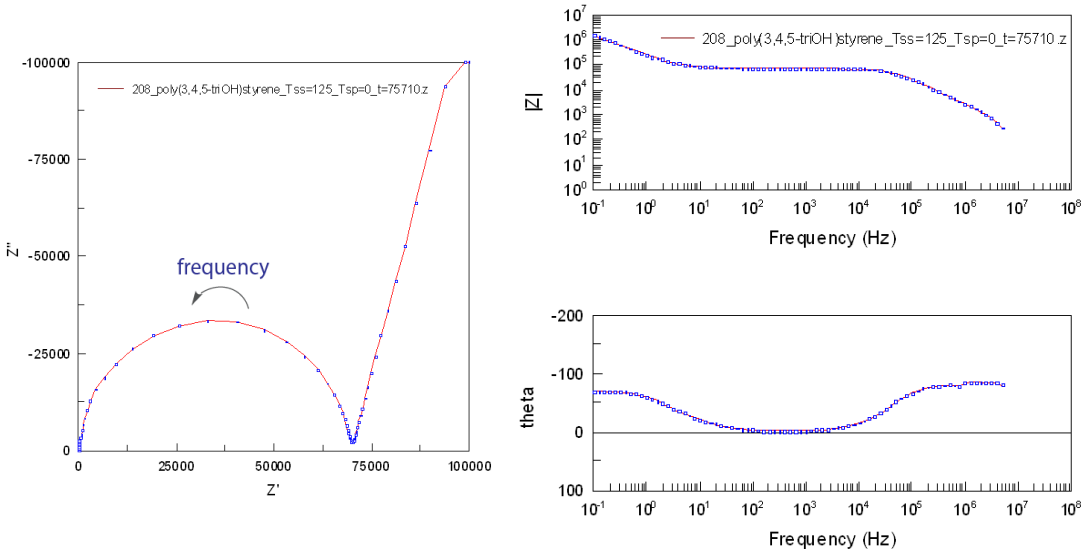

Figure A.2 Representative impedance plots (Z'' vs. Z', |Z| vs. frequency (Hz), and theta vs. frequency (Hz)) obtained from Zview.

representative impedance graphs obtained from Zview are shown in Figure A.2. The resistance (R) values were obtained by geometrically fitting a semicircular arc to the bulk response in the Z" vs. Z' plane in Zview. Z" vs. Z' plot has two intercepts on the x-axis: one near the origin ($Z' \approx 0$) and the other corresponding to the minimum imaginary response ($Z'' \approx 0$). The Z' value at the minimum imaginary response (second intercept on the x-axis) is taken as the resistance (R) value. The conductivities were derived from the equation ($\sigma = \ell/RA$), where ℓ and A are the thickness and the area of the polymer film, respectively. Conductivities lower than 10^{-9} S/cm are generally considered to be below the sensitivity of the instrument for the particular geometries used, and hence the absolute numbers below this value are not considered accurate.

A.3 References

1. Macdonald, J. R., Impedance spectroscopy: Models, data fitting, and analysis. *Solid State Ionics* **2005**, *176*, 1961-1969.

2. Ruiz-Morales, J. C.; Marrero-Lopez, D.; Canales-Vazquez, J.; Nunez, P.; Irvine, J. T. S., Application of an alternative representation to identify models to fit impedance spectra. *Solid State Ionics* **2005**, *176*, 2011-2022.

3. Zoltowski, P., Non-traditional approach to measurement models for analysis of impedance spectra. *Solid State Ionics* **2005**, *176*, 1979-1986.

BIBLIOGRAPHY

Agmon, N., The Grotthuss mechanism. *Chem. Phys. Lett.* **1995**, *244*, 456-462.

Alkorta, I.; Rozas, I.; Elguero, J., A computational approach to intermolecular proton transfer in the solid state: assistance by proton acceptor molecules. *J. Chem. Soc., Perkin Trans. 2* **1998**, 2671-2675.

Azagarsamy, M. A.; Sokkalingam, P.; Thayumanavan, S., Enzyme-Triggered Disassembly of Dendrimer-Based Amphiphilic Nanocontainers. *J. Am. Chem. Soc.* **2009**, *131*, 14184-14185.

Bae, B.; Yoda, T.; Miyatake, K.; Uchida, H.; Watanabe, M., Proton-Conductive Aromatic Ionomers Containing Highly Sulfonated Blocks for High-Temperature-Operable Fuel Cells. *Angew. Chem. Int. Ed.* **2010**, *49*, 317-320.

Bae, J. M.; Honma, I.; Murata, M.; Yamamoto, T.; Rikukawa, M.; Ogata, N., Properties of selected sulfonated polymers as proton-conducting electrolytes for polymer electrolyte fuel cells. *Solid State Ionics* **2002**, *147*, 189-194.

Baradie, B.; Dodelet, J. P.; Guay, D., Hybrid Nafion (R)-inorganic membrane with potential applications for polymer electrolyte fuel cells. *J. Electroanal. Chem.* **2000**, *489*, 101-105.

Berrada, M.; Anbaoui, Z.; Lajrhed, N.; Knouzi, N.; Vaultier, M.; Sekiguchi, H.; Carriere, F., Synthesis, characterization, and studies of heat-resistant poly(ether benzimidazole)s. *Chem. Mat.* **1997**, *9*, 1989-1993.

Berrada, M.; Carriere, F.; Abboud, Y.; Abourriche, A.; Benamara, A.; Lajrhed, N.; Kabbaj, M., Preparation and characterization of new soluble benzimidazole-imide copolymers. *J. Mater. Chem.* **2002**, *12*, 3551-3559.

Bharathi, P.; Zhao, H. D.; Thayumanavan, S., Toward globular macromolecules with functionalized interiors: Design and synthesis of dendrons with an interesting twist. *Org. Lett.* **2001**, *3*, 1961-1964.

Bozkurt, A.; Meyer, W. H., Proton conducting blends of poly(4-vinylimidazole) with phosphoric acid. *Solid State Ion.* **2001**, *138*, 259-265.

Braunecker, W. A.; Matyjaszewski, K., Controlled/living radical polymerization: Features, developments, and perspectives. *Prog. Polym. Sci.* **2007**, *32*, 93-146.

Bredas, J. L.; Poskin, M. P.; Delhalle, J.; Andre, J. M.; Chojnacki, H., Electronic-structure of hydrogen-bonded imidazole chains - Influence of the proton position *J. Phys. Chem.* **1984**, *88*, 5882-5887.

Bruce, P. G. *Solid State Electrochemistry*; Cambridge University Press: Cambridge, 1995.

Burke, S.; Eisenberg, A., Physico-chemical investigation of multiple asymmetric amphiphilic diblock copolymer morphologies in solution. *High Perform. Polym.* **2000**, *12*, 535-542.

Carrette, L.; Friedrich, K. A.; Stimming, U., Fuel cells - fundamentals and applications. *Fuel Cells* **2001**, *1*, 5-39.

Catalan, J.; Sanchezcabezudo, M.; Depaz, J. L. G.; Elguero, J.; Taft, R. W.; Anvia, F., The tautomerism of 1,2,3-triazole, 3(5)-methylpyrazole and their cations. *J. Comput. Chem.* **1989**, *10*, 426-433.

Celik, S. U.; Bozkurt, A., Proton conduction promoted by 1H-1,2,3-benzotriazole in non-humidified polymer membranes. *Electrochim. Acta* **2011**, *56*, 5961-5965.

Chen, C.; Fuller, T. F., The effect of humidity on the degradation of Nafion (R) membrane. *Polym. Degrad. Stabil.* **2009**, *94*, 1436-1447.

Chen, Y. B.; Thorn, M.; Christensen, S.; Versek, C.; Poe, A.; Hayward, R. C.; Tuominen, M. T.; Thayumanavan, S., Enhancement of anhydrous proton transport by supramolecular nanochannels in comb polymers. *Nat. Chem.* **2010**, *2*, 503-508.

Cheng, Q. Y.; Evangelista, F. A.; Simmonett, A. C.; Yamaguchi, Y.; Schaefer, H. F., Water Dimer Radical Cation: Structures, Vibrational Frequencies, and Energetics. *J. Phys. Chem. A* **2009**, *113*, 13779-13789.

Cho, A. S.; Wang, L.; Dowuona, E.; Zhou, H. Y.; Nguyen, S. T.; Broadbelt, L. J., 4-Acetoxystyrene Nitroxide-Mediated Controlled Radical Polymerization: Comparison with Styrene. *J. Appl. Polym. Sci.* **2010**, *118*, 740-750.

Cho, B. K.; Jain, A.; Gruner, S. M.; Wiesner, U., Mesophase structure-mechanical and ionic transport correlations in extended amphiphilic dendrons. *Science* **2004**, *305*, 1598-1601.

Clas, S. D.; Eisenberg, A., Synthesis and bulk physical properties of styrene-alkoxide ionomers. 1. Sodium salts of polystyrene-co-4-hydroxystyrene. *J. Polym. Sci. Pt. B-Polym. Phys.* **1986**, *24*, 2743-2756.

Costamagna, P.; Srinivasan, S., Quantum jumps in the PEMFC science and technology from the 1960s to the year 2000 Part I. Fundamental scientific aspects. *J. Power Sources* **2001**, *102*, 242-252.

Daycock, J. T.; Jones, G. P.; Evans, J. R. N.; Thomas, J. M., Rotation of imidazole in solid state and its significance in deciding nature of charge migration in biological materials. *Nature* **1968**, *218*, 672-673.

Deokar, S.; Ghadage, R. S.; Rajan, C. R.; Ponrathnam, S., Facile synthesis of poly(4-hydroxy styrene) from polystyrene. *J. Appl. Polym. Sci.* **2004**, *91*, 3192-3201.

Diat, O.; Gebel, G., Proton channels. *Nat. Mater.* **2008**, *7*, 13-14.

Donoso, P.; Gorecki, W.; Berthier, C.; Defendini, F.; Poinsignon, C.; Armand, M. B., NMR, conductivity and neutron scattering investigation of ionic dynamics in the anhydrous polymer protonic conductor PEO(H3PO4)X *Solid State Ion.* **1988**, *28*, 969-974.

Elabd, Y. A.; Hickner, M. A., Block Copolymers for Fuel Cells. *Macromolecules* **2011**, *44*, 1-11.

Elguero, J.; Fruchier, A.; Pellegrin, V., Annular tautomerism in the solid state - A high resolution NMR study. *J. Chem. Soc. Chem. Commun.* **1981**, 1207-1208.

Elliott, J. A.; Hanna, S.; Elliott, A. M. S.; Cooley, G. E., Interpretation of the small-angle X-ray scattering from swollen and oriented perfluorinated ionomer membranes. *Macromolecules* **2000**, *33*, 4161-4171.

Fischbach, I.; Spiess, H. W.; Saalwachter, K.; Goward, G. R., Solid state NMR spectroscopic investigations of model compounds for imidazole-based proton conductors. *J. Phys. Chem. B* **2004**, *108*, 18500-18508.

Godwin, A.; Hartenstein, M.; Muller, A. H. E.; Brocchini, S., Narrow molecular weight distribution precursors for polymer-drug conjugates. *Angew. Chem. Int. Ed.* **2001**, *40*, 594-597.

Goward, G. R.; Schuster, M. F. H.; Sebastiani, D.; Schnell, I.; Spiess, H. W., High-resolution solid-state NMR studies of imidazole-based proton conductors: Structure motifs and chemical exchange from H-1 NMR. *J. Phys. Chem. B* **2002**, *106*, 9322-9334.

Granados-Focil, S.; Woudenberg, R. C.; Yavuzcetin, O.; Tuominen, M. T.; Coughlin, E. B., Water-free proton-conducting polysiloxanes: A study on the effect of heterocycle structure. *Macromolecules* **2007**, *40*, 8708-8713.

Grein, F., Twist angles and rotational energy barriers of biphenyl and substituted biphenyls. *J. Phys. Chem. A* **2002**, *106*, 3823-3827.

Herz, H. G.; Kreuer, K. D.; Maier, J.; Scharfenberger, G.; Schuster, M. F. H.; Meyer, W. H., New fully polymeric proton solvents with high proton mobility. *Electrochim. Acta* **2003**, *48*, 2165-2171.

Hickner, M. A.; Ghassemi, H.; Kim, Y. S.; Einsla, B. R.; McGrath, J. E., Alternative polymer systems for proton exchange membranes (PEMs). *Chem. Rev.* **2004**, *104*, 4587-4611.

Hohenberg, P.; Kohn, W., Inhomogeneous electron gas. *Phys. Rev. B* **1964**, *136*, B864-B871.

Jayakody, J. R. P.; Chung, S. H.; Durantino, L.; Zhang, H.; Xiao, L.; Benicewicz, B. C.; Greenbaum, S. G., NMR studies of mass transport in high-acid-content fuel cell membranes based on phosphoric acid and polybenzimidazole. *J. Electrochem. Soc.* **2007**, *154*, B242-B246.

Jimenez, V.; Alderete, J. B., Complete basis set calculations on the tautomerism and protonation of triazoles and tetrazole. *Theochem-J. Mol. Struct.* **2006**, *775*, 1-7.

Kamigaito, M.; Ando, T.; Sawamoto, M., Metal-catalyzed living radical polymerization. *Chem. Rev.* **2001**, *101*, 3689-3745.

Kawada, A.; McGhie, A. R.; Labes, M. M., Protonic conductivity in imidazole single crystal. *J. Chem. Phys.* **1970**, *52*, 3121-3125.

Khurana, E.; Dal Peraro, M.; DeVane, R.; Vemparala, S.; DeGrado, W. F.; Klein, M. L., Molecular dynamics calculations suggest a conduction mechanism for the M2 proton channel from influenza A virus. *Proc. Natl. Acad. Sci. U. S. A.* **2009**, *106*, 1069-1074.

Kishimoto, K.; Suzawa, T.; Yokota, T.; Mukai, T.; Ohno, H.; Kato, T., Nano-segregated polymeric film exhibiting high ionic conductivities. *J. Am. Chem. Soc.* **2005**, *127*, 15618-15623.

Kohn, W.; Sham, L. J., Self-consistent equations including exchange and correlation effects *Physical Review* **1965**, *140*, A1133-A1138.

Kreuer, K. D., On the development of proton conducting polymer membranes for hydrogen and methanol fuel cells. *J. Membr. Sci.* **2001**, *185*, 29-39.

Kreuer, K. D., Proton conductivity: Materials and applications. *Chem. Mat.* **1996**, *8*, 610-641.

Kreuer, K. D.; Fuchs, A.; Ise, M.; Spaeth, M.; Maier, J., Imidazole and pyrazole-based proton conducting polymers and liquids. *Electrochim. Acta* **1998**, *43*, 1281-1288.

Kreuer, K. D.; Paddison, S. J.; Spohr, E.; Schuster, M., Transport in proton conductors for fuel-cell applications: Simulations, elementary reactions, and phenomenology. *Chem. Rev.* **2004**, *104*, 4637-4678.

Krishnan, R.; Binkley, J. S.; Seeger, R.; Pople, J. A., Self-consistent molecular-orbital methods .20. basis set for correlated wave-functions. *J. Chem. Phys.* **1980**, *72*, 650-654.

Laage, D.; Hynes, J. T., A molecular jump mechanism of water reorientation. *Science* **2006**, *311*, 832-835.

Lee, H. C.; Lim, H.; Su, W. F.; Chao, C. Y., Novel Sulfonated Block Copolymer Containing Pendant Alkylsulfonic Acids: Syntheses, Unique Morphologies, and Applications in Proton Exchange Membrane. *J. Polym. Sci. Pol. Chem.* **2011**, *49*, 2325-2338.

Leroux, F., Atropisomerism, biphenyls, and fluorine: A comparison of rotational barriers and twist angles. *Chembiochem* **2004**, *5*, 644-649.

Lesburg, C. A.; Christianson, D. W., X-ray crystallographic studies of engineered hydrogen-bond networks in a protein-zinc binding site. *J. Am. Chem. Soc.* **1995**, *117*, 6838-6844.

Li, Q. F.; He, R. H.; Jensen, J. O.; Bjerrum, N. J., Approaches and recent development of polymer electrolyte membranes for fuel cells operating above 100 degrees C. *Chem. Mat.* **2003**, *15*, 4896-4915.

Li, X. F.; Na, H.; Lu, H., Novel sulfonated poly(ether ether ketone ketone) derived from bisphenol S. *J. Appl. Polym. Sci.* **2004**, *94*, 1569-1574.

Macdonald, J. R., Impedance spectroscopy: Models, data fitting, and analysis. *Solid State Ionics* **2005**, *176*, 1961-1969.

Mader, J. A.; Benicewicz, B. C., Synthesis and Properties of Segmented Block Copolymers of Functionalised Polybenzimidazoles for High-Temperature PEM Fuel Cells. *Fuel Cells* **2011**, *11*, 222-237.

Markovitch, O.; Chen, H.; Izvekov, S.; Paesani, F.; Voth, G. A.; Agmon, N., Special pair dance and partner selection: Elementary steps in proton transport in liquid water. *J. Phys. Chem. B* **2008**, *112*, 9456-9466.

Martwiset, S.; Yavuzcetin, O.; Thorn, M.; Versek, C.; Tuominen, M.; Coughlin, E. B., Proton Conducting Polymers Containing 1H-1,2,3-Triazole Moieties. *J. Polym. Sci. Pol. Chem.* **2009**, *47*, 188-196.

Matyjaszewski, K.; Xia, J. H., Atom transfer radical polymerization. *Chem. Rev.* **2001**, *101*, 2921-2990.

Mauritz, K. A.; Moore, R. B., State of understanding of Nafion. *Chem. Rev.* **2004**, *104*, 4535-4585.

McLean, A. D.; Chandler, G. S., Contracted gaussian-basis sets for molecular calculations .1. 2nd row atoms, Z=11-18. *J. Chem. Phys.* **1980**, *72*, 5639-5648.

Mukherjee, B.; Maiti, P. K.; Dasgupta, C.; Sood, A. K., Jump Reorientation of Water Molecules Confined in Narrow Carbon Nanotubes. *J. Phys. Chem. B* **2009**, *113*, 10322-10330.

Munch, W.; Kreuer, K. D.; Silvestri, W.; Maier, J.; Seifert, G., The diffusion mechanism of an excess proton in imidazole molecule chains: first results of an ab initio molecular dynamics study. *Solid State Ionics* **2001**, *145*, 437-443.

Nagamani, C.; Versek, C.; Thorn, M.; Tuominen, M. T.; Thayumanavan, S., Proton Conduction in 1H-1,2,3-triazole Polymers: Imidazole-Like or Pyrazole-Like? *J. Polym. Sci. Pol. Chem.* **2010**, *48*, 1851-1858.

Nagamani, C.; Viswanathan, U.; Versek, C.; Tuominen, M. T.; Auerbach, S. M.; Thayumanavan, S., Importance of dynamic hydrogen bonds and reorientation barriers in proton transport. *Chem. Commun.* **2011**, *47*, 6638-6640.

Narayanan, S. R.; Yen, S. P.; Liu, L.; Greenbaum, S. G., Anhydrous proton-conducting polymeric electrolytes for fuel cells. *J. Phys. Chem. B* **2006**, *110*, 3942-3948.

Persson, J. C.; Jannasch, P., Block copolymers containing intrinsically proton-conducting blocks tethered with benzimidazole units. *Chem. Mat.* **2006**, *18*, 3096-3102.

Persson, J. C.; Jannasch, P., Intrinsically proton-conducting benzimidazole units tethered to polysiloxanes. *Macromolecules* **2005**, *38*, 3283-3289.

Persson, J. C.; Jannasch, P., Self-conducting benzimidazole oligomers for proton transport. *Chem. Mat.* **2003**, *15*, 3044-3045.

Pettyweeks, S.; Zupancic, J. J.; Swedo, J. R., Proton conducting interpenetrating polymer networks. *Solid State Ionics* **1988**, *31*, 117-125.

Pozio, A.; Cemmi, A.; Mura, F.; Masci, A.; Serra, E.; Silva, R. F., Long-term durability study of perfluoropolymer membranes in low humidification conditions. *J. Solid State Electrochem.* **2011**, *15*, 1209-1216.

Quinn, J. D.; Register, R. A., Microphase Separation in Block-Random Copolymers of Styrene, 4-Acetoxystyrene, and 4-Hydroxystyrene. *J. Polym. Sci. Pt. B-Polym. Phys.* **2009**, *47*, 2106-2113.

Rajan, M.; Agarwal, U. S.; Bailly, C.; George, K. E.; Lemstra, P. J., Diblock and triblock copolymers of styrene and acetoxymethylstyrene by one-pot ATRP. *J. Polym. Sci. Pol. Chem.* **2005**, *43*, 575-583.

Rikukawa, M.; Sanui, K., Proton-conducting polymer electrolyte membranes based on hydrocarbon polymers. *Prog. Polym. Sci.* **2000**, *25*, 1463-1502.

Rubatat, L.; Shi, Z. Q.; Diat, O.; Holdcroft, S.; Frisken, B. J., Structural study of proton-conducting fluorous block copolymer membranes. *Macromolecules* **2006**, *39*, 720-730.

Ruiz-Morales, J. C.; Marrero-Lopez, D.; Canales-Vazquez, J.; Nunez, P.; Irvine, J. T. S., Application of an alternative representation to identify models to fit impedance spectra. *Solid State Ionics* **2005**, *176*, 2011-2022.

Scheiner, S.; Yi, M. Y., Proton transfer properties of imidazole. *J. Phys. Chem.* **1996**, *100*, 9235-9241.

Schmidt-Rohr, K.; Chen, Q., Parallel cylindrical water nanochannels in Nafion fuel-cell membranes. *Nat. Mater.* **2008**, *7*, 75-83.

Schnell, J. R.; Chou, J. J., Structure and mechanism of the M2 proton channel of influenza A virus. *Nature* **2008**, *451*, 591-U512.

Schuster, M. E.; Meyer, W. H., Anhydrous proton-conducting polymers. *Ann. Rev. Mater. Res.* **2003**, *33*, 233-261.

Schuster, M. F. H.; Meyer, W. H.; Schuster, M.; Kreuer, K. D., Toward a new type of anhydrous organic proton conductor based on immobilized imidazole. *Chem. Mat.* **2004**, *16*, 329-337.

Shin, C. K.; Maier, G.; Scherer, G. G., Acid functionalized poly(arylene ether)s for proton-conducting membranes. *J. Membr. Sci.* **2004**, *245*, 163-173.

Shunmugam, R.; Tew, G. N., Efficient route to well-characterized homo, block, and statistical polymers containing terpyridine in the side chain. *J. Polym. Sci. Pol. Chem.* **2005**, *43*, 5831-5843.

Silverman, D. N.; Lindskog, S., The catalytic mechanism of carboinc-anhydrase - Implications of rate-limiting protolysis of water. *Accounts Chem. Res.* **1988**, *21*, 30-36.

Sivanandan, K.; Aathimanikandan, S. V.; Arges, C. G.; Bardeen, C. J.; Thayumanavan, S., Probing every layer in dendrons. *J. Am. Chem. Soc.* **2005**, *127*, 2020-2021.

Sodeye, A. I. I.; Huang, T.; Gido, S. P.; Mays, J. W., Polymer electrolyte membranes from fluorinated polyisoprene-block-sulfonated polystyrene: Membrane structure and transport properties. *Polymer* **2011**, *52*, 1963-1970.

Steele, B. C. H.; Heinzel, A., Materials for fuel-cell technologies. *Nature* **2001**, *414*, 345-352.

Sun, J. Z.; Jordan, L. R.; Forsyth, M.; MacFarlane, D. R., Acid-organic base swollen polymer membranes. *Electrochim. Acta* **2001**, *46*, 1703-1708.

Swart, M.; van der Wijst, T.; Guerra, C. F.; Bickelhaupt, F. M., pi-pi stacking tackled with density functional theory. *J. Mol. Model.* **2007**, *13*, 1245-1257.

Takamuku, S.; Jannasch, P., Fully Aromatic Block Copolymers for Fuel Cell Membranes with Densely Sulfonated Nanophase Domains. *Macromol. Rapid Commun.* **2011**, *32*, 474-480.

Teixeira, F. C.; Ramos, H.; Antunes, I. F.; Curto, M. J. M.; Duarte, M. T.; Bento, I., Synthesis and structural characterization of 1-and 2-substituted indazoles: Ester and carboxylic acid derivatives. *Molecules* **2006**, *11*, 867-889.

Tomas, F.; Abboud, J. L. M.; Laynez, J.; Notario, R.; Santos, L.; Nilsson, S. O.; Catalan, J.; Claramunt, R. M.; Elguero, J., Tautomerism and aromaticity in 1,2,3-triazole - The caseof benzotriazole. *J. Am. Chem. Soc.* **1989**, *111*, 7348-7353.

Vosko, S. H.; Wilk, L.; Nusair, M., Accurate spin-dependent electron liquid correlation energies for local spin-density calculations - A critical analysis. *Can. J. Phys.* **1980**, *58*, 1200-1211.

Wanakule, N. S.; Panday, A.; Mullin, S. A.; Gann, E.; Hexemer, A.; Balsara, N. P., Ionic Conductivity of Block Copolymer Electrolytes in the Vicinity of Order-Disorder and Order-Order Transitions. *Macromolecules* **2009**, *42*, 5642-5651.

Wang, J. T. W. W. J. T. W.; Hsu, S. L. C., Enhanced high-temperature polymer electrolyte membrane for fuel cells based on polybenzimidazole and ionic liquids. *Electrochim. Acta* **2011**, *56*, 2842-2846.

Weber, R. L.; Ye, Y. S.; Schmitt, A. L.; Banik, S. M.; Elabd, Y. A.; Mahanthappa, M. K., Effect of Nanoscale Morphology on the Conductivity of Polymerized Ionic Liquid Block Copolymers. *Macromolecules* **2011**, *44*, 5727-5735.

Westwood, G.; Horton, T. N.; Wilker, J. J., Simplified polymer mimics of cross-linking adhesive proteins. *Macromolecules* **2007**, *40*, 3960-3964.

Whittingham, M. S.; Savinell, R. F.; Zawodzinski, T., Introduction: Batteries and fuel cells. *Chem. Rev.* **2004**, *104*, 4243-4244.

Williams, R. J. P., Proton circuits in biological energy interconversions. *Annual Review of Biophysics and Biophysical Chemistry* **1988**, *17*, 71-97.

Winter, M.; Brodd, R. J., What are batteries, fuel cells, and supercapacitors? *Chem. Rev.* **2004**, *104*, 4245-4269.

Won, J.; Park, H. H.; Kim, Y. J.; Choi, S. W.; Ha, H. Y.; Oh, I. H.; Kim, H. S.; Kang, Y. S.; Ihn, K. J., Fixation of nanosized proton transport channels in membranes. *Macromolecules* **2003**, *36*, 3228-3234.

Wong, S. Y.; Putnam, D., Overcoming limiting side reactions associated with an NHS-activated precursor of polymethacrylamide-based polymers. *Bioconjugate Chem.* **2007**, *18*, 970-982.

Woudenberg, R. C.; Yavuzeetin, O.; Tuominen, M. T.; Coughlin, E. B., Intrinsically proton conducting polymers and copolymers containing benzimidazole moieties: Glass transition effects. *Solid State Ionics* **2007**, *178*, 1135-1141.

Wycisk, R.; Chisholm, J.; Lee, J.; Lin, J.; Pintauro, P. N., Direct methanol fuel cell membranes from Nafion-polybenzimidazole blends. *J. Power Sources* **2006**, *163*, 9-17.

Yang, Z.; Pelton, R., The synthesis of poly(3,4-dihydroxystyrene) and poly (sodium 4-styrenesulfonate)-co-(3,4-dihydroxystyrene). *Macromol. Rapid Commun.* **1998**, *19*, 241-246.

Yu, S.; Xiao, L.; Benicewicz, B. C., Durability studies of PBI-based high temperature PEMFCs. *Fuel Cells* **2008**, *8*, 165-174.

Yu, S.; Zhang, H.; Xiao, L.; Choe, E. W.; Benicewicz, B. C., Synthesis of Poly (2,2 '-(1,4-phenylene)5,5 '-bibenzimidazole) (para-PBI) and Phosphoric Acid Doped Membrane for Fuel Cells. *Fuel Cells* **2009**, *9*, 318-324.

Zhou, Z.; Li, S. W.; Zhang, Y. L.; Liu, M. L.; Li, W., Promotion of proton conduction in polymer electrolyte membranes by 1H-1,2,3-triazole. *J. Am. Chem. Soc.* **2005**, *127*, 10824-10825.

Zhou, Z.; Liu, R.; Wang, J. H.; Li, S. W.; Liu, M. L.; Bredas, J. L., Intra- and intermolecular proton transfer in 1H(2H)-1,2,3-triazole based systems. *J. Phys. Chem. A* **2006**, *110*, 2322-2324.

Zoltowski, P., Non-traditional approach to measurement models for analysis of impedance spectra. *Solid State Ionics* **2005**, *176*, 1979-1986.